A MECHANISTIC MODEL FOR FLOODING IN VERTICAL TUBES

A Dissertation

by

KEVIN J. HOGAN

Submitted to the Office of Graduate Studies of
Texas A&M University
in partial fulfillment of the requirements for the degree of

DOCTOR OF PHILOSOPHY

August 2009

Major Subject: Nuclear Engineering

A MECHANISTIC MODEL FOR FLOODING IN VERTICAL TUBES

A Dissertation

by

KEVIN J. HOGAN

Submitted to the Office of Graduate Studies of
Texas A&M University
in partial fulfillment of the requirements for the degree of

DOCTOR OF PHILOSOPHY

Approved by:

Chair of Committee,	Karen Vierow
Committee Members,	Yassin Hassan
	Frederick Best
	Debjyoti Banerjee
Head of Department,	Raymond J. Juzaitis

August 2009

Major Subject: Nuclear Engineering

ABSTRACT

A Mechanistic Model for Flooding in Vertical Tubes. (August 2009)
Kevin J. Hogan, B.S., University of Maryland; M.S.N.E., Purdue University
Chair of Advisory Committee: Dr. Karen Vierow

In a counter-current two-phase flow system, flooding can be defined as the onset of flow reversal of the liquid component which results in an upward co-current flow. Flooding in the surge line of pressurized water reactors poses a significant technical challenge in the analysis of several postulated nuclear reactor accident scenarios.

Despite the importance of flooding in these analyses, previous work does not identify a universally accepted rigorous physics-based model of flooding, even for the simple case of flooding in adiabatic, vertical tubes. This can be attributed to a lack of conclusive understanding of the physics of two-phase counter-current flow, specifically the mechanism of flooding, and the large amount of uncertainty among data from various flooding experiments. This deficiency in phenomenological and experimental knowledge has led to the use of many empirical and semi-empirical correlations for specific system conditions and geometries. The goal of this work is the development of a model for flooding in vertical, adiabatic tubes from first principles.

To address a source of uncertainty in the analysis of flooding, a model for the prediction of average film thickness in annular co- and counter-current flows has been developed by considering the conservation of momentum of the liquid and gas flows. This model is shown to be a quantitative improvement over the most commonly used models, those of Nusselt and Belkin, Macleod, Monrad, and Rothfus. The new model better considers the effects of interfacial shear and tube curvature by using closure relations known to represent forces appropriately in co- and counter-current flow.

Previous work based on semi-empirical flooding models has been analyzed to develop a new theory on the hydrodynamic mechanism which causes flooding. It is postulated that the growth of an interfacial wave due to interfacial instability results in a flow reversal to ensure that momentum is conserved in the counter-current flow system by causing a partial or complete co-current flow.

A model for the stability of interfacial waves in a counter-current flow system is proposed and has been developed herein. This model accurately represents the geometric and flow conditions in vertical adiabatic tubes and has been shown to have limits that are consistent with the physical basis of the system. The theory of waves of finite amplitude was employed to provide closure to an unknown parameter in the new model, the wave number of the wave that generates the interfacial instability. While this model underpredicts the flooding superficial gas velocity, the result is a conservative estimate of what conditions will generate flooding for a system. In the context of the analysis of a nuclear reactor, specifically a pressurized water reactor, conservatism means that the gas flow rate predicted to cause flooding for a fixed liquid flow rate will be less than the flow rate found experimentally, meaning that liquid delivery to the core would be safely underestimated. Future work includes the improvement of the closure relation for the limiting wave number that will cause unstable interfacial waves, as well as an assessment of the applicability of the stability-based model to flooding in the presence of phase change and flooding in complex geometries.

To my wife

ACKNOWLEDGMENTS

I would like to thank Prof. Karen Vierow for all of her guidance and supervision during the past five years, particularly for the three years spent at Texas A&M University. My work with her during this time has enabled me to become a capable researcher. I would also like to acknowledge my committee members, Prof. Yassin Hassan, Prof. Frederick Best, and Prof. Debjyoti Banerjee, as their comments and suggestions have contributed to this work.

Special thanks go to Prof. Richard Lahey, formerly of Rensselaer Polytechnic Institute, and Prof. Qiao Wu, of Oregon State University, for stimulating discussions on the nature of flooding. I would also like to thank Dr. DuWayne Schubring, formerly of the University of Wisconsin, for helping me with the selection of experimental film thickness data. Prof. Tsvetkov's advice was invaluable in the mathematical development of the stability-based model of flooding. I am also very grateful to librarian Jane Stevens for assisting in the procurement of several references that were used in the course of this work.

I would like to thank the members of the Laboratory for Nuclear Heat Transfer Systems for their support of my work, particularly Adam Bingham, James Corson, Matt Solmos, and Niki Williams for discussions and reviews of my derivations and methods. Aaron Totemeier and Adam Bingham also deserve many thanks for their help concerning the design and implementation of the LaTeX template used to construct this dissertation.

This work would not have been possible without the encouragement and support of my parents, Will and Gerrie Hogan, and my wife, Melissa Hogan. I would also thank to thank my wife for the endless hours of proofreading and discussions about this research.

NOMENCLATURE

a	distance from tube centerline to gas-liquid interface, m
f	Fanning friction factor
g	gravitational constant, 9.8 m/s^2
j_k	superficial velocity, m/s
j_k^*	Wallis parameter, $\langle j_k \rangle \sqrt{\rho_k / \left(gD\left(\rho_f - \rho_g\right)\right)}$
k	wave number, $2\pi/\lambda$, 1/m
p	pressure, N
r	radial cylindrical coordinate
s	modified Bessel function order
v	velocity, m/s
z	axial cylindrical coordinate
A	area, m^2
D	diameter, m
D^*	dimensionless diameter, $\sqrt{\text{Bo}}$
N	number of points
P	wetted perimeter, m
Q	volumetric flow rate, m^3
R	tube radius, m
T	temperature, K
U	velocity, m/s
$\overline{V}_{gj}$	drift velocity, $\left(1 - \langle \alpha_g \rangle\right) \overline{v_r}$, m/s
$\dot{m}$	mass flow rate, m/s
$\overline{v_r}$	relative velocity, see Equation 3.17, m/s
Bo	Bond number, $D^2 g \left(\rho_f - \rho_g\right)/\sigma$
Ku_k	Kutateladze number for phase k, $\sqrt{D^*} j_k^*$
Re	Reynolds number (vD/ν)

Re_Γ	Reynolds number of the liquid film ($4\Gamma/\mu_f$)
$\bar{\Psi}$	time averaged Ψ
$\langle\Psi\rangle$	area averaged Ψ, $\frac{1}{A}\int_A \Psi dA$
$\langle\langle\Psi\rangle\rangle$	mean weight averaged Ψ, $\langle\alpha\Psi\rangle/\langle\alpha\rangle$

Greek symbols:

α	void fraction, α_g
α_k	volume fraction of phase k
δ	film thickness, m
δ^*	dimensionless film thickness, $\delta\left(g_z\rho_f\left(\rho_f-\rho_g\right)/\mu_f^2\right)^{1/3}$
δ_{exp}	film thickness, experimental, m
δ_{model}	film thickness, calculated from a model, m
ϵ	surface roughness, m
μ	dynamic viscosity, $\mathrm{Pa}\cdot\mathrm{s}$
ν	kinematic viscosity, m^2/s
ϕ	potential, m^2/s
ρ	density
σ	surface tension
σ_{model}	standard deviation of values from experimental data
τ	shear
θ	azimuthal cylindrical coordinate
ω	angular frequency, rad/s
Γ	mass flow per wetted perimeter, $\dot{m}/\left(\pi D\right)$
Φ_1	variable

Subscripts:

f	liquid
g	gas

h	hydraulic
i	interfacial
k	k-phase; liquid or gas
w	wall
z	axial direction
0	initial

TABLE OF CONTENTS

Page

Page

LIST OF TABLES

LIST OF FIGURES

FIGURE Page

FIGURE Page

FIGURE Page

FIGURE Page

FIGURE Page

1. INTRODUCTION

In a counter-current two-phase flow system, flooding can be defined as the onset of flow reversal of the liquid component which results in an upward co-current flow. This flow reversal includes significantly more liquid than that which reverses flow at low gas flow rates due to entrainment. Flooding can be perceived as a limit to two-phase counter-current flow, meaning that pairs of liquid and gas flow rates exist that define the envelope for stable countercurrent flow for a given system. The ability to predict flooding in a system is important to the analysis of hypothetical accidents in nuclear reactors. Several accident scenarios have been postulated that include the possible occurrence of flooding. For example, flooding can occur in the AP600 reactor design due to the draining of the pressurizer through the surge line during a small break loss of coolant accident [1]. The difficulty in analyzing the two-phase flow in the surge line is compounded due to the geometric complexities of the surge line itself, as can be seen in the schematic given by Figure 1.1. In all PWRs, degradation of emergency core cooling system performance during a LOCA following flooding and flow reversal can interfere with accident mitigation [2, 3]. In addition, the progression of events that may cause a steam generator tube rupture strongly depends on the timing of the occurrence of flooding in the reactor hot leg [4].

Despite the importance of this phenomenon, a clear, rigorous physics-based model of flooding, even for the simple case of flooding in adiabatic, vertical tubes, is not available. This can be attributed to a lack of conclusive understanding of the mechanisms [2, 5, 6] and the large amount of uncertainty among data from various flooding experiments [7]. This deficiency in phenomenological and experimental knowledge has led to the use of many empirical and semi-empirical correlations for specific system conditions and geometries. Many "analytical" models have been created and

This dissertation follows the style of International Journal of Heat and Mass Transfer.

utilize lengthy derivations, only to include a coefficient or parameters determined by analyzing data from experiments on flooding. The development of a model for flooding in vertical, adiabatic tubes from first principles that does not include empirical parameters would both identify the mechanisms governing flooding and allow for the derivation of models for flooding in the presence of phase change and non-vertical orientations.

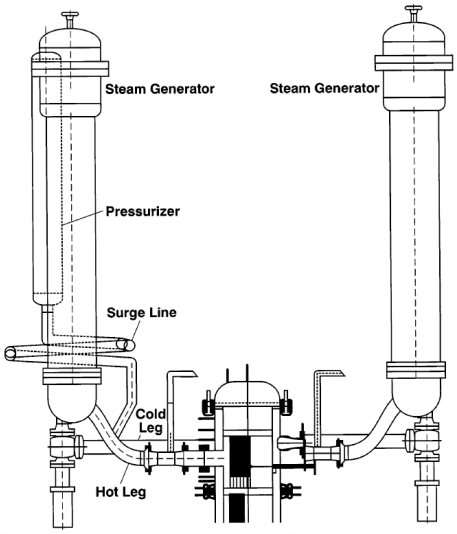

Fig. 1.1. PWR schematic (from [8]).

1.1 Objectives

The objectives of this research are to:

1. Develop a model for average annular film thickness for co- and counter-current flow by considering the parameters governing the system

2. Survey previous experimental and analytical work to identify the mechanism of flooding and define flooding in this context

3. Derive a model for flooding based on the mechanism that has been identified by considering as many relevant parameters as possible

1.2 Technical Approach

This document is structured to describe a complete model for flooding in vertical, adiabatic tubes in a narrative fashion. To this end, each section will build on the work described in the previous sections, culminating in a description of how the model could be feasibly implemented when it is completed.

A review of experimental work and models of flooding is presented in Section 2. In Section 3, a model is proposed to estimate the void fraction and average liquid film thickness for annular counter- and co-current flows. This model will both serve as the basis for the analysis described in Section 4 and will provide closure to the mechanistic model that will be developed in Section 5. Section 4 investigates previous work on semi-empirical models of flooding and will pose a mechanism by which flooding can occur. This mechanism will lead to the development of a physics-based model for flooding in Section 5. In Section 6, this physics-based model will be analyzed and validated against experimental data. Finally, conclusions and recommendations based on this work are detailed in Section 7.

2. PREVIOUS WORK

Experimental and analytical research on flooding and associated phenomena have been conducted for more than fifty years [9]. This research has yielded numerous experimental data sets, experimental observations, and empirical, semi-empirical, and analytical models of flooding. In spite of this, many parametric dependencies of flooding are not entirely understood, and no analytical model of flooding exists that is widely accepted as correct. A review of published literature will show which observations and trends are commonly agreed upon, which are currently inconclusive, and the state of models for flooding. A majority of the work conducted in these areas has been summarized by Bankoff and Lee [2], McQuillan [7], and Zapke and Kroger [10].

2.1 Experimental Studies

Much experimental research conducted on the topic of flooding has used a configuration with the following characteristics:

- a counter-current flow of liquid and gas
- a horizontal test section (possibly a segment of test section), or an inclined-to-vertical test section, with liquid flowing downward and gas rising upward

While this is the general configuration for all these experiments, there are several different goals of flooding experiments. Bankoff and Lee [2] identified these as:

- determination of the onset of flooding
- investigation of the effect of gas flow delivery rate at constant liquid injection during flooding (and vice-versa)
- exploration of hanging film (described in Section 2.1.1) and flow reversal

The determination of flooding in these experiments is accomplished by studying the liquid and gas flow conditions that cause the flow pattern to change to a co-current flow. This results in a set of pairs of flow rates that cause flooding in that specific experimental apparatus. Investigating the effect of a changing delivery rate of one fluid while the other fluid is held constant allows for the observation of the events that function as precursors to flooding, as well as the study of the behavior of the liquid-gas interface as flooding is experimentally approached.

2.1.1 Characteristics of Flooding

The indications of flooding are generally agreed upon by most researchers. The main indicator of flooding is a reduction in liquid delivery rate when compared to liquid injection rate, signaling that a considerable amount of liquid flow has become co-current with the gas flow. An increase in the pressure drop from the liquid inlet to the gas inlet is also known to occur in small diameter tubes [2, 11]. This is possibly related to another indicator of flooding, the appearance of large amplitude interfacial waves at the gas-liquid interface. A hysteresis effect is noted following flooding, meaning that to stop the significant co-current flow, the gas flow rate must be reduced significantly below the rate that caused flooding [2, 12]. Recently it has been reported that these indicators can occur without a dynamic change in the system; hence, flooding happens spontaneously and can occur without an external perturbation of a countercurrent system [13].

Important definitions and phenomena related to flooding include the locus of flooding, hold-up and partial delivery, hanging (or "standing") film, flow reversal, and deflooding.

The locus of flooding, as defined by Wallis [11] is the axial location where flooding occurs in a tube. The liquid upstream of the locus of flooding may be partially reversed, leading to the partial delivery of the liquid, or fully reversed, leading to liquid hold-up [14]. Liquid hold-up occurs when the downward flow of the liquid

has completely reversed and is no longer penetrating downstream, past the locus of flooding [2, 12, 15]. "Gas hold-up," though not used frequently in literature, is used to refers to the portion of gas located downstream with respect to the gas flow of the locus of flooding [5, 16, 17]. Specifically, this may refer to either the volume average void fraction or the radius of the gas core downstream of the locus of flooding [18].

The hanging film phenomenon is observed following the discontinuance of liquid partial delivery downstream of the locus of flooding [19]. The contact angle between the leading edge of the film and the tube wall has been found to be correlated to the tube diameter, though this contact angle is asymptotic for large tubes (see Sections 2.1.2 and 2.2.1). The film that remains along the periphery of the tube remains stagnant. It has been hypothesized that a large tube diameter may represent a physical limit for the largest possible contact angle between the liquid film and wall [20]. Shearer and Davidson [21] noted that the existence of this hanging film implies that the interfacial shear may have a minimal effect on flooding. Furthermore, they postulate that this assumption could be supported by Nicklin and Davidson's [22] result that film thickness in an annular flow is unaffected by the flow rate of the gas. It should be noted that Bankoff and Lee [2] disagree with this assumption due to the fact that large-amplitude interfacial waves appear and effectively increase the roughness of the gas-liquid interface.

Flow reversal, beyond simple entrainment of droplets, occurs immediately following flooding. The region of the tube downstream of the locus of flooding of the gas can be described as a churn-annular flow [5]. The growth of interfacial waves is likely to contribute to flow reversal, and the co-current flow that results may be driven by interfacial shear force [23]. Most likely, a model for the reversed flow would need to be derived without regard to the flow conditions that caused the flooding [24].

Deflooding, a term used in literature as early as 1966 by Clift, Pritchard, and Nedderman [25], describes the transition from co-current flow and partial delivery to an annular, counter-current flow. It has been well-established that the pairs of liquid

and gas flow rates that define flooding for a given system are not equivalent to the pairs of flow rates found for deflooding. This hysteresis effect has been documented by numerous researchers [2,26]. The gas and liquid flow rate pairs that cause deflooding are determined by decreasing the gas flow rate in a system undergoing flow reversal until the annular film redevelops [2, 5].

2.1.2 Parameters Studied

The major parameters affecting flooding are the orientation of the system, the geometry (including the inlet and outlet conditions and the cross section shape and size), and the fluid properties, including the presence of phase change [2, 10, 27, 28]. The effect of each of these parameters on pairs of liquid and gas flow rates that cause flooding has been studied extensively, though a survey of literature shows that there is not a concurrence of opinion on trends for each of these parameters.

Inclination can cause the flow structure to change between annular flow and stratified flow and can affect the influence of gravity on the flow [10, 17, 28, 29]. This may affect where the locus of flooding is located along a channel [2, 30]. For vertical tubes without phase change, flooding tends to occur near the gas inlet. For a specific inclination, the locus of flooding appears to always be in the same location for a given system. Inlet and outlet conditions affect the local velocity profiles of both the liquid and the gas and can affect the momentum of each phase [2].

A variety of inlet and outlet geometries have been studied, but primarily empirical models have been developed to account for these effects [2, 9, 10, 31]. Cross sectional geometries, including circular tubes, rectangular ducts and flat plates, were studied, and the cross sectional shape was shown to have an appreciable effect on flooding. In addition, for small hydraulic diameter closed channels, the onset of flooding is a function of the hydraulic diameter. Beyond a specific transition point, where the Bond number is greater than 160, the diameter has very little effect on flooding [2].

It is also known that obstructions, bends, and elbows affect flooding but there has been little work in this area due to the added complications [27, 32–34].

The effects of temperature and pressure on flooding are treated implicitly by considering their effects on fluid properties. Of all the fluid properties, the density of liquid and gas are known to have the most significant effect on flooding. An increase in gas density is known to cause a decrease in the gas flow rate needed to cause flooding for a given liquid flow rate. The opposite is true for the liquid: increasing the liquid density increases the flow rate of the gas [2,10]. The gas viscosity has been shown to have little effect on flooding whereas flooding is a property of the viscosity of the liquid [10]. Recently, Zapke and Kroger [10] have reported that for large liquid viscosities, flooding is not a function of viscosity. While this trend is accepted, there is no consensus regarding the relationship between viscosity and the relative velocities needed to cause flooding. Some researchers have noted the effects of surface tension, but various researchers have found conflicting trends [2, 6, 10]. Condensation of the gas phase has also been studied and has yielded a variety of results. Condensation appears to affect flooding as a function of the location of the locus of flooding relative to the injection point of the gas [2,29]. A possible explanation for the many conflicting trends is the difficulty in isolating individual fluid properties [10]. Understanding the mechanism that causes flooding through both a theoretical and mathematical approach could clarify the functional dependencies of flooding on fluid properties. Conversely, the inclusion of these functional dependencies in an analytical model would be integral to the accuracy and general success of the model.

2.2 Models of Flooding

The uncertainties and complexities surrounding the parametric dependencies of flooding significantly contribute to the difficulty in modeling flooding. As a result of the experimental work on flooding, numerous empirical correlations for flooding in complicated geometries and configurations have been developed [2]. These mod-

els are generally unable to predict the flooding in experimental facilities that are not identical to the facility the model was developed to represent. Historically, all models have been developed to try to predict flooding in systems with similar sets of features. Bankoff and Lee [2] categorize all flooding models into four groups: theories based on stability of a traveling wave, envelope theories, static equilibrium theories, and theories based on models of slug formation. These categories are based on the assumptions on which the models are based, including assumptions about the mechanistic cause of flooding and system configuration, which Bankoff and Lee determined were most important. Alternatively, the models could be characterized by the following criteria:

degree of empiricism If a variable parameter in a model represents a phenomenon based on experimental results and cannot be derived for any given facility, then the value of that individual parameter is not easily found. This undermines the physical interpretation of the model and, in general, differentiates between models considered "semi-empirical" and "analytical" models. However, most models of flooding rely on experimental data, even if the model itself is derived from first principles. While these models are technically empirical, they are referred to as both theoretical and analytical models in literature to differentiate them from models which are, to a significant degree, empirical. This distinction would separate the Wallis and Kutateladze-like correlations from analytical models that are assumed to be better understood (see Section 2.2.1).

reliance on first principles The form of the field equations used to model flooding strongly influences the form of the final flooding criteria. For example, while models of flooding based on the theory of slug formation are conceptually similar, some models for the onset of slug formation are similar to models Bankoff and Lee identify in the category of theories on the stability of a traveling wave. Additionally, envelope theories can conceptually be related to models that fit into other categories that are identified by Bankoff and Lee [2].

Therefore, an alternative method of characterizing flooding models is to determine if the model is semi-theoretical or analytical, and then determine which analytical models are of similar origin.

2.2.1 Semi-Theoretical Models

Because the prediction of flooding relies on numerous parameters, the prevalent method of determining the flow rates that lead to flooding for a particular system is the use of semi-empirical correlations. Variations of the Wallis correlation and Kutateladze-like correlations are the primary methods of predicting flooding in vertical, adiabatic tubes [2, 11].

The Wallis correlation [11, 15] is given as

$$\left[j_g^*\right]^{1/2} + m\left[j_f^*\right]^{1/2} = c. \tag{2.1}$$

The coefficient m is proportional to the Reynolds number and ranges from 0.8 to 1.0, where $m = 1$ corresponds to a turbulent flow. The parameter c accounts for geometric considerations, including tube end effects and fluid injection methods, and ranges from 0.7 to 1.0. The Wallis correlation is based on a dimensional number, the Wallis parameter (j_k^*), which represents a balance of momentum flux and hydrostatic forces. For each fluid, liquid (f) and gas (g), the Wallis parameter is

$$j_f^* = \langle j_f \rangle \sqrt{\frac{\rho_f}{gD\left(\rho_f - \rho_g\right)}} \tag{2.2}$$

$$j_g^* = \langle j_g \rangle \sqrt{\frac{\rho_g}{gD\left(\rho_f - \rho_g\right)}}. \tag{2.3}$$

In these equations, the volumetric flux, or superficial velocity, for a phase k is defined as

$$\langle j_k \rangle = \frac{Q_k}{A} = \langle \alpha_k \rangle \left\langle \langle v_k \rangle \right\rangle, \tag{2.4}$$

and the following averaging definitions are used [35]:

$$\langle F_k \rangle = \frac{1}{A} \int_A F_k dA \tag{2.5}$$

$$\langle\langle F_k \rangle\rangle = \frac{\langle \alpha_k F_k \rangle}{\langle \alpha_k \rangle}. \tag{2.6}$$

Kutateladze [36] presented his eponymous dimensionless group as a number that determined the break up of droplets suspended in a gas stream. Wallis and Kuo [19] later pointed out that the Kutateladze number emerges from a two-dimensional potential flow analysis of the hanging film phenomena using the Bernoulli equation. Pushkina and Sorokin [37] demonstrated that the gas velocity needed to reverse flow for a given liquid velocity could be determined as a function of the Kutateladze number for tubes with diameters between 6 mm and 309 mm. Tien [38] and Chung, Liu, and Tien [39] posed a model, refered to as a "Kutateladze-like" correlation, for flooding using the Kutateladze number in the form of

$$\mathrm{Ku}_g^{1/2} + m\mathrm{Ku}_f^{1/2} = c \tag{2.7}$$

where m and c are approximately 1 and 1.79, respectively. It should be noted that m and c in Equation 2.7 are not fundamentally equivalent to the values posed in Equation 2.1 and must be found empirically for a given experimental system. The liquid and gas Kutateladze numbers are defined as

$$\mathrm{Ku}_f = \langle j_f \rangle \left[\frac{\rho_f^2}{g\sigma(\rho_f - \rho_g)} \right]^{1/4} \tag{2.8}$$

$$\mathrm{Ku}_g = \langle j_g \rangle \left[\frac{\rho_g^2}{g\sigma(\rho_f - \rho_g)} \right]^{1/4}. \tag{2.9}$$

The Kutateladze number can then be written in terms of the Wallis number as

$$\mathrm{Ku}_k = [D^*]^{1/2} j_k^* \tag{2.10}$$

with the dimensionless diameter, D^*, defined both in terms of the Bond number, Bo, and known parameters as

$$D^* = [\mathrm{Bo}]^{1/2} = D\sqrt{\frac{g(\rho_f - \rho_g)}{\sigma}}. \tag{2.11}$$

Generally, the Wallis correlation is used for systems where the dimensionless diameter, D^*, is less than 40. For larger values of D^*, it has been noted that there appears

to be no dependence on tube diameter [2, 15] and a Kutateladze-like correlation is used.

Criticism

Both the Wallis and Kutateladze-like correlations strongly rely on experimental data in order to calculate the occurence of flooding. While the Wallis parameter represents a ratio of forces, attempts to represent experimental data with this quantity have not established clear trends. McQuillan and Whalley [7] found significant scatter in a plot of the gas Wallis parameter versus the liquid Wallis parameter, implying that either the Wallis parameter does not account for the appropriate phenomena involved in flooding or that more parameters must be considered. While uncertainty in experimental flooding data, such as not observing precisely the minimum pairs of velocities to cause flooding and entrance and exit plenum effects, can lead to experimental error, error found in the analysis of several experimental data sets using the Wallis parameter is larger than that of experimental error alone.

The Kutateladze number was used in analysis before it was derived from field equations, and the form of the Kutateladze-like correlations was determined by inserting the Kutateladze number into an equation similar to that of the Wallis correlation [38, 39]. The derivation of the Kutateladze number by Wallis and Kuo does not result in a model commonly used to predict flooding, nor does it explain the form of Kutateladze-like correlations.

The use of Wallis and Kutateladze-like correlations together to predict flooding in tubes of all diameters implies that a change in the diameter of a tube could change the mechanism that causes flooding. A model that is valid for all tube diameters would be more justified than a piece-wise model, as the two correlations are not conceptually continuous. Though a gravitational term is included in both the Wallis and Kutateladze numbers, the effect of gravity on flooding has not been studied.

Based on the forms of Equations 2.1 and 2.7, the gravity term effectively acts as a constant, and is present in each number to provide dimensionless terms.

The model presented herein will address some of the known deficiencies of the Wallis and Kutateladze-like correlations. The formation of dimensionless groups that more accurately capture the physics of flooding can be determined by using field equations to derive an appropriate model of flooding. While experimental uncertainty will still be present in analyses of experimental flooding data, the characterization of flow parameters using suitable nondimensional numbers will allow for more useful comparisons of data between different experimental facilities. The new model will also address the discontinuity between large and small diameter tubes by assuming that flooding has a continuous dependence on tube diameter and this dependence diminishes for larger tubes.

2.2.2 Analytical Models

Analytical models are created by assuming flooding is caused by certain mechanisms, and then applying appropriate equations in order to generate a model that can be analyzed. Many models of flooding are the result of lengthy rigorous derivations, only to fit a coefficient to experimental data as a final step. A majority of these models are given by Bankoff and Lee [2]. Though these models may rely on first principles, they are nevertheless semi-empirical. The development of a model to predict flooding in a vertical, adiabatic counter-current flow system without a major presence of empirical parameters "tuned" to experimental data will both yield insight into the mechanisms behind flooding and will provide an analytical basis for the development of future models in complex systems.

Among the analytical models that have been developed are drift-flux models for flooding. Drift-flux models of flooding have been shown to correlate to flooding data to a reasonable degree of accuracy. Wallis [11] developed an early drift-flux model for flooding and showed that these models can predict the qualitative trends

found in flooding. Ohkawa and Lahey [40] later developed an addition to this model for predicting flooding based on one-dimensional drift-flux techniques by deriving the distribution parameter and drift velocity of the gas. Using the Zuber-Findlay relationship [41], they defined flooding in terms of the maximum value of the gas superficial velocity for a given liquid superficial velocity [40]. These models tend to qualitatively predict the occurrence of flooding, but empirical coefficients derived from experimental data are used to provide closure relations to these models. Consequently, these models contain a high degree of empiricism.

This work aims to analyze flooding using an approach based on one-dimensional drift-flux momentum equations for each phase with closure relations that are not derived from experimental data on flooding. The model predictions reveal deficiencies in current techniques, the implications of which are discussed in relation to future developments in the modeling of flooding.

3. A MODEL FOR AVERAGE FILM THICKNESS

The ability to estimate the average film thickness for a counter-current annular system of liquid and gas allows for the estimation of the void fraction and diameter of the gas core of the flow pattern, both of which must be provided as closure relations for many models of flooding. The development of a new model for the average film thickness of the liquid layer in counter-current annular flow will improve the estimate of the thickness of the film, as well as provide a more theoretically sound basis for this calculation. Additionally, this model will be used as the basis for the work described in Section 4.

3.1 Earlier Models

The models most commonly used to predict the average film thickness in counter-current annular systems are presented by Wallis [11] and Bankoff and Lee [2] and are based on the work of Nusselt [42] and Belkin, Macleod, Monrad, and Rothfus [43]. The use of these models requires the gas velocity be low enough that interfacial shear stresses and the pressure drop are negligible, and the curvature of the tube can be ignored. A dimensionless film thickness, δ^*, has been defined in the model posed by Wallis [11] as

$$\delta^* = \delta \left(\frac{g_z \rho_f \left(\rho_f - \rho_g \right)}{\mu_f^2} \right)^{\frac{1}{3}}. \tag{3.1}$$

To determine the magnitude of the nondimensional film thickness, the Reynolds number of the liquid film must be calculated as

$$\mathrm{Re}_\Gamma = \frac{4\Gamma}{\mu_f} = \frac{4\dot{m}}{\pi D \mu_f}. \tag{3.2}$$

If $\mathrm{Re}_\Gamma < 1000$, δ^* can be calculated as

$$\delta^*_{\mathrm{lam}} = 0.909 \mathrm{Re}_\Gamma{}^{\frac{1}{3}}. \tag{3.3}$$

For $\mathrm{Re}_\Gamma > 1000$, the dimensionless film thickness can be found by using the following model that was posed by Belkin, Macleod, Monrad, and Rothfus [43]:

$$\delta^*_{\mathrm{turb}} = 0.315 \left(\mathrm{Re}_\Gamma \sqrt{f_{wf}} \right)^{\frac{2}{3}}. \tag{3.4}$$

In Equation 3.4, f_{wf} is the Fanning friction factor, which can be calculated by using the Colebrook equation [44]:

$$\frac{1}{\sqrt{4f_{wf}}} = -2 \log \left(\frac{\epsilon}{3.7D} + \frac{2.51}{\mathrm{Re}_f \sqrt{4f_{wf}}} \right). \tag{3.5}$$

The friction factor must be solved for iteratively, and Re_f, the liquid Reynolds number, is defined as [45]

$$\mathrm{Re}_f = \frac{4\rho_f \left| v_f \right| \delta}{\mu_f} \approx \frac{\rho_f \left| \langle j_f \rangle \right| D}{\mu_f}. \tag{3.6}$$

These empirical correlations have been shown to provide reasonable agreement with experimental data. Because the liquid film is known to remain at an approximately constant thickness until the occurrence of flooding [2], the prediction of the average film thickness in a counter-current annular flow should describe the geometry of the flow pattern.

While the gas flow and tube curvature were assumed not to have an effect on the average film thickness before flooding, this could be explored by applying the conservation of momentum equation to the system. The development of a new model that considers the balance of momentum between the fluids would provide a more theoretically sound basis for this calculation that considers both the downward flow of the liquid and upward flow of the gas.

3.2 New Theoretical Model for Average Film Thickness

Solving for the geometric configuration before the occurence of flooding can be accomplished by considering the momentum balance before the appearance of the large-amplitude waves that are characteristic of flooding, as well as the onset of

flow reversal and partial delivery. By considering the conservation of momentum in the axial direction in a cylindrical coordinate system, where the centerline ($r = 0$) corresponds to the center of the tube (see Figure 3.1), a relationship between the liquid volumetric flow rate into the tube, the gas volumetric flow rate into the tube, and the mean film thickness around the tube (vis-à-vis the void fraction) can be determined. Using equations developed by Ishii, Chawla, and Zuber [45] to provide a constitutive equation for the drift velocity in two-phase annular flow, this relationship will be developed. The conservation of momentum for the gas phase is given as

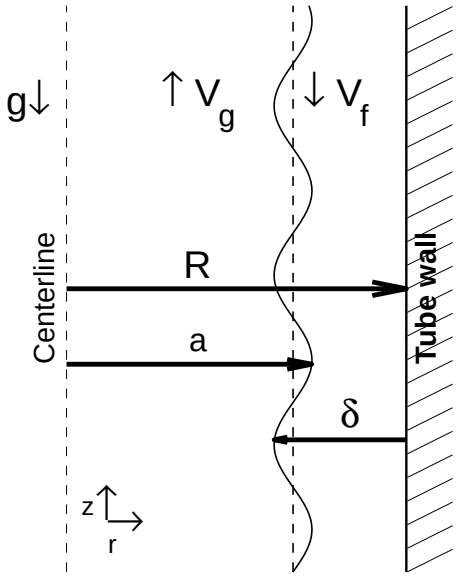

Fig. 3.1. Cylindrical coordinate system.

$$-\left(\frac{dp_m}{dz} + \rho_g g_z\right) = \frac{\tau_i P_i}{\langle \alpha_g \rangle A} \tag{3.7}$$

while that of the liquid is [45]

$$-\left(\frac{dp_m}{dz} + \rho_f g_z\right) = \frac{\tau_{wf} P_{wf}}{(1 - \langle \alpha_g \rangle) A} - \frac{\tau_i P_i}{(1 - \langle \alpha_g \rangle) A}. \tag{3.8}$$

Subtracting Equation 3.7 from Equation 3.8 yields Equation 3.9

$$\rho_g g_z - \rho_f g_z = \frac{\tau_{wf} P_{wf}}{(1 - \langle \alpha_g \rangle) A} - \frac{\tau_i P_i}{(1 - \langle \alpha_g \rangle) A} - \frac{\tau_i P_i}{\langle \alpha_g \rangle A}. \tag{3.9}$$

To use Equation 3.9 as a relationship between Q_f, Q_g, and α, the following parameters must be defined:

- pipe diameter, D
- pipe flow area, $A = \left(\frac{D}{2}\right)^2 \pi$
- wall wetted perimeter, $P_{wf} = D\pi$
- liquid viscosity, μ_f
- liquid density, ρ_f
- gas density, ρ_g
- gravitational acceleration, g_z

Therefore, parameters that must be determined by constitutive relations are the:

- wall shear of the fluid, τ_{wf}
- interfacial shear, τ_i
- interfacial wetted perimeter, P_i

Bankoff and Lee [2] identified several closure relations that are valid for both co- and counter-current flow up until the point of flooding. Using these relations allows for the development of a model to predict the average film thickness of both co- and counter-current flows.

The wall shear of liquid is defined as [35]

$$\tau_{wf} = \frac{f_{wf}\rho_f \langle\langle v_f \rangle\rangle |\langle\langle v_f \rangle\rangle|}{2} - \frac{\Delta\rho g_z \delta}{3}. \tag{3.10}$$

As noted in Section 3.1, the wall friction factor is a function of the Reynolds number. The wall friction factor is

$$f_{wf} = \frac{16}{Re_f} \tag{3.11}$$

for laminar flow or the Colebrook Equation (Equation 3.5) for turbulent flow. The transition to turbulent flow for this internal flow is $Re = 2300$ [35, 44].

The thickness of the liquid film, δ, can also be defined as a function of the void fraction as

$$\delta = \frac{1}{2}\left(1 - \sqrt{\alpha_g}\right) D. \tag{3.12}$$

The interfacial shear for both counter-current and co-current annular flow is defined as [35, 46]

$$\tau_i = \frac{f_i \rho_g \left|\overline{v_r}\right| \overline{v_r}}{2}. \tag{3.13}$$

The interfacial friction factor is known to be a function of the void fraction for annular flows with thin film layers and can be written [2]

$$f_i = 0.005 \left[1 + 75 \left(1 - \langle \alpha_g \rangle\right)\right]. \tag{3.14}$$

The relative velocity, $\overline{v_r}$, can be found by considering two definitions of the drift velocity, $\overline{V}_{gj}$,

$$\overline{V}_{gj} = \left(1 - \langle \alpha_g \rangle\right) \overline{v_r} \tag{3.15}$$

and

$$\overline{V}_{gj} = \langle \langle v_g \rangle \rangle - \langle j \rangle . \tag{3.16}$$

Combining Equation 3.15 and Equation 3.16 gives

$$\overline{v_r} = \frac{\langle \langle v_g \rangle \rangle - \langle j \rangle}{1 - \langle \alpha_g \rangle}, \tag{3.17}$$

which expresses $\overline{v_r}$ as a function of the velocity of the gas, the void fraction and, because $\langle j \rangle = \langle j_f \rangle + \langle j_g \rangle$, known values [35]. The interfacial wetted perimeter,

$$P_i = \left(D - 2\delta\right) \pi, \tag{3.18}$$

is a function of the film thickness, and as given in Equation 3.12, is a function of the void fraction.

Therefore, by substituting the previous equations into closure relations and the conservation equation, Equation 3.9 has only three remaining variables: the void

fraction, $\langle \alpha_g \rangle$, and the gas and liquid velocities, $\langle\langle v_g \rangle\rangle$ and $\langle\langle v_f \rangle\rangle$ (or, alternatively, $\langle j_g \rangle$ and $\langle j_f \rangle$). Since $\langle j_k \rangle = Q_k/A$ is a definition of the superficial velocity of each fluid, $\langle \alpha \rangle$, the void fraction, is the only unknown in Equation 3.9, it can be found simply by solving the equation. The average film thickness can then be found using Equation 3.12.

3.3 Model Assessment

The model developed in Section 3.2 provides a physical basis more consistent with the physics in annular flow when compared to the model posed by Wallis [11] by Equation 3.1, as well as an improved numerical result when calculating average annular film thickness.

3.3.1 Model Analysis

The model for average film thickness that has been developed does not necessarily take all relevant phenomena into account, but it significantly improves upon the popular model described by Wallis [11]. The previous model neglects tube curvature and assumes that interfacial shear stresses and pressure drop are not signficant. As the new model is based on the conservation of momentum between the flows, interfacial shear stresses are explicitly treated using Equation 3.13. Tube curvature affects both the interfacial parameters of the flow, as well as the geometric considerations of the system. Both of these aspects are treated in this new formulation by using constitutive relations that have been shown to be valid at varied flow conditions and system geometries. The rigorous nature of this model also allows for the use of different closure relations based on the analyst's requirements, though the constitutive equations given in this paper have been noted above to be valid for a wide range of co- and counter-current flows. The pressure gradient of the two-phase flow is not ne-

glected, but rather not necessary due to the mathematical construction of the model shown in Equation 3.9.

Much like the models presented by Wallis [11], the proposed model does not explicitly consider entrance effects or frictional wall losses over significant lengths; however, the use of a field equation based on the conservation of momentum could allow for the implicit consideration of these parameters based on their contributions to the loss of momentum. While the new model does not account for under-developed flows, quantitative results have shown this uncertainty to be small in comparison to the uncertainty in using the models of Nusselt and Belkin on fully-developed flows (see Section 3.3.2). The limited knowledge of the exact transition from laminar to turbulent flows is an uncertainty that contributes to the use of both models, though it has been found by examination that the model is not very sensitive to this transition between friction factor models.

3.3.2 Model Validation

In order to quantitatively assess the model described in Section 3.2 for the prediction of average annular film thickness in co- and counter-current flows, experimental data is analyzed with the new model. The new model for average film thickness by determining the average film thickness is assessed by determining the average film thickness from the area area averaged void fraction. To calculate the void fraction in the test section of the experiment, the following parameters are used as input to the model:

- liquid volumetric flow rate, Q_f
- gas volumetric flow rate, Q_g
- liquid density, ρ_f
- gas density, ρ_g

- liquid viscosity, μ_f
- tube diameter, D

From this input, the output variables that can be found are:

- average film thickness, $\bar{\delta_f}$
- superficial fluid velocities, $\langle j_k \rangle$
- void fraction, $\langle \alpha_g \rangle$
- average distance from tube centerline to the gas-liquid interface, $\bar{a}$
- mean weight averaged velocities, $\langle \langle v_k \rangle \rangle = \langle j_k \rangle \, / \, \langle \alpha_k \rangle$

Approach

While it would be ideal for the application of this research to validate the new model for average annular film thickness by using several sets of counter-current annular flow experimental data, scarcity of this data and the low fidelity of the data that can be found prevent this from being possible. Several reports which appear to contain this data are not commonly available. Data presented by Bharathan, Wallis, and Richter [47] was procured for the purposes of validation, but the uncertainty in measurements of liquid flow rates is large enough to impede the use of this data for analysis purposes. Limited data reported by Lacy [48] appears to be of relatively high quality and can be used as validation data.

Despite the limited availability of counter-current annular film thickness data, a variety of available co-current annular film thickness data allows for the validation of the new film thickness model against several experimental data sets. The co-current flow film thickness data that have been chosen to validate the new model are those of Asali [49], Fore and Dukler [50], MacGillivray [51], and Wolf, Jayanti, and Hewitt [52]. The co- and counter-current experimental configurations used to

provide the data from these researchers are similar in that they all consist of a vertical test section which is instrumented to find the average annular film thickness for gas-liquid flows. Each experiment is conducted by adjusting the respective fluid flow rates to desired values, allowing the film thickness to reach a steady state, and measuring the film thickness at the desired locations along the test section. The film thickness in each experiment is measured via conductance probes and is then averaged in time, space, or both. The average film thickness value is reported. The boundary conditions and data reported are modeled using the method previously discussed in this section.

Co-current Flow Validation

Each set of experimental data is characterized by the parameters specified in Table 3.1 (the pressure for each experiment is one atmosphere unless noted.) Data points are characterized by experimental facility, fluid properties, and prescribed pairs of liquid and gas flow rates. Many values in Table 3.1 are from the source reference literature, though liquid and gas flow rates have been recast as superficial velocities for the purpose of this analysis, and the densities for MacGillivray [51] and Wolf, Jayanti, and Hewitt [52] and liquid viscosity for the latter work were found by using EES [53]. The validation is performed by calculating the film thickness for a given system using both the Wallis and the new models, and then comparing these results to the film thickness reported from each experiment. The results are quantitatively assessed with the following equation:

$$\sigma_{\text{model}} = \sqrt{\frac{\sum_{i=1}^{N} \left(\frac{\delta_{\text{model}}}{\delta_{\text{exp}}} - 1 \right)_i^2}{N-1}}, \tag{3.19}$$

where σ_{model} is the standard deviation for results of a given model, N is the number of points analyzed, δ_{model} is the film thickness calculated by the model (either Wallis or the "New Model" developed in this work), and δ_{exp} is the film thickness reported

from the experiment. The significance of this standard deviation, σ_{model}, is that this standard deviation quantifies the magnitude of relative error for a specific model calculated using the experimental and calculated film thicknesses. In other words, if a group of calculations is performed and a standard deviation for model x is calculated, σ_x, Chebyshev's inequality [54], among other methods, can be used to quantify how many points of data must fall within $\pm\sigma_x$ (calculated as a percentage) of the film thickness reported from experimentation, δ_{exp}.

The quantitative results calculated using Equation 3.19 are shown in Table 3.2. The standard deviation calculated for each set of data is similar in most cases, and, as such, one value is reported per literature source. Error is only given in the reference literature for the data of MacGillivray [51]. This error is reported to be 0.104 mm for each data point, which is quite large as this value is approximately 50% of most of the data presented.

The data provided by Wolf, Jayanti, and Hewitt [52] is reported at seven points along the tube, with data taken at 0.05 m, 0.25 m, 0.44 m, 0.94 m, 1.07 m, 3.85 m, and 10.4 m from the tube inlet, with the gradient in film height shown to be as large as 0.017 mm/m. As the liquid film flows down the tube, overall film thickness changes due to inlet and outlet effects of both fluids, as well as an increase in momentum due to shear forces and gravity. The calculated film thicknesses for this data set were compared to data from 0.94 m downstream of the liquid inlet, which is located at $L/D \approx 30$. Film thickness values reported at 0.94 m are similar to those at 1.07 m from the tube inlet, and the axial location at 0.94 m are significantly closer to the length of most experimental flooding test sections than the next data point at 3.85 m.

Figures 3.2, 3.3, 3.4, 3.5, 3.6, and 3.7 show the major qualitative trends for each set of experimental data. A plot of all points analyzed is given as Figure 3.8. While Table 3.2 and the aforementioned figures show a general improvement in film thickness prediction by an order of magnitude, investigation of the qualitative and quantitative

Table 3.1
Experimental parameters for co-current validation data.

Study	Working Fluids	Tube I.D. (mm)	j_f (m/s)	j_g (m/s)	ρ_f (kg/m^3)	ρ_g (kg/m^3)	μ_f (kPa $\cdot$ s)
Asali	air-water	42.0	$0.00076 - 0.11269$	$10.1 - 59.9$	990	1.28	1.1
	air-glyc. solution	42.0	$0.0028 - 0.0288$	$34.0 - 141.8$	1056	1.28	2.1
	air-glyc. solution	42.0	$0.0026 - 0.0475$	$20.3 - 49.1$	1120	1.28	5.3
	air-water	22.9	$0.0116 - 0.1276$	$25.6 - 96.0$	990	1.28	1.1
	air-water ($P = 2$atm)	42.0	$0.0002 - 0.0047$	$0.84 - 1.34$	990	2.34	1.1
	air-glyc. solution	42.0	$0.0120 - 0.1035$	$36.5 - 55.7$	1056	1.28	2.59
Fore and	air-water	50.8	$0.00001 - 0.00012$	$36.5 - 55.7$	999	1.27	1
Dukler	air-glyc. solution	50.8	$0.006 - 0.057$	$15.8 - 34.1$	1128	1.27	6
MacGillivray	air-water	9.525	$0.076 - 0.315$	$13.0 - 29.4$	998.2	1.306	1
	helium-water	9.525	$0.098 - 0.312$	$22.2 - 62.4$	998.3	0.2267	1
Wolf, Jayanti, and Hewitt	air-water	31.8	$0.01 - 0.122$	$25.5 - 55.4$	977.1	2.781	0.89

Table 3.2
Comparison of film thickness model performance.

Study	No. of points	σ_{Wallis} (%)	$\sigma_{\text{New Model}}$ (%)	Figure(s)
Asali	182	290	58	3.2
Fore and Dukler	65	40	48	3.3, 3.4
MacGillivray	328	124	18	3.5, 3.6
Wolf, Jayanti, and Hewitt	28	191	14	3.7
All co-current cases	603	188	38	3.8
Lacy	21	10 to 23	22 to 49	3.14, 3.15

results shows that the new model appears to perform poorly in the prediction of average film thicknesses for a subset of data from Asali [49], as well as the data presented by Fore and Dukler [50]. A majority of the results that have been calculated for the previously presented experimental data is similar to Figure 3.9 in that the new model appears to clearly outperform the model posed by Wallis. Three specific groups of film thickness data from Asali [49], for which $j_g = 13.8\text{ m/s}, 20.3\text{ m/s}, 20.3\text{ m/s}$, respectively, in 0.042 m tubes with air and water at atmospheric pressure, are incorrectly predicted by the new model and overpredicted by Wallis' model in such a way that the standard deviation between the two models and experimental data implies that the Wallis model better predicts the liquid film thickness. The cases can be characterized as having low liquid and gas superficial velocities when compared to the rest of the data provided by Asali, and comparisons of the experimental data and predicted film thickness are shown in Figures 3.10, 3.11, and 3.12. The spectrum of cases analyzed by Fore and Dukler [50], represented by the specific case shown in Figure 3.13, poorly predict experimental data at low gas flow rates, but significantly improve for higher gas superficial velocities. This is true for both the air-water and air-glycerine solution experimental results reported by Fore and Dukler. This dis-

crepancy can be explained by considering the fact that the Wallis interfacial friction factor correlation, Equation 3.14, is valid for rough, wavy films [35], which tend not to form at low flow rates. This limitation of the Wallis correlation is for the particular situation of low gas flow rates, which should not be of concern in near-flooding counter-current flow systems.

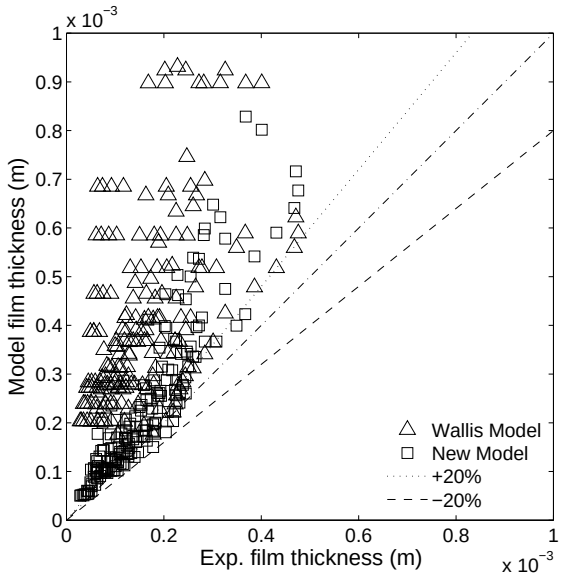

Fig. 3.2. Average film thicknesses for Asali [49].

Counter-current Flow Validation

Data reported by Lacy [48] includes film thickness measurements for air-water counter-current flow in a 55.8 mm tube. Liquid was introduced to the test section via a "feed section," and film thicknesses were measured at points above, inside, and below this feed section. The new model can be used to calculate film thickness in the region below the feed, which is downstream of the gas inlet.

As these experiments are conducted by varying gas flow rates to co-current and post-flooding conditions at five predetermined liquid flow rates, a total of 21 exper-

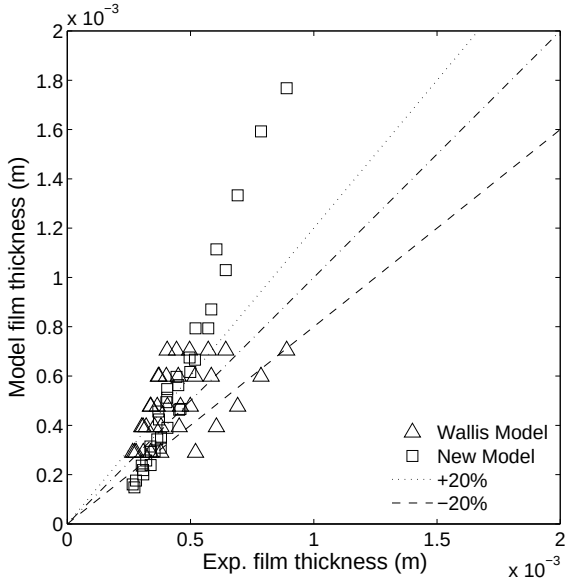

Fig. 3.3. Average film thicknesses for Fore and Dukler [50] (air-water cases).

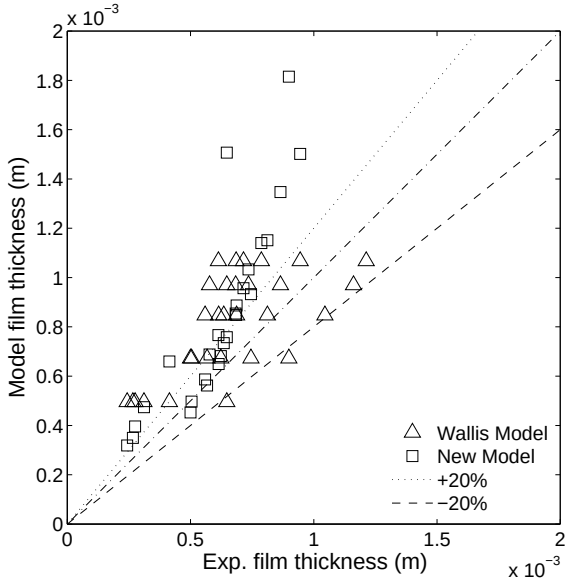

Fig. 3.4. Average film thicknesses for Fore and Dukler [50] (air-water/glyc. cases).

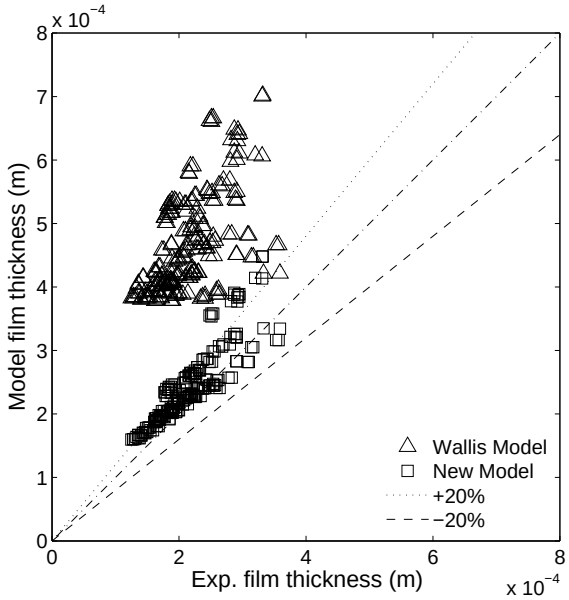

Fig. 3.5. Average film thicknesses for MacGillivray [51] (air-water cases).

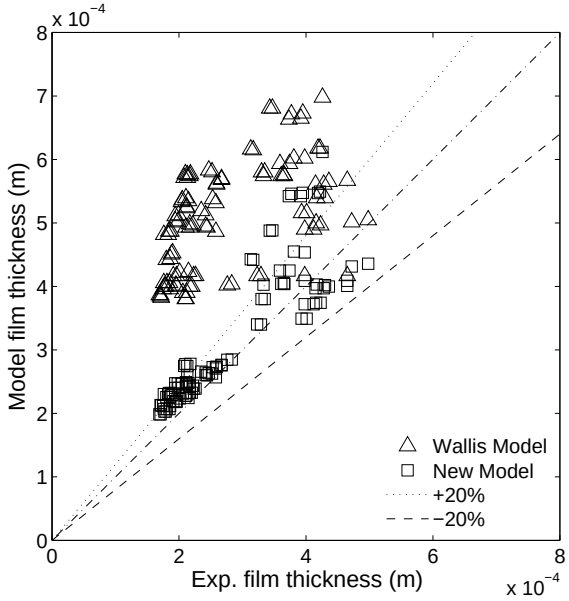

Fig. 3.6. Average film thicknesses for MacGillivray [51] (helium-water cases).

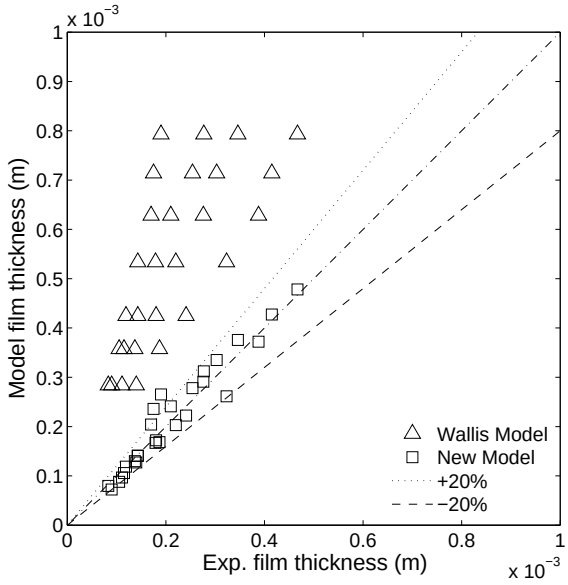

Fig. 3.7. Average film thicknesses for Wolf, Jayanti, and Hewitt [52].

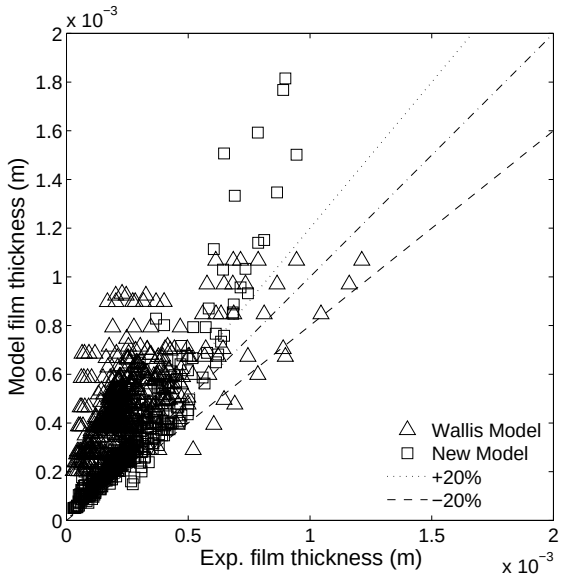

Fig. 3.8. Average film thicknesses for all validation data.

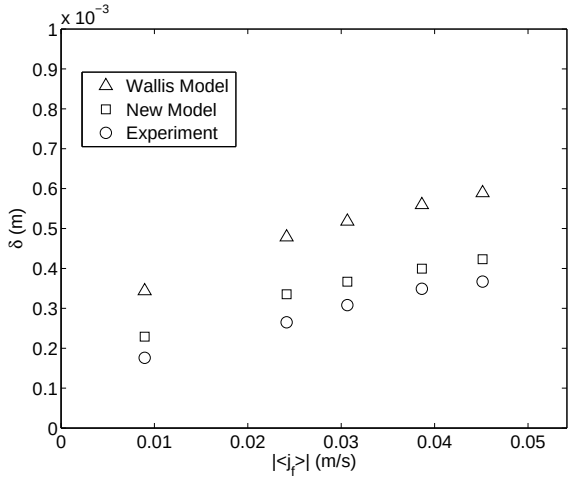

Fig. 3.9. Typical analysis of the data of Asali ($j_g = 29.8$ m/s).

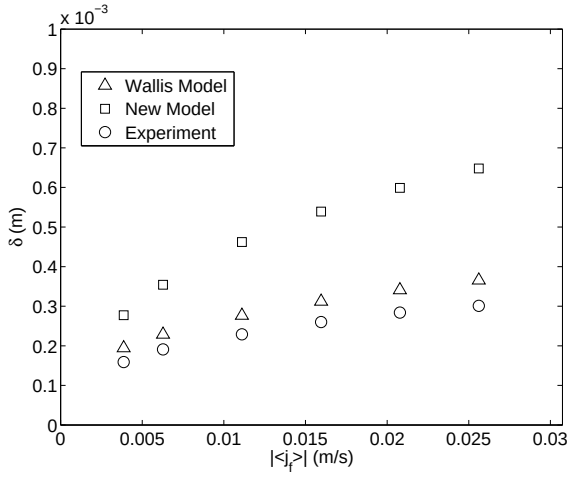

Fig. 3.10. Overpredicted subset of the data of Asali ($j_g = 13.8$ m/s).

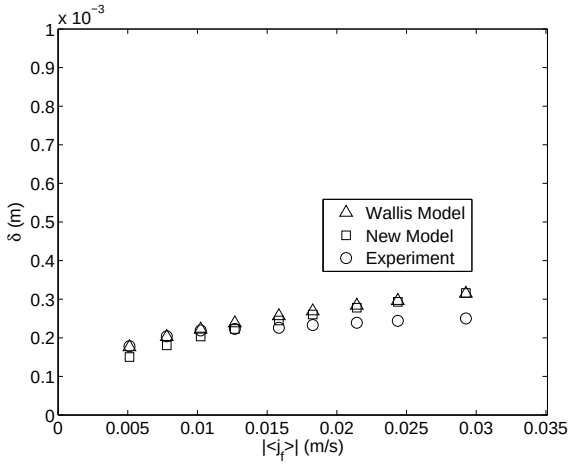

Fig. 3.11. Overpredicted subset of the data of Asali ($j_g = 20.3$ m/s, first case).

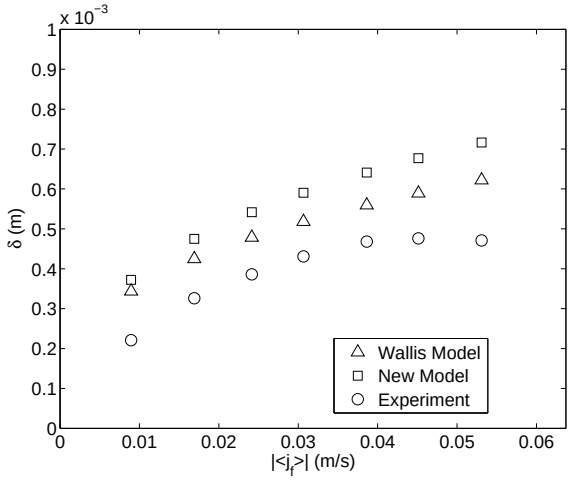

Fig. 3.12. Overpredicted subset of the data of Asali ($j_g = 20.3$ m/s, second case).

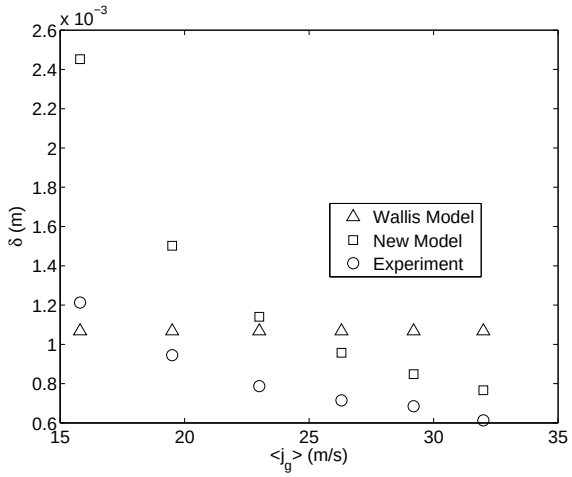

Fig. 3.13. Typical analysis of the data of Fore and Dukler (j_f = 0.059 m/s, air-glyc. solution).

imental data points are considered to be usable as validation data for the annular film thickness model. Specifically, the liquid flow superficial velocities of the points considered range from 0.006 m/s to 0.062 m/s and the gas superficial velocities from 7.6 m/s to 14.8 m/s. The film thicknesses are measured using conductivity probes and are reported at distances of 0.07 m, 0.12 m, 1.74 m, and 1.79 m below the liquid feed of Lacy's test section. Error on measured values is not reported.

Liquid film thicknesses for Lacy's test section are predicted using the new model for average annular film thickness. Qualitative results of this analysis are shown in Figure 3.14, and numerical results of the validation with Lacy's data are presented on Table 3.2. From Figure 3.14 it can be seen that while the model presented by Wallis [11] tends to underpredict the liquid film thickness, the new model tends to overpredict the film thickness. This comparison uses the measurements taken at the conductivity probe 1.74 m from the liquid inlet. The quantitative analysis is summarized by the values given in Table 3.2. A qualitative result given in Figure 3.15 shows that the deviation from experimental data for each model appears to be on the same order of magnitude. While there is a clear discrepancy between the experimental data and the film thickness values predicted by the new model, it can be noted that the results of the Wallis model shown in Figure 3.15 are relatively constant for each gas flow rate, while the new model is predicting a trend more similar to the trend of the experimental data. The lack of significant improvement in predictive capability of the new model for average film thickness is unexpected considering the improvement shown in a majority of the co-current film thickness calculations. It is hypothesized that the limited test section length allowed the film thickness to be affected by inlet and outlet conditions along the entire length of the tube, thereby decreasing the accuracy of both models. Further analysis and validation using additional counter-current film thickness data is necessary to determine whether the new model is applicable for the predicition of average annular film thickness when compared to the model presented by Wallis.

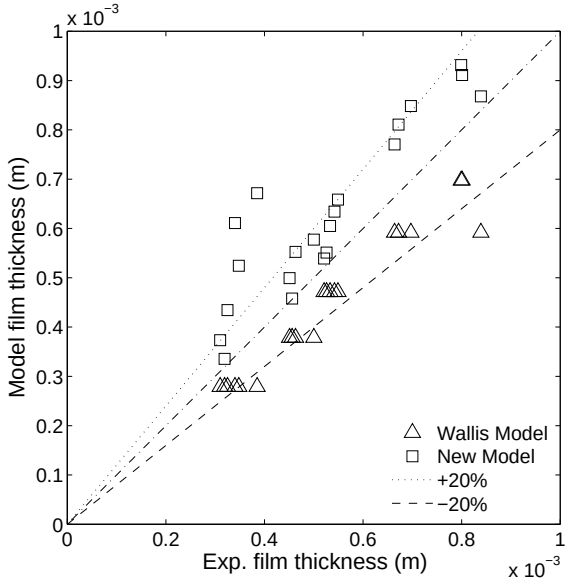

Fig. 3.14. Average film thicknesses for Lacy [48].

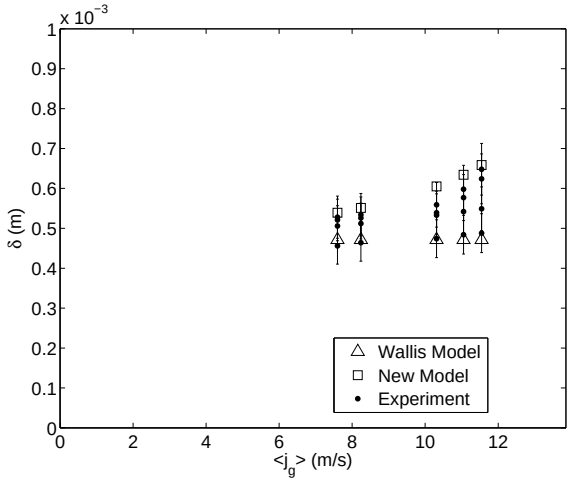

Fig. 3.15. Typical analysis of the data of Lacy ($j_f = 0.031$ m/s).

Results of New Film Thickness Model

Overall performance of the new model for the prediction of average annular film thickness appears to be significantly better than the results of the model posed by Wallis [11] based on the work of Nusselt [42] and Belkin, Macleod, Monrad, and Rothfus [43]. While the new model does not correctly predict the film thickness for low gas flow rates, this is consistent with the underlying assumptions inherent in the closure relations to the model. At this time, it is apparent that the new model provides a reasonable prediction of counter-current film thicknesses, though the quantitative improvement shown in the co-current cases is not present. This may be a function of the limited counter-current film thickness data used in this validation. Future work should include the procurement of additional counter-current annular flow data that could be used to assess the performance of the model, specifically for the application of predicting flooding, as well as possibly testing the formulation with a variety of closure relations posed by other researchers.

4. THEORETICAL ANALYSIS OF FLOODING

It is well known that one-dimensional drift-flux models using empirical or semi-empirical closure relations for the distribution parameter and drift velocity can be used to predict flooding [2, 11, 40]. These drift-flux models are based on the Zuber-Findlay relationship for the gas superficial velocity of the flow [41]. To develop a model based on this relationship, closure relations that rely on data from flooding experiments have been used in previous work. For example, Ohkawa and Lahey [40] used the semi-empirical Kutateladze correlation in terms of the liquid and gas superficial velocities with empirical closure relations based on experimental data. While correlations based on the drift-flux model qualitatively can be used to predict flooding, closure relations based on data that consider the occurrence of flooding, as opposed to the flow conditions that can lead to flooding, seem to be more dependent on fitting data than mechanistically capturing relevant phenomena. In this section, the work of Ohkawa and Lahey [40] will be used in conjunction with the previous model for liquid film thickness to analyze the mechanism of flooding.

4.1 Model Development

Using the Zuber-Findlay relationship, Ohkawa and Lahey [40] found that the gas superficial velocity that causes flooding for a given liquid superficial velocity can be found by satisfying the equation

$$\left.\frac{\partial j_g}{\partial \alpha_g}\right|_{j_f} = 0. \tag{4.1}$$

According to this equation, the superficial velocity of the gas that will cause flooding is the maximum value of the gas superficial velocity with respect to the void fraction for a constant liquid superficial velocity. Therefore, if the gas superficial velocity can be calculated as a function of the liquid superficial velocity and the void fraction, a plot representing the superficial velocities that cause flooding for a given

system can be generated. Using the above criteria for flooding, it should be possible to generate a flooding curve for a given system using the mass and momentum conservation equations obtained from the one-dimensional drift-flux model as well as the appropriate closure relations for this model [35].

A model of flooding based on Equation 4.1 can be developed by considering the following system of equations developed in Section 3.2:

$$\rho_g g_z - \rho_f g_z = \frac{\tau_{wf} P_{wf}}{(1 - \langle \alpha_g \rangle) A} - \frac{\tau_i P_i}{(1 - \langle \alpha_g \rangle) A} - \frac{\tau_i P_i}{\langle \alpha_g \rangle A} \tag{3.9}$$

$$\tau_{wf} = \frac{f_{wf} \rho_f \langle \langle v_f \rangle \rangle |\langle \langle v_f \rangle \rangle|}{2} - \frac{\Delta \rho g_z \delta}{3} \tag{3.10}$$

$$f_{wf} = \frac{16}{Re_f} \tag{3.11}$$

$$\frac{1}{\sqrt{4 f_{wf}}} = -2 \log \left(\frac{\epsilon}{3.7 D} + \frac{2.51}{\mathrm{Re}_f \sqrt{4 f_{wf}}} \right). \tag{3.5}$$

$$\delta = \frac{1}{2} \left(1 - \sqrt{\alpha_g} \right) D \tag{3.12}$$

$$\tau_i = \frac{f_i \rho_g |\overline{v_r}| \overline{v_r}}{2} \tag{3.13}$$

$$f_i = 0.005 \left[1 + 75 \left(1 - \langle \alpha_g \rangle \right) \right] \tag{3.14}$$

$$\overline{v_r} = \frac{\langle \langle v_g \rangle \rangle - \langle j \rangle}{1 - \langle \alpha_g \rangle} \tag{3.17}$$

$$P_i = (D - 2\delta) \pi. \tag{3.18}$$

Using this system of equations, a relationship between the gas superficial velocity, the liquid superficial velocity, and the void fraction can be determined. In order to use Equation 4.1 to determine the conditions necessary to cause flooding, a liquid flow rate for a specific system must be determined. Discrete values of the void fraction (α_g) between 0 and 1 can be selected, and the system of equations can be solved for each discretized value of α_g. A physical interpretation of Equation 4.1 would imply that flooding for a given system with a known liquid superficial velocity of j_f would occur when the value of j_g, the superficial velocity of the gas, is at a maximum with respect to the void fraction, α_g. Using this methodology, the flooding conditions for the system can be determined.

4.2 Analysis

A qualitative three dimensional plot showing the superficial gas velocity as a function of the void fraction and the liquid superficial velocity is shown in Figure 4.1. The behavior exhibited by this surface is qualitatively similar to the surface given by Ohkawa and Lahey [40], Figure 4.2, for drift-flux models of flooding. Figure 4.2 shows the superficial gas velocity derived using the Zuber-Findlay relationship and closure relations for the distribution parameter and drift velocity. Figure 4.3 shows a qualitative flooding curve generated from the solution of Equation 3.9. This curve is consistent with both previous analyses and experimental data. Therefore, using a model based on the one-dimensional Zuber-Findlay drift-flux relationship and a model based on the one-dimensional drift-flux momentum equation, both based on the superficial velocity of each phase, similar behavior of both the surface describing the gas superficial velocity and the flooding curve can be generated.

Despite these similarities, the value of the gas superficial velocity found by considering the conservation of momentum to cause flooding overestimates the experimentally found gas superficial velocities, but generally by no more than a factor of three. When compared to experimental flooding data for an adiabatic, vertical test section, the model based on the conservation of momentum overpredicts the superficial gas velocity. This is illustrated using experimental data from Williams [55] and Tien, Chung, and Liu [56]. Both sets of flooding data are based on experimental facilities that use liquid injection methods to induce vertical adiabatic counter-current flows. (These experiments will be discussed in more detail in Section 6.2.) A comparison of predicted flooding conditions and experimental data of Williams [55] and Tien, Chung, and Liu [56] is shown in Figure 4.4 and Figure 4.5. As dimensionless superficial velocities have been shown to correlate poorly to experimental data [7], the results are also presented in terms of the liquid and gas superficial velocities as Figure 4.6 and Figure 4.7. Figures 4.4 and 4.6 show comparisons between the flooding conditions predicted by Equations 3.9 and 4.1 and the data of Williams [55], which

is based on an air-water countercurrent flow in a 76.2mm inner diameter tube. Figures 4.5 and 4.7 compare the results of Equations 3.9 and 4.1 with data from Tien, Chung, and Liu [56]. The experimental setup that generated the Tien, Chung, and Liu data consisted of fluids of various properties in 16 $-$70 mm inner diameter tubes. This data set was selected because data from this experiment spans several tube and fluid property combinations. It should be noted that not all data from Tien, Chung, and Liu [56] has been analyzed in Figures 4.5 and 4.7. Additionally, the spread of the experimental data of Tien, Chung, and Liu [56] when recast as the Wallis parameter implies that this data may be of questionable quality; this issue will be addressed in Section 6.2. This shows that Equation 4.1 also overpredicts the gas superficial velocity that will cause flooding when compared to data that has been demonstrated to be reproducible. In summary, it is noted that using a momentum-based approach to model flooding overpredicts the gas flow rate that will cause flooding to occur for a specified liquid flow rate.

Modeling flooding using the one-dimensional drift-flux momentum equations with closure relations that are not curve-fit to experimental flooding data should create an accurate flooding curve if Equation 4.1 is satisfied. Since the one-dimensional drift-flux momentum equations are derived from physics, the closure relations are known to model both co-current and countercurrent annular flow reasonably well. Further, Equation 4.1 has been shown to predict flooding. Therefore, it can be inferred that additional phenomena that are not currently considered in the momentum balance are affecting the flow.

4.3 Discussion

The quantitative discrepancies and qualitative similarities between this model based on conservation of the liquid and gas momentum and models that utilize the distribution parameter and drift velocity as closure relations suggest that there is a fundamental difference in the closure relations used in both models and this difference

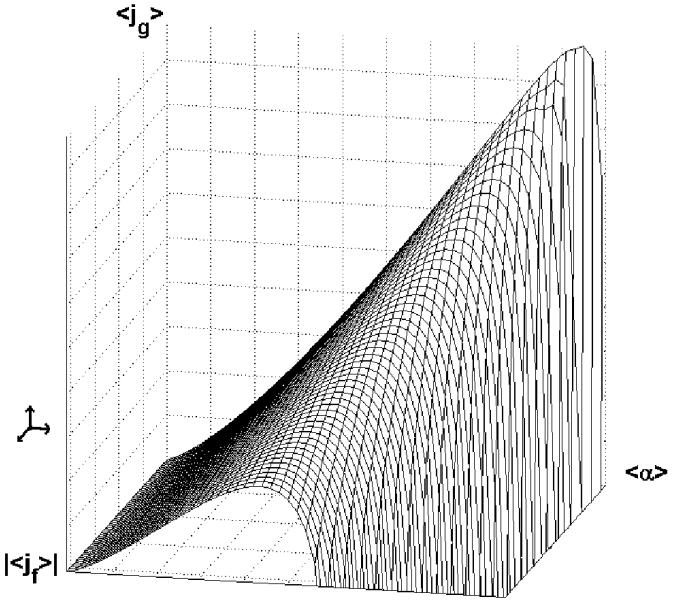

Fig. 4.1. Gas superficial velocity in terms of the liquid superficial velocity and the void fraction.

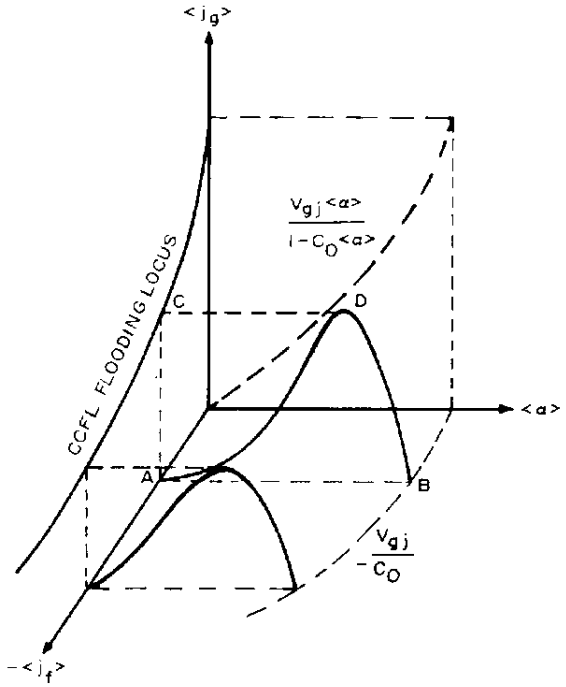

Fig. 4.2. Qualitative plot of drift-flux models of flooding (from Okawa and Lahey [40]).

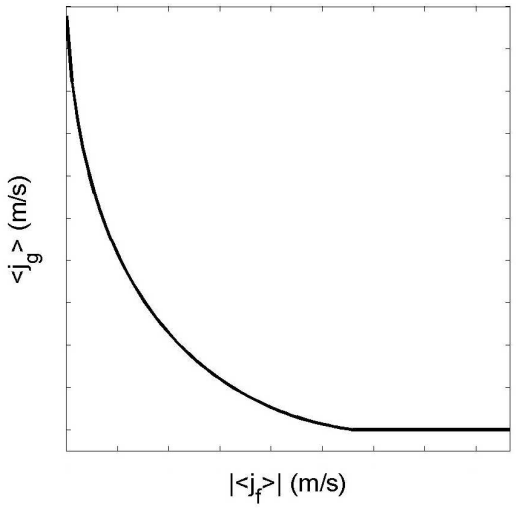

Fig. 4.3. Qualitative flooding curve based on the new model.

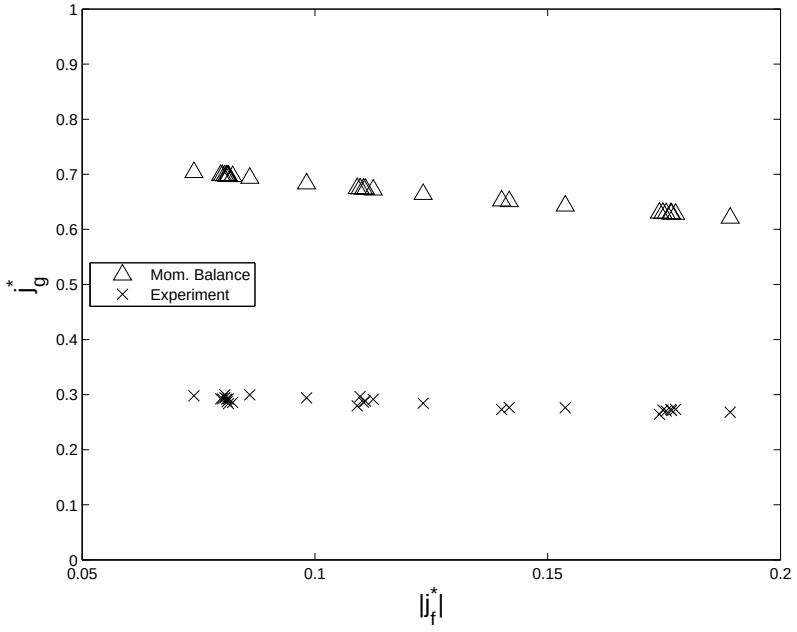

Fig. 4.4. Comparison between Williams' air-water data [55] and momentum-based model of Wallis parameters for flooding.

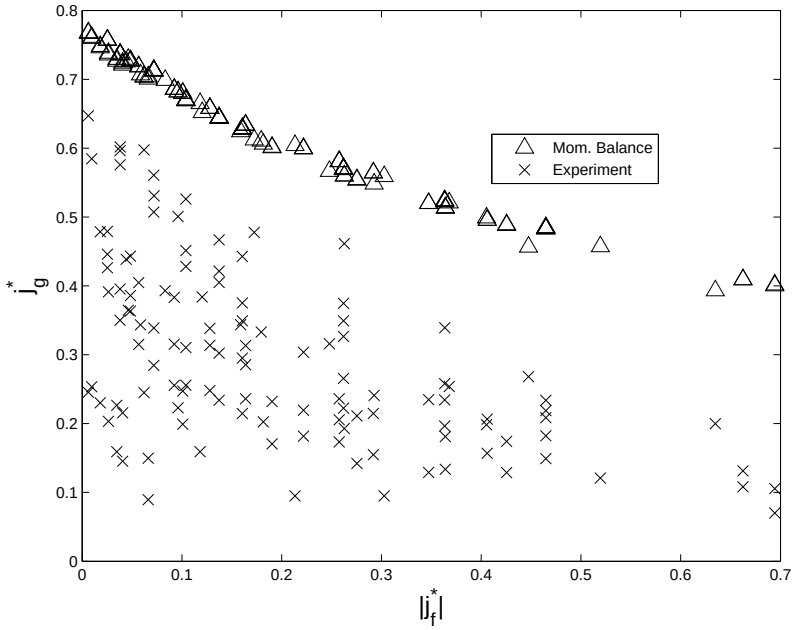

Fig. 4.5. Comparison between Tien, Chung, and Liu's data [56] and momentum-based model of Wallis parameters for flooding .

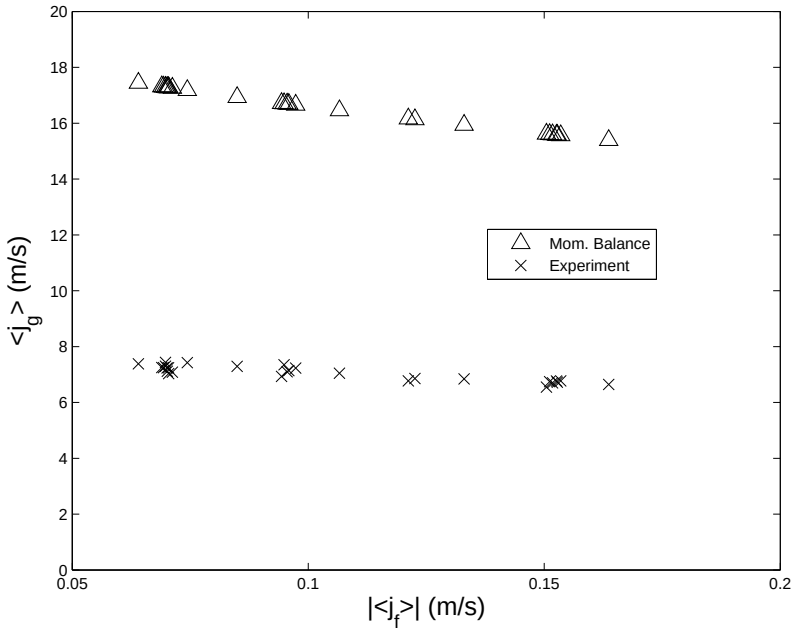

Fig. 4.6. Comparison between Williams' air-water data [55] and momentum-based model of superficial velocities for flooding.

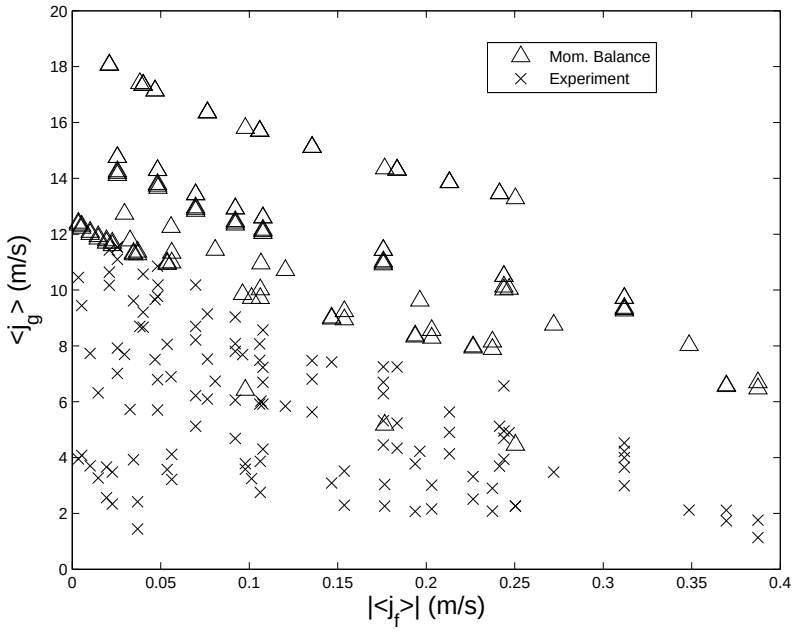

Fig. 4.7. Comparison between Tien, Chung, and Liu's data [56] and momentum-based model of superficial velocities for flooding.

may be obscured by the empirical factors used in models based on the Zuber-Findlay relationship. It is known from experimental observations that when flooding occurs, a fast-growing wave appears at the gas-liquid interface. Several stability analyses have been performed on gas-liquid countercurrent flow systems, and they have shown that if this instability is a Kelvin-Helmholtz or similar instability [35,57,58], the wave will grow radially inward from the liquid film as a uniform circle of fluid. Following this wave growth, the local cross-sectional void fraction will be significantly smaller than the void fraction that arises from a pure conservation of momentum. This change in void fraction would instantaneously change the value of all of the closure relations that depend on the film thickness.

In Figure 4.8, the gas superficial velocity is plotted with respect to the void fraction for a specified liquid superficial velocity. By using Equation 4.1 and the model developed above, the gas superficial velocity that will cause flooding due to the conservation of momentum and the previously discussed closure relations is located at the maximum value of the gas superficial velocity on the curve. A system with a gas superficial velocity and void fraction located at point "A" could exist in a stable counter-current flow pattern. If this system is operating at a constant liquid superficial velocity and an instability causes significant interfacial wave growth, the flow would be represented by point "B" in Figure 4.8. The void fraction in the channel has decreased while maintaining the same gas superficial velocity. This point is now located above the curve, whereas before this wave growth occurred, the flow parameters would have matched that of "A" and been located on the curve. The reduction of void fraction does not allow for the gas and liquid superficial velocities that are specified, resulting in the reversal of flow in order to conserve momentum. Using this principle, it may be possible to predict the occurrence of flooding both by considering the momentum balance of the gas and liquid and by evaluating the stability of the gas-liquid interface. Therefore, the development of a model for the

prediction of the onset of the interfacial instability could enable the prediction of the occurence of flooding.

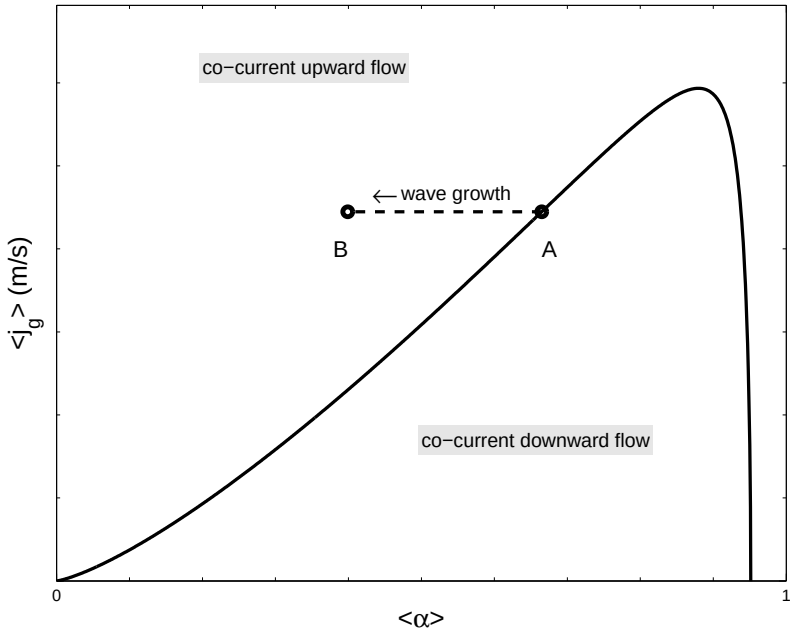

Fig. 4.8. Superficial gas velocity versus void fraction for a specific liquid flow rate.

5. STABILITY-BASED MODEL OF FLOODING

Section 4 described a theory on the mechanism that causes flooding. This theory maintains that flooding occurs so that momentum is conserved following the growth of large-amplitude waves at the gas-liquid interface. In order to predict the occurence of flooding, the criteria for the growth of this wave should be analytically derived.

If the counter-current annular flow pattern is considered to be a cylinder of gas surrounded by an annulus of water, it should be possible to extend Rayleigh's [57,59] work on the vibrations of cylindrical jets. (It should be noted here that the word "jet" refers to the cylindrical gas flow, as opposed to its common usage.) The stability criteria that Rayleigh developed were previously used for Zuber's [60] analysis of critical heat flux. Zuber [60] and Wallis [9] noted the hydrodynamic similarities between flooding and the work of Rayleigh, and hypothesized that a model of this type could be applied to flooding. While Rayleigh derived his model by assuming that the pressure change due to fluid, the Bernoulli effect, is negligible due to near-zero fluid velocities in the overall system being analyzed, the relative motion between the liquid and gas flow should have a significant destabilizing effect in flooding. The model for wave growth proposed herein will only be valid for vertical, counter-current annular flows and will not directly account for inlet and outlet effects, but the success of an analytical approach should provide a theoretical basis for analysis of other scenarios where flooding may occur.

5.1 Previous Work

Bankoff [2] categorized potential flow models of flooding as stability theories of a traveling wave. These potential flow models are used to calculate flooding criteria based on interfacial instability. These models tend to be analogous to slugging models, such as Mishima and Ishii's [61] model of slugging in a rectangular duct

and Georgevich's [62] integral approach to predict interfacial wave growth due to instability.

Models that fit into the category of potential flow models include Imura, Kusada, and Funatsu [63], Chung, Liu, and Tien [38], Yao and Sun [64], and Shibata and Kaminaga [65]. Each of these models employs assumptions that are not consistent with the physics of flooding [2]. The model developed by Imura, Kusada, and Funatsu [63] relies on an empirical correlation for the mean film thickness and the dimensionless wave number. In their model, Chung, Liu, and Tien [39] neglected the flow pattern and the curvature of the tube. Closure relations for this model are a function of the wave number, which makes their correlation empirical in this regard. Yao and Sun [64] define flooding as the conditions at which partial delivery has ceased. This is not a conservative assumption when analyzing flooding in nuclear reactors. Yao and Sun also use a simplified dynamic interface condition that is not representative of the shape of the interface. The analyses of Imura, Kusada, and Funatsu, Tien, Chung, and Lei, and Yao and Sun all rely on linearized kinematic conditions at the gas-liquid interface. None of the models consider the appropriate form of the solution of the governing differential equation with respect to boundary conditions. Shibata and Kaminaga [65] compared linear and non-linear wave models at the interface and found that the non-linear condition yields a better result when compared to experimental data. The model Shibata derived from non-linear analysis is in rectangular coordinates and does not capture the unique mathematical properties of stability analysis on cylinders. Both the stability analysis of a stationary jet (Rayleigh, 1878) and the analysis of Imura, Kusada, and Funatsu [63] find that the stability criteria of cylindrical systems are expressed in terms of modified Bessel functions, which do not arise from stability analysis in a rectangular plane. The model based on the non-linear analysis of Shibata consists of many terms and is not convenient to solve.

Previous work indicates that a comprehensive physics-based model for the prediction of flooding in vertical adiabatic tubes based on stability criteria should consider phenomena in a cylindrical coordinate system, account for curvature of the interface, use non-linear kinematic conditions and not require empirical closure relations. The development of this stability-based model would allow for the prediction of flooding based on the premise that flooding is caused by the need for momentum of the liquid and gas flows to be conserved. A change of the void fraction in the system affects the closure relations of this momentum balance by reducing the flow area of the gas, increasing the flow area of the liquid, and reducing the interfacial area between the fluids.

5.2 Model Development

The stability-based model of flooding is developed using the following procedure:

1. develop the potential functions of the liquid and gas flow
2. determine the interfacial fluid pressures from the fluid potential functions
3. relate the interfacial fluid pressures using the Young-Laplace equation
4. solve the Young-Laplace equation for the wave speed
5. derive stability criteria as when the wave speed contains an imaginary component
6. provide closure for the unknown wave number in the stability criteria

5.2.1 Calculation of Fluid Potential

The cylindrical coordinate system presented in Section 3.2 is used to derive the model of stability criteria. The liquid, "f", flows downward in an annulus around

the gas core, "g." The film thickness at that axial level, δ, can be used to find the radius at a specific axial location of the gas core, a, by substracting the film thickness from the radius of the tube, R. The gravitational force acts downward, parallel to both flows.

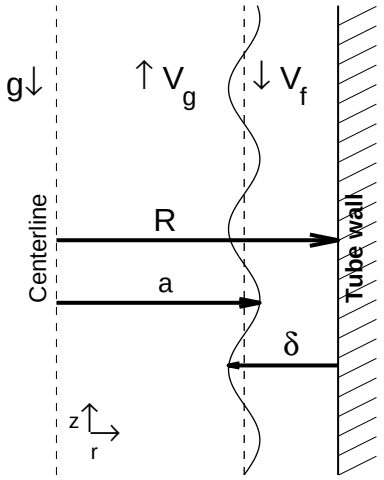

Fig. 5.1. Cylindrical coordinate system (not to scale).

To begin the stability analysis, the continuity equation for phase k is

$$\frac{\partial \rho_k}{\partial t} + \nabla \cdot \rho_k \vec{v}_k = 0. \tag{5.1}$$

In an adiabatic system, the flow can be assumed to be incompressible. Therefore,

$$\nabla \cdot \vec{v}_k = 0 \tag{5.2a}$$

$$\frac{1}{r}\frac{\partial \left(r v_{kr}\right)}{\partial r} + \frac{1}{r}\frac{\partial v_{k\theta}}{\partial \theta} + \frac{\partial v_{kz}}{\partial z} = 0. \tag{5.2b}$$

By making the additional assumptions that the fluid is inviscid and irrotational, potential flow theory may be used. The definitions of the radial, azimuthal, and longitudinal velocities in terms of the velocity potential of each phase [44], ϕ_k, are

$$v_{kr} = -\frac{\partial \phi_k}{\partial r} \tag{5.3a}$$

$$v_{kz} = -\frac{\partial \phi_k}{\partial z} \tag{5.3b}$$

$$v_{k\theta} = -\frac{1}{r}\frac{\partial \phi_k}{\partial \theta}. \tag{5.3c}$$

Substituting Equation 5.3 into 5.2 yields the continuity equation for potential flow,

$$\nabla^2 \phi_k = 0 \tag{5.4a}$$

$$\frac{\partial^2 \phi_k}{\partial z^2} + \frac{\partial^2 \phi_k}{\partial r^2} + \frac{1}{r}\frac{\partial \phi_k}{\partial r} + \frac{1}{r^2}\frac{\partial^2 \phi_k}{\partial \theta^2} = 0. \tag{5.4b}$$

The potential of each fluid, ϕ_k, can be written as

$$\phi_k = \Phi_{1,k} e^{ik(z-ct)} - U_k z \tag{5.5}$$

where k in the exponential is the wave number, z is the axial position, c is the wave speed, t is time, and i is equal to $\sqrt{-1}$. The exponential term accounts for the motion of a wave within the flow in space and time, and the rightmost velocity term accounts for the initial velocity of the fluid. It should be noted that this rightmost velocity term is a linear function of z, and the second derivative of this term with respect to z must be zero. The term $\Phi_{1,k} = \Phi_{1,k}(r, \theta)$ satisfies the initial conditions of the partial differential equation. Substituting Equation 5.5 into Equation 5.4 results in a differential equation for $\Phi_{1,k}$,

$$\begin{aligned} 0 = &- k^2 \Phi_{1,k} e^{ik(z-ct)} \\ &+ \frac{\partial^2 \Phi_{1,k}}{\partial \theta^2} e^{ik(z-ct)} \\ &+ \frac{1}{r}\frac{\partial \Phi_{1,k}}{\partial r} e^{ik(z-ct)} \\ &+ \frac{1}{r^2}\frac{\partial^2 \Phi_{1,k}}{\partial \theta^2} e^{ik(z-ct)}, \end{aligned} \tag{5.6}$$

which can be reduced to form the equation

$$\frac{\partial^2 \Phi_{1,k}}{\partial r^2} + \frac{1}{r}\frac{\partial \Phi_{1,k}}{\partial r} + \frac{1}{r^2}\frac{\partial^2 \Phi_{1,k}}{\partial \theta^2} - \Phi_{1,k}k^2 = 0. \tag{5.7}$$

Equation 5.7 is similar to the modified Bessel differential equation, but in cylindrical coordinates. The general solution to this equation is

$$\Phi_{1,k} = A_{1,k} I_s(kr)\cos(s\theta) + A_{2,k} K_s(kr)\cos(s\theta) \tag{5.8}$$

where $A_{1,k}$ and $A_{2,k}$ are constants determined by boundary conditions, I_s is the modified Bessel function of the first kind of order s and K_s is the modified Bessel function of the second kind of order s (see Appendix A).

5.2.2 Interfacial Liquid Pressure

For the liquid component of the potential, ϕ_f, one of the boundary conditions is that the radial velocity must be zero at the wall, or where $r = R$. In terms of the potential, this means

$$-\frac{\partial \phi_f(R)}{\partial r} = 0 \tag{5.9}$$

and because ϕ_k is a separable function (as per Equation 5.5) that can be defined $\phi_k = \Phi_{1,k} f(z,t)$, the following equation is equivalent to Equation 5.9:

$$-\frac{\partial \Phi_{1,f}(R)}{\partial r} = 0. \tag{5.10}$$

The solution to Equation 5.8 that meets the boundary condition posed by Equation 5.10 is not trivial and is not readily presented in previous literature. This solution can be found by rewriting Equation 5.8 as

$$\Phi_{1,k} = B_f\big(C_1 I_s(kr)\cos(s\theta) + C_2 K_s(kr)\cos(s\theta)\big) \tag{5.11}$$

where $A_{1,f} = B_f C_1$ and $A_{2,f} = B_f C_2$. Writing Equation 5.8 in this manner allows for B_f to satisfy the boundary condition at the gas-liquid interface and C_1 and C_2 to satisfy the boundary condition at the tube wall.

A solution to Equation 5.11 that satisfies the boundary condition posed by Equation 5.10 can be shown to be (see Appendix B)

$$C_1 = \frac{1}{\left(I_{s+1}(kR) + \dfrac{sI_s\left(kR\right)}{kR}\right)} \tag{5.12a}$$

$$C_2 = \frac{-1}{\left(-K_{s+1}(kR) + \dfrac{sK_s\left(kR\right)}{kR}\right)}. \tag{5.12b}$$

The boundary condition for the liquid at the gas-liquid interface is

$$-\frac{\partial \phi_g}{\partial r} = \frac{\partial \eta}{\partial t} + U_g \frac{\partial \eta}{\partial z}. \tag{5.13}$$

The parameter η represents the radial position of the single wave that exists at the gas-liquid interface and is defined as

$$\eta = \eta_0 e^{ik(z-ct)} \cos\left(s\theta\right) + \bar{a} \tag{5.14}$$

where $\bar{a}$ is the time-average distance from the center of the gas core to the interface. The axial location is given by the parameter z, time is represented by t, and the wave speed is defined by c. The wave number, k, is related to the wavelength, λ, by $k = 2\pi/\lambda$. The distance between the tube centerline and the gas-liquid interface is $a\left(z\right)$, which is equal to η for the wave which is defined by Equation 5.14. The boundary condition given by Equation 5.13 requires that the radial velocity, $-\dfrac{\partial \phi_k}{\partial r}$, must equal the change in the wave height with respect to time and the change in wave height in space, $U_g \dfrac{\partial \eta}{\partial z}$, at the gas-liquid interface. The value of B_f that satisfies this condition can be found by substituting Equations 5.8 and 5.14 into Equation 5.13. Evaluating Equation 5.13 at $r = a$, B_f is found to be

$$B_f = \frac{ika\eta_0\left(U_f - c\right)}{cos\left(s\theta\right)\left[C_2\left(K_{s+1}\left(ka\right)ka - sK_s\left(ka\right)\right) - C_1\left(I_{s+1}\left(ka\right)ka + sI_s\left(ka\right)\right)\right]}. \tag{5.15}$$

The pressure in the liquid at the gas-liquid interface, P_f, can now be found by using the unsteady Bernoulli equation,

$$P_k = \rho_k\big(\frac{d\phi_k}{dt} + \frac{1}{2}\nabla\phi_k \cdot \nabla\phi_k - G + F(t)\big), \tag{5.16}$$

where G, the Bernoulli constant, and $F(t)$, a forcing function, are both equal to zero. The convective term of the Bernoulli equation, $\frac{1}{2}\nabla\phi \cdot \nabla\phi$, is small and negligible [57, 59]. Therefore, the Bernoulli equation of the liquid can be written

$$P_f = \rho_f \frac{d\phi_f}{dt}. \tag{5.17}$$

Using the chain rule, Equation 5.17 can be written in terms of partial derivatives of ϕ_f as

$$P_f = \rho_f \left(\frac{\partial \phi_f}{\partial t} + U_f \frac{\partial \phi_f}{\partial z} \right). \tag{5.18}$$

Substituting the potential flow solution, Equation 5.4, into Equation 5.18 using the boundary conditions described gives the liquid pressure at the interface, P_f, as

$$P_f = ik\rho_f B_f \left(U_f - c\right) \cos\left(s\theta\right) \left(C_1 I_s\left(ka\right) + C_2 K_s\left(ka\right)\right) e^{ik(z-ct)} - \rho_f U_f^2. \tag{5.19}$$

5.2.3 Interfacial Gas Pressure

Similar to the liquid potential, the potential of the gas must satisfy Equation 5.8 and can be determined by considering a pair of boundary conditions. At the centerline of the tube, $r = 0$, the gas potential must be finite. Since

$$\lim_{x \to 0} K_s\left(x\right) = \infty, \tag{5.20}$$

the coefficient $A_{2,g}$ in Equation 5.8 must be zero to satisfy this boundary condition. The boundary condition for the gas potential at the gas-liquid interface is similar to that of the liquid potential,

$$-\frac{\partial \phi_g}{\partial r} = \frac{\partial \eta}{\partial t} + U_g \frac{\partial \eta}{\partial z}. \tag{5.21}$$

Using a method similar to the one posed for the gas-liquid interfacial boundary condition, $A_{1,g}$ can be calculated as

$$A_{1,g} = \frac{\eta_0 kai\left(c - U_g\right)}{cos\left(s\theta\right)\left(kaI_{s+1}\left(ka\right) + sI_s\left(ka\right)\right)}. \tag{5.22}$$

The Bernoulli equation for the gas is written as

$$P_g = \rho_g \frac{d\phi_g}{dt} \tag{5.23}$$

which is written in terms of partial derivatives of ϕ_g as

$$P_g = \rho_g \left(\frac{\partial \phi_g}{\partial t} + U_g \frac{\partial \phi_g}{\partial z} \right). \tag{5.24}$$

Substituting Equations 5.22 and 5.8 into Equation 5.24, the gas pressure at the gas-liquid interface is found to be

$$P_g = -ik\rho_g A_{1,g} \left(c - U_g\right) I_s \left(ka\right) \cos\left(s\theta\right) e^{ik(z-ct)} - \rho_g U_g^2. \tag{5.25}$$

For consistency, B_k will be used to define the parameter that satisfies the interfacial boundary condition, meaning $B_g = A_{1,g}$. Therefore,

$$P_g = -ik\rho_g B_g \left(c - U_g\right) \cos\left(s\theta\right) I_s \left(ka\right) e^{ik(z-ct)} - \rho_g U_g^2. \tag{5.26}$$

5.2.4 Relationship Between Fluid Pressures

The pressures of the gas and the liquid at the gas-liquid interface (i.e., where $r = a$) can be related by the Young-Laplace equation [35, 66] as

$$-\sigma \left(\frac{1}{R_1} + \frac{1}{R_2} \right) = P_f - P_g \tag{5.27}$$

where σ is the surface tension and $1/R_1$ and $1/R_2$ are the principal curvatures of the system. The curvature in the azimuthal direction [57] is

$$\frac{1}{R_1} = \frac{1}{a} - \frac{1}{a^2} \left(\eta + \frac{\partial^2 \eta}{\partial \theta^2} \right), \tag{5.28}$$

and the curvature in the axial direction is

$$\frac{1}{R_2} = \frac{\partial^2 \eta}{\partial z^2}. \tag{5.29}$$

Substituting η into the definition for the principal curvatures yields

$$\left(\frac{1}{R_1} + \frac{1}{R_2} \right) = \frac{1}{a} - \frac{\eta_0 e^{ik(z-ct)} \cos\left(s\theta\right) \left(1 + s^2\right)}{a^2} + k^2 \eta_0 e^{ik(z-ct)} \cos\left(s\theta\right). \tag{5.30}$$

Therefore, Equations 5.30, 5.19 and 5.26 can be used with Equation 5.27 to establish a relationship between the pressure of the liquid and gas near the interface. The resulting equation can be simplified using the method of undetermined coefficients [67] to generate two equations. The first, the pressure between the unperturbed liquid and gas flows, is

$$-\frac{\sigma}{a} = \rho_g U_g^2 - \rho_f U_f^2. \tag{5.31}$$

The second equation that can be formed describes the relationship between the pressure of the liquid and gas at the interface due to the wave,

$$\begin{aligned} -\frac{\sigma\eta_0 e^{ik(z-ct)}\left(k^2a^2+s^2-1\right)}{a^2} = ik\cos\left(s\theta\right)e^{ik(z-ct)}\,[\ &\rho_f B_f U_f C_{\mathrm{IK}} \\ &-\rho_g A_{1,g} U_g I_s\left(ka\right) \\ &+c\left(\rho_g A_{1,g} I_s\left(ka\right)\right. \\ &\left.-\rho_f B_f C_{\mathrm{IK}}\ )\ ] \end{aligned} \tag{5.32}$$

with $C_{\mathrm{IK}} = C_1 I_s\left(ka\right) + C_2 K_s\left(ka\right)$.

5.2.5 Determination of the Value of s

Stability criteria are found by determining what system parameters cause the wave speed, c, to become imaginary. The wave speed is found by substituting Equations 5.12, 5.15, and 5.22 into Equation 5.32 and solving for c. While the relationship between the liquid and gas pressures for all orders s of the modified Bessel functions of the first and second kind has been given by Equation 5.32, deriving stability criteria from this general solution leads to unwieldy algebraic manipulation. General stability criteria valid for all s have been found herein, and this result is given in Appendix C. Studying this result will allow for the simplification of the development of the stability criteria for counter-current annular flow and will clarify the procedure used in this derivation.

If s is a non-zero value, Equation 5.3 will result in a non-zero velocity in the azimuthal direction. This flow would be inconsisent with experimental observation.

Using the fact that s must equal zero to correctly model the counter-current flow system, Equation 5.32 will be simplified in such a way that the derivation of stability criteria will be expressed clearly. A derivation of unique stability criteria for the case $s = 0$ is provided for enhanced methodological clarity in Appendix D.

5.2.6 Wave Speed and Stability Criteria

Using the fact that the order of the modified Bessel functions, s, is zero, Equation 5.32 can be rearranged by the order of the wave speed as

$$\begin{aligned} 0 = &- \left(\frac{ka^2 \rho_f \xi}{\gamma \cos(s\theta)} - \frac{ka^2 \rho_g I_0(ka)}{I_1(ka) \cos(s\theta)} \right) c^2 \\ &- \left(-\frac{2ka^2 \rho_f U_f \xi}{\gamma \cos(s\theta)} + \frac{2ka^2 \rho_g U_g I_0(ka)}{I_1(ka) \cos(s\theta)} \right) c \\ &+ \left(-\frac{-\sigma\gamma + \rho_f k U_f^2 a^2 \xi + \sigma k^2 a^2 \gamma}{\gamma \cos(s\theta)} + \frac{\rho_g k I_0(ka) U_g^2 a^2}{I_1(ka) \cos(s\theta)} \right) \end{aligned} \tag{5.33}$$

where the parameters ξ and γ are used for convenience to define

$$\xi = I_0(ka) K_1(kR) + I_1(kR) K_0(ka) \tag{5.34}$$

and

$$\gamma = K_1(kR) I_1(ka) - I_1(kR) K_1(ka). \tag{5.35}$$

A graph of ξ and γ for a constant value of ka is shown in Figure 5.2.

Equation 5.33 is a quadratic equation in the wave speed; therefore, the wave speed can be determined by using the quadratic formula,

$$c = -\frac{X_2}{2X_1} \pm \frac{\sqrt{{X_2}^2 - 4X_1X_3}}{2X_1}, \tag{5.36}$$

given that Equation 5.33 is in the form $X_1c^2 + X_2c + X_3$=0. Equation 5.36 can be rewritten in terms of simplifying variables C_a and C_b as

$$c = C_a \pm C_b. \tag{5.37}$$

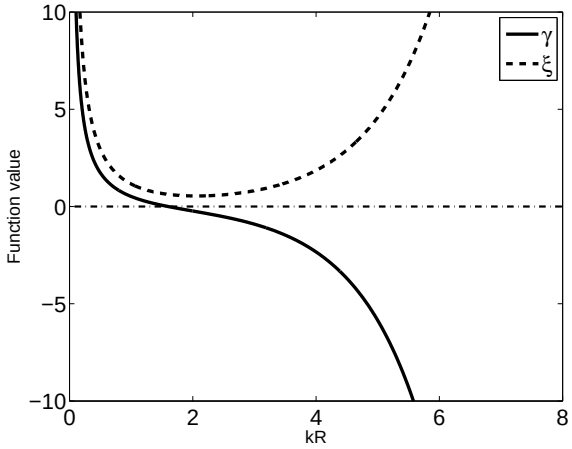

Fig. 5.2. A qualitative graph of γ and ξ.

For planar analysis of Kelvin-Helmholtz instability, the negative value of C_b is used to develop an appropriate solution [35]; analogously, the negative solution will be used for this analysis. Using this formulation,

$$C_a = \frac{\rho_f U_f \xi I_1(ka) - \rho_g U_g \gamma I_0(ka)}{\rho_f \xi I_1(ka) - \rho_g \gamma I_0(ka)} \tag{5.38}$$

and

$$C_b = \sqrt{-\frac{\sigma\gamma\left(k^2a^2-1\right)I_1(ka)}{ka^2\left(\rho_f\xi I_1(ka)-\rho_g\gamma I_0(ka)\right)} + \frac{\rho_f\rho_g\xi\gamma\left(U_f-U_g\right)^2 I_1(ka)\,I_0(ka)}{\left(\rho_f\xi I_1(ka)-\rho_g\gamma I_0(ka)\right)^2}}. \tag{5.39}$$

Since the condition for stability criteria is that the wave speed must not contain an imaginary component, $C_b^2 \geq 0$ would provide the necessary criteria. Therefore, the gas-liquid interface is stable if the following condition is met:

$$0 < -\frac{\sigma\gamma\left(k^2a^2-1\right)I_1(ka)}{ka^2\left(\rho_f\xi I_1(ka)-\rho_g\gamma I_0(ka)\right)} + \frac{\rho_f\rho_g\xi\gamma\left(U_f-U_g\right)^2 I_1(ka)\,I_0(ka)}{\left(\rho_f\xi I_1(ka)-\rho_g\gamma I_0(ka)\right)^2}. \tag{5.40}$$

5.2.7 Velocity Field Characterizations

From Sections 5.2.2 and 5.2.3, the potential functions of the liquid and gas are known to be

$$\phi_f = B_f e^{ik(z-ct)}\left(\frac{I_0(kr)}{I_1(kR)} + \frac{K_0(kr)}{K_1(kR)}\right) - U_f z \tag{5.41}$$

and

$$\phi_g = B_g e^{ik(z-ct)} I_0(kr) - U_g z. \tag{5.42}$$

Using the definitions of the axial, azimuthal, and radial velocities given by Equation 5.3, the liquid velocities in terms of the potential function are

$$v_{fr} = -B_f k e^{ik(z-ct)} \left(\frac{I_1(kr)}{I_1(kR)} - \frac{K_1(kr)}{K_1(kR)} \right) \tag{5.43a}$$

$$v_{fz} = -iB_f k e^{ik(z-ct)} \left(\frac{I_0(kr)}{I_1(kR)} + \frac{K_0(kr)}{K_1(kR)} \right) + U_f \tag{5.43b}$$

$$v_{f\theta} = 0 \tag{5.43c}$$

and the velocities of the gas are

$$v_{gr} = -B_g k e^{ik(z-ct)} I_1(kr) \tag{5.44a}$$

$$v_{gz} = -iB_g k e^{ik(z-ct)} I_0(kr) + U_g \tag{5.44b}$$

$$v_{g\theta} = 0. \tag{5.44c}$$

The assumption that $s = 0$ leads to an azimuthally symmetric flow, meaning that $v_{k\theta} = 0$. This symmetry allows for the flow to be considered two-dimensional. Stream functions, Ψ_k, for each fluid can now be generated by considering the definition of the stream function for the $r - z$ plane [68]:

$$v_{kr} = -\frac{1}{r}\frac{\partial \Psi_k}{\partial z} \tag{5.45a}$$

$$v_{kz} = \frac{1}{r}\frac{\partial \Psi_k}{\partial r}. \tag{5.45b}$$

The stream functions can then be found by integrating Equation 5.45 for the liquid and gas flows. Integration of the liquid axial velocity yields

$$\Psi_f = irB_f e^{ik(z-ct)} \left(\frac{K_1(kr)}{K_1(kR)} - \frac{I_1(kr)}{I_1(kR)} \right) + \frac{1}{2} U_f r^2 + F_f(z), \tag{5.46}$$

while integration of the gas axial velocity results in the stream function

$$\Psi_g = -irB_g e^{ik(z-ct)} I_1(kr) + \frac{1}{2} U_g r^2 + F_g(z). \tag{5.47}$$

These stream functions actually satisfy both conditions of Equation 5.45, meaning $F_f(z) = F_g(z) = 0$. Therefore, the liquid and gas stream functions are

$$\Psi_f = irB_f e^{ik(z-ct)} \left(\frac{K_1(kr)}{K_1(kR)} - \frac{I_1(kr)}{I_1(kR)} \right) + \frac{1}{2} U_f r^2, \tag{5.48}$$

and

$$\Psi_g = -irB_g e^{ik(z-ct)} I_1(kr) + \frac{1}{2} U_g r^2. \tag{5.49}$$

In summary, Table 5.1 (see page 61) characterizes the flow as developed in this section.

5.2.8 Consideration of Waves of Finite Amplitude

Kordyban and Ranov [69] and Mishima and Ishii [61] have previously shown that the limiting amplitude of waves in planar systems can be used in order to study wave stability in the context of slugging in co-current flow. This is accomplished by determining the maximum value of the product of the wave number and wave amplitude that may occur in a given system. This principle of waves of finite amplitude will be used to determine the maximum wave amplitude present given the model that has been developed thus far.

Derivation

The wave profile as limited by the finite amplitude of liquid waves can be calculated using the knowledge that for an irrotational flow, the gas-liquid interface can be determined by considering the stream function for the flow. Therefore, by using the stream function developed in Section 5.2.7 as Equation 5.49, a function for the gas-liquid interface can be determined by setting the value of Ψ_f equal to a constant. As this calculation is in reference to the actual height of the wave, the position to be

Table 5.1
Summary of flow characteristics.

Eq.	Liquid (f)	Eq.	Gas (g)
(5.41)	$\phi_f = B_f e^{ik(z-ct)} \left(\frac{I_0(kr)}{I_1(kR)} + \frac{K_0(kr)}{K_1(kR)} \right) - U_f z$	(5.42)	$\phi_g = B_g e^{ik(z-ct)} I_0(kr) - U_g z$
(5.48)	$\Psi_f = irB_f e^{ik(z-ct)} \left(\frac{K_1(kr)}{K_1(kR)} - \frac{I_1(kr)}{I_1(kR)} \right) + \frac{1}{2} U_f r^2$	(5.49)	$\Psi_g = -irB_g e^{ik(z-ct)} I_1(kr) + \frac{1}{2} U_g r^2$
(5.43a)	$v_{fr} = -B_f k e^{ik(z-ct)} \left(\frac{I_1(kr)}{I_1(kR)} - \frac{K_1(kr)}{K_1(kR)} \right)$	(5.44a)	$v_{gr} = -B_g k e^{ik(z-ct)} I_1(kr)$
(5.43b)	$v_{fz} = -iB_f k e^{ik(z-ct)} \left(\frac{I_0(kr)}{I_1(kR)} + \frac{K_0(kr)}{K_1(kR)} \right) + U_f$	(5.44b)	$v_{gz} = -iB_g k e^{ik(z-ct)} I_0(kr) + U_g$
(5.43c)	$v_{f\theta} = 0$	(5.44c)	$v_{g\theta} = 0$
(5.19)	$P_{if} = \frac{i\rho_f k B_f e^{ik(z-ct)} (U_f - c) \xi}{I_1(kR) K_1(kR)} - U_f^2 \rho_f$ with $\xi = K_1(kR) I_0(ka) + I_1(kR) K_0(ka)$	(5.26)	$P_{ig} = i\rho_g B_g k e^{ik(z-ct)} (U_g - c) I_0(ka) - U_g^2 \rho_g$

solved for will be defined as η. Since any streamline can be identified as $\Psi_k = 0$ [44], let $\Psi_k = 0$ at the gas-liquid interface. Along the resulting streamline,

$$0 = irB_f e^{ik(z-ct)} \left(\frac{K_1(k\eta)}{K_1(kR)} - \frac{I_1(k\eta)}{I_1(kR)} \right) + \frac{1}{2} U_f \eta^2, \tag{5.50}$$

the pressure must be constant.

The maximum attainable wave amplitude can then be found by considering the unsteady Bernoulli equation for the liquid film [70],

$$\frac{d\phi_f}{dt} + \frac{P_f}{\rho_f} + \frac{1}{2} \nabla\phi_f \cdot \nabla\phi_f = 0. \tag{5.51}$$

Despite the fact that it is small, the convective term is included in this equation to ensure the pressure is completely constant over the streamline. For flow along a streamline, both sides of the following equation must be constant:

$$P_f = -\rho_f \left(\frac{\partial\phi_f}{\partial t} + U_f \frac{\partial\phi_f}{\partial z} + \frac{1}{2} \nabla\phi_f \cdot \nabla\phi_f \right). \tag{5.52}$$

This equation must be evaluated at the gas-liquid interface, where $r = a$.

To satisfy this requirement at the gas-liquid interface, the value of ϕ_f must be substituted into Equation 5.52. This equation will include an unknown, B_f, which must be defined in order to find the maximum wave amplitude. The parameter B_f can now be defined in terms of the result of Equation 5.50, as

$$B_f = -\frac{\frac{1}{2} i U_f \eta I_1(kR) K_1(kR) e^{ik(z-ct)}}{I_1(k\eta) K_1(kR) - K_1(k\eta) I_1(kR)}. \tag{5.53}$$

In order to satisfy the condition that the pressure is constant along the interface, the right hand side of Equation 5.52 should be zero. Using this information and substituting Equation 5.53 and Equation 5.41 into Equation 5.52 yields the equation

$$\begin{aligned} 0 = &-(k\eta)^2 - 4 - \frac{4k\eta \left(K_0(k\eta) I_1(kR) + K_1(kR) I_0(k\eta) \right)}{\Omega} \\ &+ \frac{(k\eta)^2 \left(I_1(kR) K_0(k\eta) + K_1(kR) I_0(k\eta) \right)^2}{\Omega^2}, \end{aligned} \tag{5.54}$$

where $\Omega = I_1(k\eta) K_1(kR) - K_1(k\eta) I_1(kR)$. Equation 5.54 must be solved implicitly, as $k\eta = f(kR)$.

Using this equation, a maximum value of $k\eta$, $(k\eta)_{\max}$, can be obtained as a function of kR, which will be used as the effect of the finite amplitude of the wave on the stability criteria previously derived.

Implementation

In order to implement the theory of waves of finite amplitude into the inequality posed by Equation 5.40, a closure relation must be provided for the wave number, or, more practically, the quantity ka. As previously discussed, the values of $k\eta$ that satisfy Equation 5.54 will allow for the determination of the maximum value of $k\eta$, $(k\eta)_{\max}$. In order to accomplish this, the roots of Equation 5.54 must be found. To determine an appropriate method of solving the equation, the left hand side can be rewritten

$$\begin{aligned} f\left(k\eta\right) = &- \left(k\eta\right)^2 - 4 - \frac{4k\eta\left(K_0\left(k\eta\right)I_1\left(kR\right) + K_1\left(kR\right)I_0\left(k\eta\right)\right)}{\Omega} \\ &+ \frac{\left(k\eta\right)^2\left(I_1\left(kR\right)K_0\left(k\eta\right) + K_1\left(kR\right)I_0\left(k\eta\right)\right)^2}{\Omega^2}. \end{aligned} \tag{5.55}$$

The roots can then be found by studying the function given in Equation 5.55 by considering that when the value of the residual is zero, Equation 5.54 is satisfied.

Plotting Equation 5.55 for specific values of kR allows for the understanding of the behavior of the roots of Equation 5.55 as a function of $k\eta$. This can be accomplished by considering the non-zero values of the function, Equation 5.55, to be considered as a residual, an error in the calculation of the roots of the function. For small, near-zero values of kR, Equation 5.55 has no real roots for positive values of $k\eta$, and Equation 5.54 has no solutions. The functions are not equivalent for $k\eta = 0$, as seen in Figure 5.3, but quickly converge to the same value and diverge from zero, as in Figure 5.4. As kR is increased, the function is no longer monotonically increasing, as seen in Figure 5.5. The minimum of each function decreases as the value of kR increases. This can be further studied by restricting the range of the scale of the ordinate. For larger values of kR, Equation 5.55 has two real roots for positive values

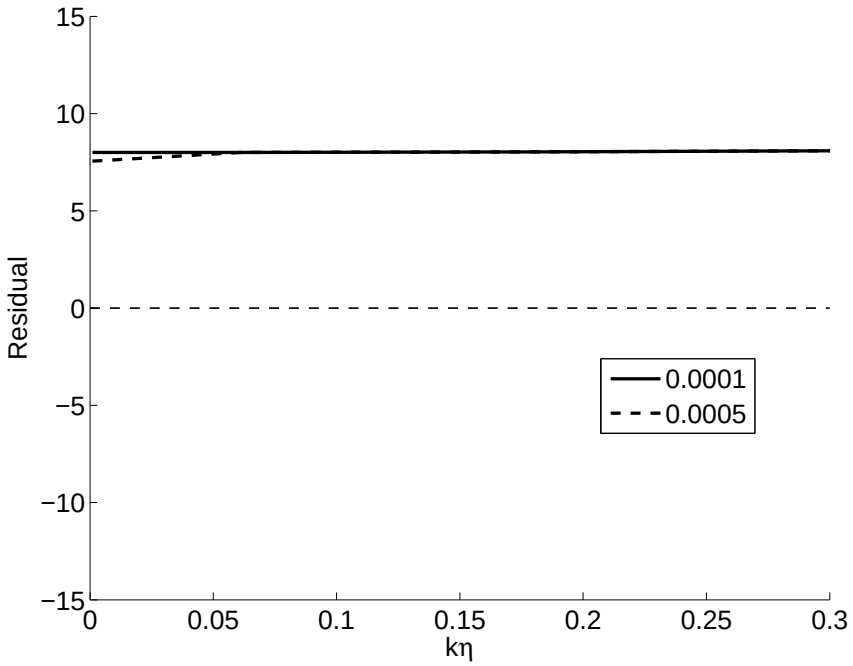

Fig. 5.3. Plot of Equation 5.55 for $kR = 0.0001$,0.0005 (for small kR).

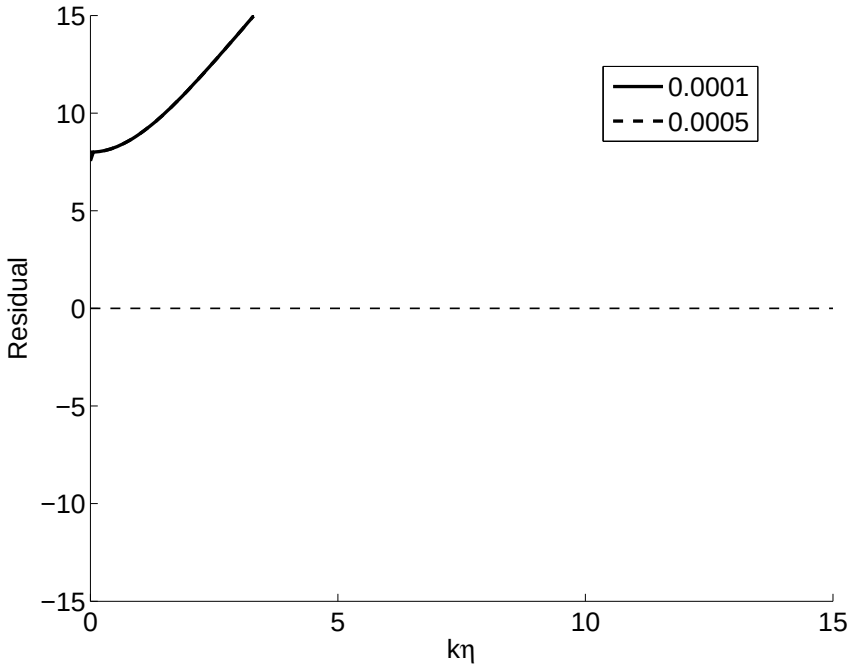

Fig. 5.4. Plot of Equation 5.55 for $kR = 0.0001$,0.0005.

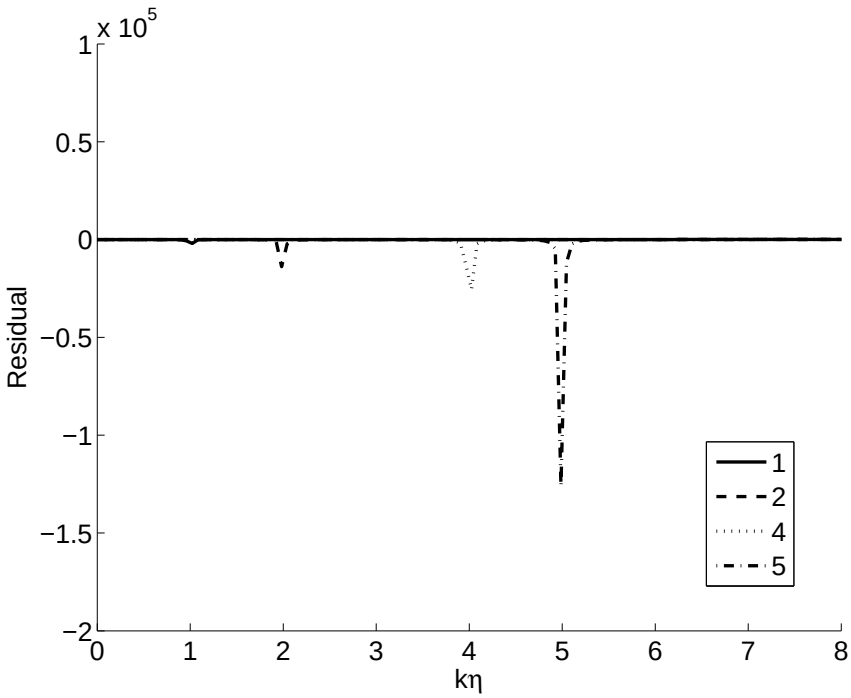

Fig. 5.5. Plot of Equation 5.55 for $kR = 1, 2, 4, 5$.

of $k\eta$: one root closer to zero (herein referred to as the "left" root) and a root further from zero (the "right" root). Figure 5.6 shows several plots of Equation 5.55 that show the existence of both roots. In this figure, both the left and right roots appear to increase in magnitude for greater values of kR. In Figure 5.7, it can be seen that the

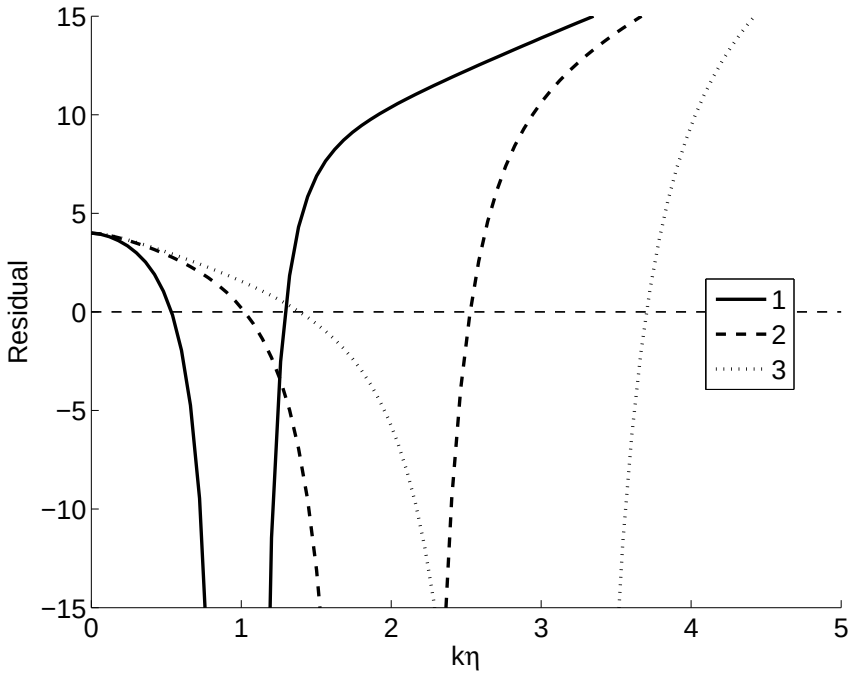

Fig. 5.6. Plot of Equation 5.55 for $kR = 1, 2, 3$.

distance between the left roots for each value of kR decreases for increasing values of kR. Despite this apparent convergence, the distance between the left and right roots is increasing. For $kR \approx 4$ and larger (as shown in Figure 5.8), the left root converges on a specific value, while the right root appears to grow towards infinity. With this knowledge, it should be possible to use the known solution to Equation 5.54, the left root, as the value of $(k\eta)_{\max}$ as a function of kR. Plotting the value of $(k\eta)_{\max}$ versus kR in Figure 5.9, it can be seen that the value of $(k\eta)_{\max}$ clearly converges on a value, specifically 1.5997. With this knowledge, the effect of finite wave amplitude

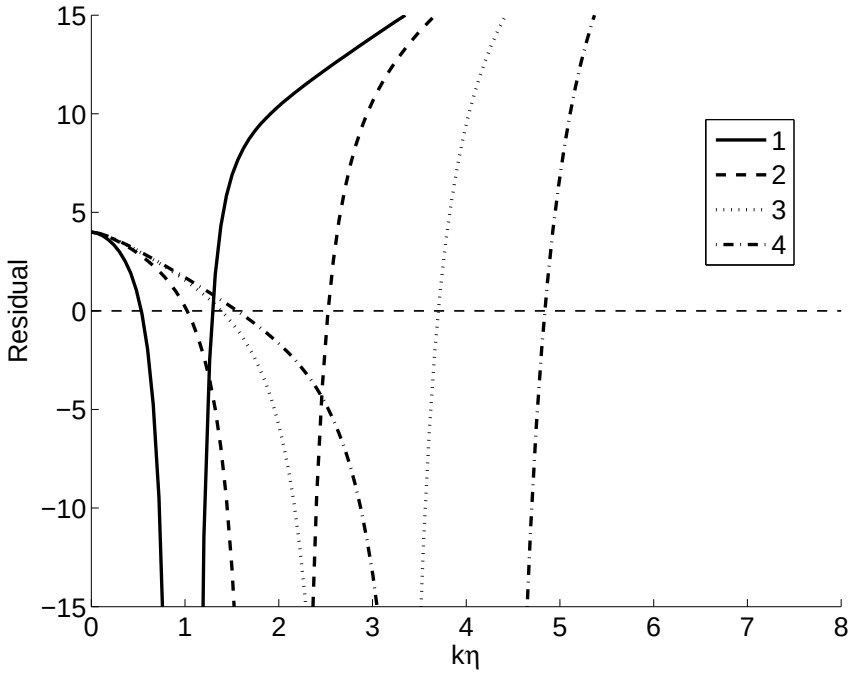

Fig. 5.7. Plot of Equation 5.55 for $kR = 1, 2, 3, 4$.

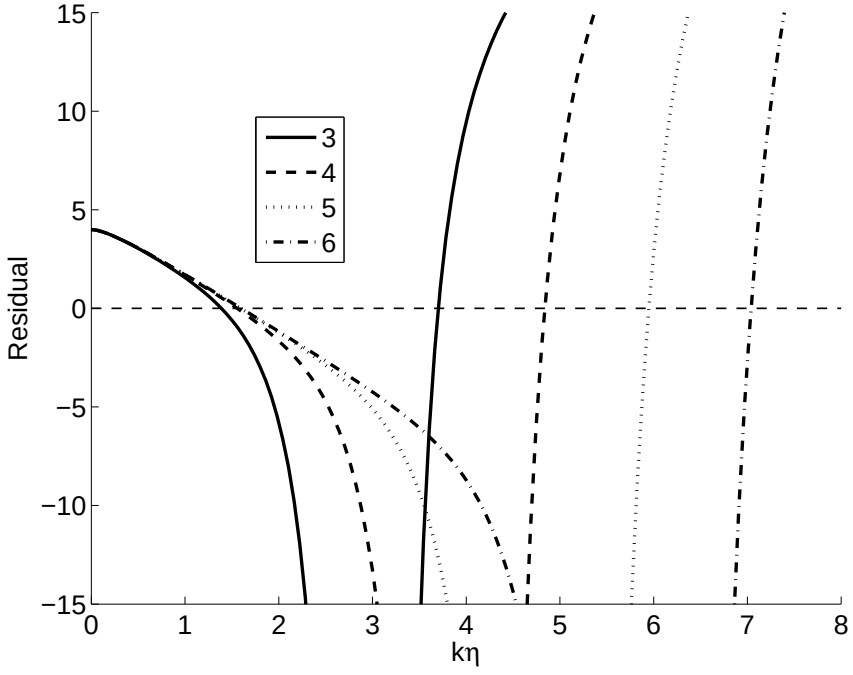

Fig. 5.8. Plot of Equation 5.55 for $kR = 3, 4, 5, 6$.

on the stability of a counter-current annular flow will be accounted for by assuming $(k\eta)_{\max} = 1.6$ in this analysis.

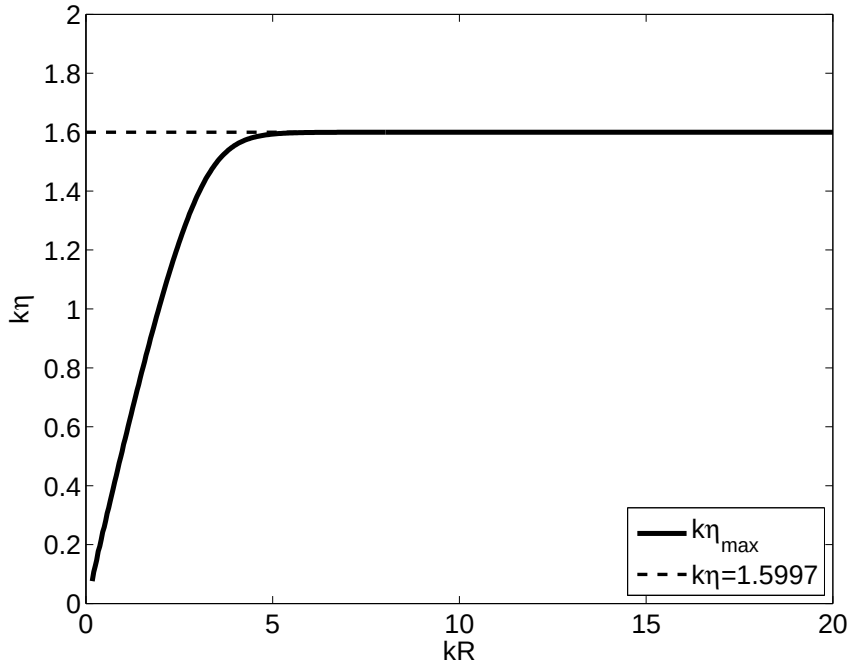

Fig. 5.9. Value of $(k\eta)_{\max}$ versus kR at the wave cusp.

5.2.9 Analysis of the Limiting Wave

Using the solution generated in Section 5.2.8, the wave number, k from Equation 5.40 can be eliminated in the context of the product of the wave number and the distance from the tube centerline to the gas-liquid interface, a. Therefore, determination of the product kR is necessary in order to remove the wave number as a variable in this analysis. This is accomplished by considering the dependence of Equation 5.40 on the parameter kR.

The stability criteria previously developed as Equation 5.40 is

$$0 < -\frac{\sigma\gamma\left(k^2a^2-1\right)I_1\left(ka\right)}{ka^2\left(\rho_f\xi I_1\left(ka\right)-\rho_g\gamma I_0\left(ka\right)\right)}+\frac{\rho_f\rho_g\xi\gamma\left(U_f-U_g\right)^2 I_1\left(ka\right)I_0\left(ka\right)}{\left(\rho_f\xi I_1\left(ka\right)-\rho_g\gamma I_0\left(ka\right)\right)^2}. \qquad (5.40)$$

with $\xi = I_0(ka)\,K_1(kR) + I_1(kR)\,K_0(ka)$ and $\gamma = K_1(kR)\,I_1(ka) - I_1(kR)\,K_1(ka)$. Since the value of kR is only present in ξ and γ, and the quantity ka is known, limiting values of ξ and γ may be determined. To accomplish this, both sides of Equation 5.40 are multiplied by the quantity $(\rho_f \xi I_1(ka) - \rho_g \gamma I_0(ka))$, which is valid if it is assumed that γ will always be negative. This operation results in the inequality

$$0 < -\frac{\sigma\gamma\left(k^2a^2-1\right)\left(\rho_f \xi I_1(ka) - \rho_g \gamma I_0(ka)\right) I_1(ka)}{ka^2} + \rho_f \rho_g \xi \gamma \left(U_f - U_g\right)^2 I_1(ka)\, I_0(ka). \tag{5.56}$$

Dividing both sides of this inequality by the quantity $\xi\gamma$, which will be negative since $\gamma < 0$, yields

$$0 > -\frac{\sigma\left(k^2a^2-1\right)\left(\rho_f \xi I_1(ka) - \rho_g \gamma I_0(ka)\right) I_1(ka)}{\xi ka^2} + \rho_f \rho_g \left(U_f - U_g\right)^2 I_1(ka)\, I_0(ka). \tag{5.57}$$

Finally, distributing the quantity ξ results in the inequality

$$0 > -\frac{\sigma\left(k^2a^2-1\right) I_1(ka)\left(\rho_f I_1(ka) - \rho_g \dfrac{\gamma}{\xi} I_0(ka)\right)}{ka^2} + \rho_f \rho_g \left(U_f - U_g\right)^2 I_1(ka)\, I_0(ka). \tag{5.58}$$

Equation 5.58 is equivalent to Equation 5.40 for the assumptions that $\gamma < 0$ and $\xi > 0$. In Equation 5.58 a single term can be expressed that represents the effect of γ and ξ. As the value of ka was established to be approximately 1.6 in Section 5.2.8, Equation 5.59 can be written as $\gamma/\xi = f(kR)$:

$$\frac{\gamma}{\xi} = \frac{K_1(kR)\,I_1(ka) - I_1(kR)\,K_1(ka)}{I_0(ka)\,K_1(kR) + I_1(kR)\,K_0(ka)}. \tag{5.59}$$

A graphical representation of Equation 5.59 is shown in Figure 5.10. Based on this graphical result, it can be seen that for $kR > 5$, the expression γ/ξ asymptotically approaches the value -1.2803. Assuming this asymptotic value is approached, then the equation $\gamma/\xi = -1.2803$ can be used as a closure relation in the instability

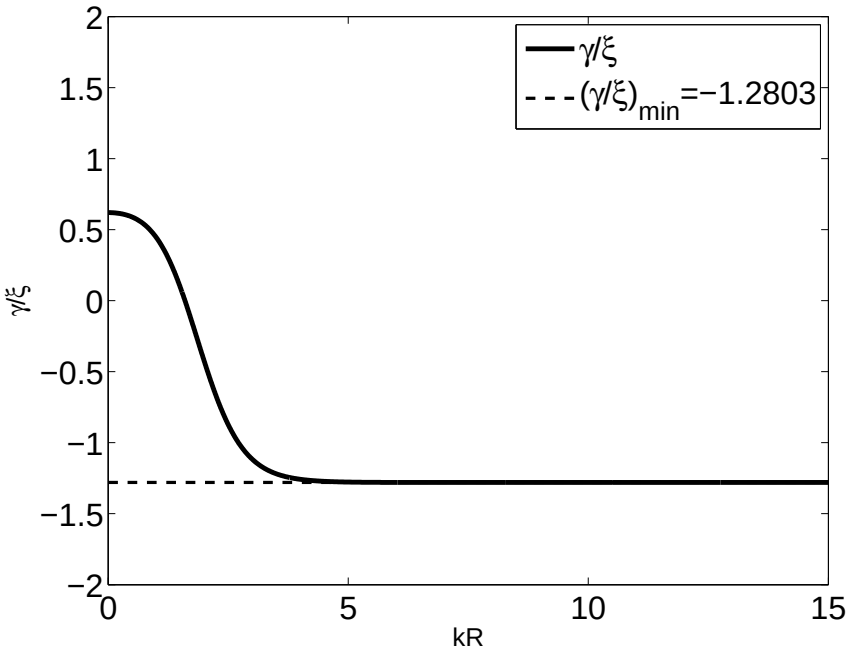

Fig. 5.10. Functional dependence of γ/ξ on kR.

criteria rewritten as Equation 5.58. Therefore, the resulting stability criteria posed for an adiabatic, counter-current annular flow is

$$0 > -\frac{\sigma\left(k^2a^2-1\right)I_1\left(ka\right)\left(\rho_f I_1\left(ka\right)-\rho_g\frac{\gamma}{\xi}I_0\left(ka\right)\right)}{ka^2}+\rho_f\rho_g\left(U_f-U_g\right)^2 I_1\left(ka\right)I_0\left(ka\right) \tag{5.58}$$

with $ka = 1.6$ and $\gamma/\xi = -1.2803$.

6. MODEL ASSESSMENT

The model developed in Section 5 provides a method of predicting flooding using the assumption that flooding is caused by instability-driven wave growth. To assess this model, its mathematical limits will be investigated and a comparison of this model with experimental data will be used for validation.

6.1 Analysis

In order to verify that the model given in Section 5 is suitable for the calculation of stability criteria for flooding, several analyses will be performed. First, equivalence to Rayleigh's solution to the problem of vibrations of a cylindrical jet, as given by Lamb [57], will be verified as a limiting case. Then, the asymptotic dependence of flooding on tube diameter will be investigated with the new model. From this, the transition from the applicability of the Wallis model to that of the Kutateladze-like correlations and dependence of this transition on the Bond number will be demonstrated. Finally, dimensionless parameters derived from the new model will be discussed.

6.1.1 Simplification to Rayleigh's Model

In *Hydrodynamics*, Lamb [57] describes the solution developed by Rayleigh for interfacial instability on a vibrating cylindrical jet. This derivation is conducted given the assumptions that a cylindrical column of fluid is surrounded by an infinite field of a different fluid. The column of fluid is parallel to gravity and is analyzed using the same coordinate system given by Figure 5.1. The system is adiabatic, and neither fluid is undergoing motion. Given these considerations, this stability model should be a limiting case of the model given in Section 5, where the radius of the tube is infinite and the velocities of both fluids, U_f and U_g, are zero. To verify that

the newly developed model is analytically sound, it should be possible to show that it can reduce to Rayleigh's model given these assumptions.

As shown in Section 5, the interfacial stability of an annular counter-current flow that has been developed is based on the equation

$$C_b = \sqrt{-\frac{\sigma\gamma\left(k^2a^2-1\right)I_1\left(ka\right)}{ka^2\left(\rho_f\xi I_1\left(ka\right)-\rho_g\gamma I_0\left(ka\right)\right)}+\frac{\rho_f\rho_g\xi\gamma\left(U_f-U_g\right)^2 I_1\left(ka\right)I_0\left(ka\right)}{\left(\rho_f\xi I_1\left(ka\right)-\rho_g\gamma I_0\left(ka\right)\right)^2}}, \quad (5.39)$$

where C_b is the component of the wave speed that may become imaginary. In order to show that the new stability model can be simplified to give Rayleigh's model, it must be noted that Lamb presents Rayleigh's result in terms of the angular frequency, ω, which is defined in terms of the wave speed, c, and the wave number, k, as

$$\omega = kc. \quad (6.1)$$

Substituting Equation 5.37 into Equation 6.1, the angular frequency is written

$$\omega = kC_a + kC_b, \quad (6.2)$$

or, analogous to Equation 5.37

$$\omega = \Omega_a + \Omega_b, \quad (6.3)$$

with $\Omega_a = kC_a$ and $\Omega_b = kC_b$. Using these definitions, Ω_b is written

$$\Omega_b = \sqrt{-\frac{ka\sigma\gamma\left(k^2a^2-1\right)I_1\left(ka\right)}{a^3\left(\rho_f\xi I_1\left(ka\right)-\rho_g\gamma I_0\left(ka\right)\right)}+k^2\frac{\rho_f\rho_g\xi\gamma\left(U_f-U_g\right)^2 I_1\left(ka\right)I_0\left(ka\right)}{\left(\rho_f\xi I_1\left(ka\right)-\rho_g\gamma I_0\left(ka\right)\right)^2}}. \quad (6.4)$$

This equation in terms of Ω_B can then be used to derive a new inequality for interfacial stability, as Ω_b is imaginary when the expression under the radical is less than zero. Mathematically, this is expressed as

$$0 < \sqrt{-\frac{ka\sigma\gamma\left(k^2a^2-1\right)I_1\left(ka\right)}{a^3\left(\rho_f\xi I_1\left(ka\right)-\rho_g\gamma I_0\left(ka\right)\right)}+k^2\frac{\rho_f\rho_g\xi\gamma\left(U_f-U_g\right)^2 I_1\left(ka\right)I_0\left(ka\right)}{\left(\rho_f\xi I_1\left(ka\right)-\rho_g\gamma I_0\left(ka\right)\right)^2}}. \quad (6.5)$$

Now that this inequality has been formulated, simplifying assumptions can be imposed to derive Rayleigh's equation. To begin, the limit of Equation 6.5 as the radius,

R, tends toward infinity must be found. As only γ and ξ are explicit functions of the tube radius, the following equations are posed:

$$\lim_{R\to\infty}\gamma = \lim_{R\to\infty} K_1(kR)\, I_1(ka) - \lim_{R\to\infty} I_1(kR)\, K_1(ka) \tag{6.6}$$

$$\lim_{R\to\infty}\xi = \lim_{R\to\infty} I_0(ka)\, K_1(kR) + \lim_{R\to\infty} I_1(kR)\, K_0(ka)\,. \tag{6.7}$$

Two functions in the definitions of γ and ξ are calculated based on the tube diameter. These are a modified Bessel function of the second kind, $K_1(kR)$ and a modified Bessel function of the first kind, $I_1(kR)$. As the limit of the modified Bessel function of the second kind is zero as kR goes to infinity (see Appendix A), terms involving this function go to zero. Therefore, Equations 6.6 and 6.7 are equivalent to

$$\lim_{R\to\infty}\gamma = -\lim_{R\to\infty} I_1(kR)\, K_1(ka) \tag{6.8}$$

and

$$\lim_{R\to\infty}\xi = \lim_{R\to\infty} I_1(kR)\, K_0(ka)\,. \tag{6.9}$$

For clarity, Equation 6.5 is now written

$$0 < \beta_1 + \beta_2, \tag{6.10}$$

with β_1 and β_2 defined as

$$\beta_1 = -\frac{ka\sigma\gamma\left(k^2a^2-1\right) I_1(ka)}{a^3\left(\rho_f\xi I_1(ka) - \rho_g\gamma I_0(ka)\right)} \tag{6.11}$$

and

$$\beta_2 = \frac{k^2\rho_f\rho_g\xi\gamma\left(U_f-U_g\right)^2 I_1(ka)\, I_0(ka)}{\left(\rho_f\xi I_1(ka) - \rho_g\gamma I_0(ka)\right)^2}. \tag{6.12}$$

In order to find the limit of the inequality posed by Equation 6.5, the equation

$$\lim_{R\to\infty}\left(\beta_1+\beta_2\right) = \lim_{R\to\infty}\beta_1 + \lim_{R\to\infty}\beta_2 \tag{6.13}$$

must be simplified using Equations 6.8 and 6.9. This task is accomplished by first identifying which parameters are functions of R, specifically by identifying the dependence of β_1 and β_2 on γ and ξ, which can be written as

$$\lim_{R\to\infty}\beta_1 = \lim_{R\to\infty} -\frac{ka\sigma\gamma(R)\left(k^2a^2-1\right) I_1(ka)}{a^3\left(\rho_f\xi(R) I_1(ka) - \rho_g\gamma(R) I_0(ka)\right)} \tag{6.14}$$

and

$$\lim_{R\to\infty}\beta_2 = \lim_{R\to\infty} k^2 \frac{\rho_f\rho_g\xi\left(R\right)\gamma\left(R\right)\left(U_f-U_g\right)^2 I_1\left(ka\right)I_0\left(ka\right)}{\left(\rho_f\xi\left(R\right)I_1\left(ka\right)-\rho_g\gamma\left(R\right)I_0\left(ka\right)\right)^2}. \tag{6.15}$$

Substituting Equations 6.8 and 6.9 into Equations 6.14 and 6.15, yields

$$\lim_{R\to\infty}\beta_1 = \lim_{R\to\infty} -\frac{ka\sigma\left(-I_1\left(kR\right)K_1\left(ka\right)\right)\left(k^2a^2-1\right)I_1\left(ka\right)}{a^3\left(\rho_f\left(I_1\left(kR\right)K_1\left(ka\right)\right)I_1\left(ka\right)-\rho_g\left(-I_1\left(kR\right)K_0\left(ka\right)\right)I_0\left(ka\right)\right)} \tag{6.16}$$

and

$$\lim_{R\to\infty}\beta_2 = \lim_{R\to\infty} k^2 \frac{\rho_f\rho_g\left(I_1\left(kR\right)K_0\left(ka\right)\right)\left(-I_1\left(kR\right)K_1\left(ka\right)\right)\left(U_f-U_g\right)^2 I_1\left(ka\right)I_0\left(ka\right)}{\left(\rho_f\left(I_1\left(kR\right)K_1\left(ka\right)\right)I_1\left(ka\right)-\rho_g\left(-I_1\left(kR\right)K_0\left(ka\right)\right)I_0\left(ka\right)\right)^2}. \tag{6.17}$$

It can be seen that $I_1\left(kR\right)$ can be factored from the numerator and denominator of both Equation 6.16 and Equation 6.17, simplifying these equations to

$$\lim_{R\to\infty}\beta_1 = \lim_{R\to\infty} -\left(\frac{I_1\left(kR\right)}{I_1\left(kR\right)}\right)\frac{ka\sigma\left(-K_1\left(ka\right)\right)\left(k^2a^2-1\right)I_1\left(ka\right)}{a^3\left(\rho_f\left(K_1\left(ka\right)\right)I_1\left(ka\right)-\rho_g\left(-K_0\left(ka\right)\right)I_0\left(ka\right)\right)} \tag{6.18}$$

and

$$\lim_{R\to\infty}\beta_2 = \lim_{R\to\infty} \left(\frac{I_1\left(kR\right)}{I_1\left(kR\right)}\right) k^2 \frac{\rho_f\rho_g\left(K_0\left(ka\right)\right)\left(-K_1\left(ka\right)\right)\left(U_f-U_g\right)^2 I_1\left(ka\right)I_0\left(ka\right)}{\left(\rho_f\left(K_1\left(ka\right)\right)I_1\left(ka\right)-\rho_g\left(-K_0\left(ka\right)\right)I_0\left(ka\right)\right)^2}. \tag{6.19}$$

Therefore, the limit of these functions as the radius becomes infinite can be expressed as

$$\lim_{R\to\infty}\beta_1 = \frac{ka\sigma I_1\left(ka\right)K_1\left(ka\right)\left(k^2a^2-1\right)}{a^3\left(\rho_f K_0\left(ka\right)I_1\left(ka\right)-\rho_g\left(-K_1\left(ka\right)\right)I_0\left(ka\right)\right)} \tag{6.20}$$

and

$$\lim_{R\to\infty}\beta_2 = -k^2\frac{\rho_f\rho_g I_0\left(ka\right)I_1\left(ka\right)K_0\left(ka\right)K_1\left(ka\right)\left(U_f-U_g\right)^2}{\left(\rho_f K_0\left(ka\right)I_1\left(ka\right)-\rho_g\left(-K_1\left(ka\right)\right)I_0\left(ka\right)\right)^2}. \tag{6.21}$$

Similar to the analysis of Kelvin-Helmholtz instability of planar flow in a channel [35], modified liquid and gas densities can be expressed by considering the effect of depth on the density of each fluid as

$$\hat{\rho}_f = \rho_f K_0\left(ka\right)I_1\left(ka\right) \tag{6.22}$$

and

$$\hat{\rho}_g = -\rho_g K_1\left(ka\right)I_0\left(ka\right). \tag{6.23}$$

Equations 6.20 and 6.21 are then written

$$\lim_{R\to\infty}\beta_1 = \frac{ka\sigma I_1(ka)\,K_1(ka)\,(k^2a^2-1)}{a^3\,(\hat{\rho}_f-\hat{\rho}_g)} \tag{6.24}$$

and

$$\lim_{R\to\infty}\beta_2 = -k^2\frac{\rho_f\rho_g I_0(ka)\,I_1(ka)\,K_0(ka)\,K_1(ka)\,(U_f-U_g)^2}{(\hat{\rho}_f-\hat{\rho}_g)^2}. \tag{6.25}$$

Substituting Equation 6.24 and Equation 6.25 into Equation 6.10 yields

$$0 < \frac{ka\sigma I_1(ka)\,K_1(ka)\,(k^2a^2-1)}{a^3\,(\hat{\rho}_f-\hat{\rho}_g)} - k^2\frac{\rho_f\rho_g I_0(ka)\,I_1(ka)\,K_0(ka)\,K_1(ka)\,(U_f-U_g)^2}{(\hat{\rho}_f-\hat{\rho}_g)^2}. \tag{6.26}$$

By making the reasonable assumption that the modified Bessel functions of the first and second kinds are always positive, Equation 6.26 can be divided by the quantity $I_0(ka)\,K_1(ka)$ to give

$$0 < \frac{ka\sigma I_1(ka)\,(k^2a^2-1)}{a^3 I_0(ka)\,(\hat{\rho}_f-\hat{\rho}_g)} - k^2\frac{\rho_f\rho_g I_1(ka)\,K_0(ka)\,(U_f-U_g)^2}{(\hat{\rho}_f-\hat{\rho}_g)^2}. \tag{6.27}$$

By employing the assumption of stationary fluids, where $U_f = U_g = 0$, it is easily seen that

$$0 < \frac{ka\sigma I_1(ka)\,(k^2a^2-1)}{a^3 I_0(ka)\,(\hat{\rho}_f-\hat{\rho}_g)}. \tag{6.28}$$

Equation 6.28 is the stability condition of Rayleigh which is posed by Lamb [57]. Therefore, by making the appropriate assumption of a stationary column of fluid surrounded by an infinite field of stationary fluid, the new stability model for counter-current annular flow in a tube reduces to the stability model posed in historical literature.

6.1.2 Investigation of Bond Number Dependence

Previous literature [2] has noted that for tubes with dimensionless diameters greater than 40, flooding in these systems does not appear to be a function of tube diameter. As the dimensionless diameter has been defined as $D^* = \sqrt{\mathrm{Bo}}$,

the stability-based model of flooding can be analyzed to see if this behavior can be derived from the model.

The inequality presented as Equation 5.58 can be rewritten using the convention that positive values represent stabilizing forces as

$$0 < \frac{\sigma\left(k^2a^2-1\right)I_1\left(ka\right)\left(\rho_f I_1\left(ka\right)-\rho_g\frac{\gamma}{\xi}I_0\left(ka\right)\right)}{ka^2}-\rho_f\rho_g\left(U_f-U_g\right)^2 I_1\left(ka\right)I_0\left(ka\right). \tag{6.29}$$

As the quantities ka and kR have been calculated in Section 5, Equation 6.29 can also be formulated

$$0 < \frac{\sigma\left(k^2a^2-1\right)I_1\left(ka\right)\left(\rho_f I_1\left(ka\right)-\rho_g\frac{\gamma}{\xi}I_0\left(ka\right)\right)}{\left(a\right)\left(ka\right)}-\rho_f\rho_g\left(U_f-U_g\right)^2 I_1\left(ka\right)I_0\left(ka\right). \tag{6.30}$$

It can be seen from Equation 6.30 that if ka and kR are known, the inequality could be expressed by writing a, the film thickness, in terms of $\bar{a}$, the average annular film thickness that can be calculated using the model presented in Section 3. The relative velocity that is used for these calculations is actually defined as the relative superficial velocity, $\langle j_f \rangle - \langle j_g \rangle$, as is consistent with previous literature (such as Mishima and Ishii [61]).

To examine the dependence of the stability-based model of flooding on tube diameter, Equation 6.30 will be considered a function of tube diameter. While the film thickness model that is employed explicitly depends on the tube diameter, the superficial velocities of each fluid are also determined based on the cross-sectional dimensions of the tube.

Due to the nonlinear nature of Equation 6.30, the effect of tube diameter on the new model of flooding is not easily studied by simply calculating the limit of the function as the diameter tends towards infinity. To address this, a numerical investigation is conducted to examine the gas flow rate needed to cause flooding for a specific liquid flow rate as a function of tube diameter. The parameters used

for this study are given in Table 6.1. Results of this investigation are shown in

Table 6.1
Parameters for diameter dependence investigation.

Parameter	Value
D	$0.04\text{ m} - 0.4\text{ m}$
$\lvert Q_f \rvert$	$0.002\text{ m}^3/\text{s}$
$\lvert j_f \rvert$	$0.0028\text{ m/s} - 0.1592\text{ m/s}$
$\lvert j_f^* \rvert$	$0.0017 - 0.0045$
ρ_f	997.1 kg/m^3
ρ_g	1.18 kg/m^3
σ	0.07197 N/m
μ_f	0.0008905 Ns/m^2
$\sqrt{\text{Bo}}$	$14 - 110$

Figures 6.1, 6.2, 6.3, 6.4, and 6.5. (Plots of the gas volumetric flow rate, gas superficial velocity, average annular liquid film thickness, void fraction, and gas Wallis parameter as a function of tube diameter are provided in Appendix E). Each parameter has been plotted in terms of the square root of the Bond number, equivalent to the dimensionless diameter, D^*, which is used to characterize the transition from "small" to "large" tube diameters. As expected, Figure 6.1 shows that the volumetric gas flow rate is increases with the tube diameter for a fixed liquid volumetric flow rate. Since the diameter of the tube is increasing, the superficial velocity of both the gas and liquid for fixed volumetric flow rates decreases as tube size increases. This phenomenon is shown in Figure 6.2. It is important to note that the change in gas superficial velocity is decreasing for increasing diameter size and Bond number. The film thicknesses corresponding to the fixed liquid volumetric flow rate and the gas flow rate that causes flooding are not monotonic.

While it is expected that the film thickness should decrease for increasing tube diameter, Figure 6.3 presents a non-linear dependence of annular liquid film thickness on tube diameter. At $\sqrt{\text{Bo}} \approx 40$, a discontinuity appears due to the transition between laminar and turbulent wall friction factor models in the liquid film thickness model. The film thickness then continues to decrease until $\sqrt{\text{Bo}} \approx 60$, where the film thickness appears to reach a minimum. A maximum film thickness is then obtained at $\sqrt{\text{Bo}} \approx 100$, followed by another decrease in film thickness. This complex functional dependence of the film thickness on diameter is caused by not only the obvious changing of the tube diameter, but also the effect of the tube diameter on the superficial velocities used to calculate the film thickness. While a large tube should intuitively decrease in film thickness for a fixed liquid flow rate, the dependence of the film thickness on tube diameter becomes non-linear as the difference between superficial velocities continues to increase. Similarly, Figure 6.4 shows the void fraction calculated from this predicted average annular film thickness. It is important to note that while the initial change in void fraction is significant, the more complex behavior of the film thickness that develops for $\sqrt{\text{Bo}} > 60$ has less of a profound effect on the void fraction. Considering these results, the Wallis parameter for the gas appears to show an asymptotic dependence on the square root of the Bond number, D^*, as shown in Figure 6.5. For these values of the gas Wallis parameter, the liquid Wallis parameter, j_f^*, has an overall range of 0.0017 to 0.0045, and is relatively steady at a range of 0.0017 to 0.0027 for $\sqrt{\text{Bo}} \approx 40$. From this analysis, the trend towards a lack of diameter dependence for large-diameter tubes (those with dimensionless diameters greater than 40) can be inferred.

6.1.3 Dimensionless Characterization

While flooding has been categorized historically by the Wallis number, Kutateladze number, and the Bond number, it has been noted in literature, particularly by McQuillan and Whalley [7], that these parameters alone do not sufficiently charac-

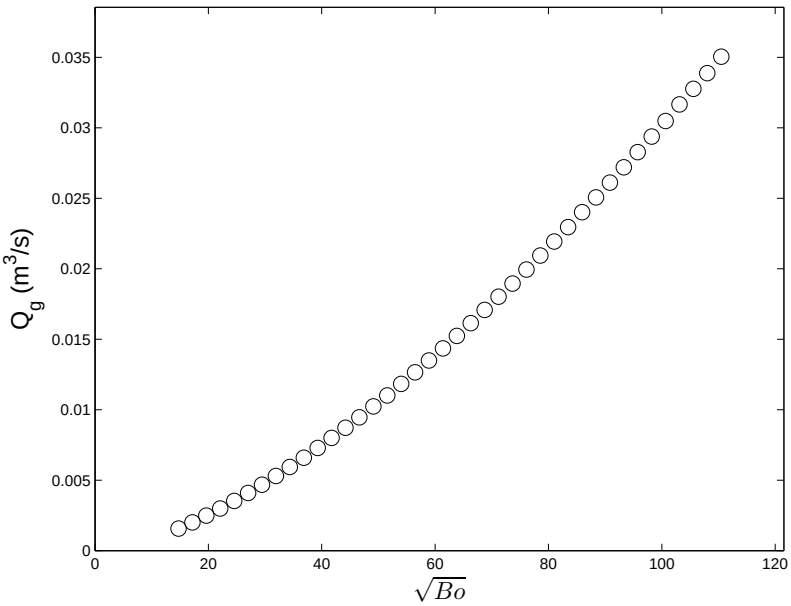

Fig. 6.1. Gas volumetric flow rate as a function of the square root of the Bond number for diameter dependence demonstration case.

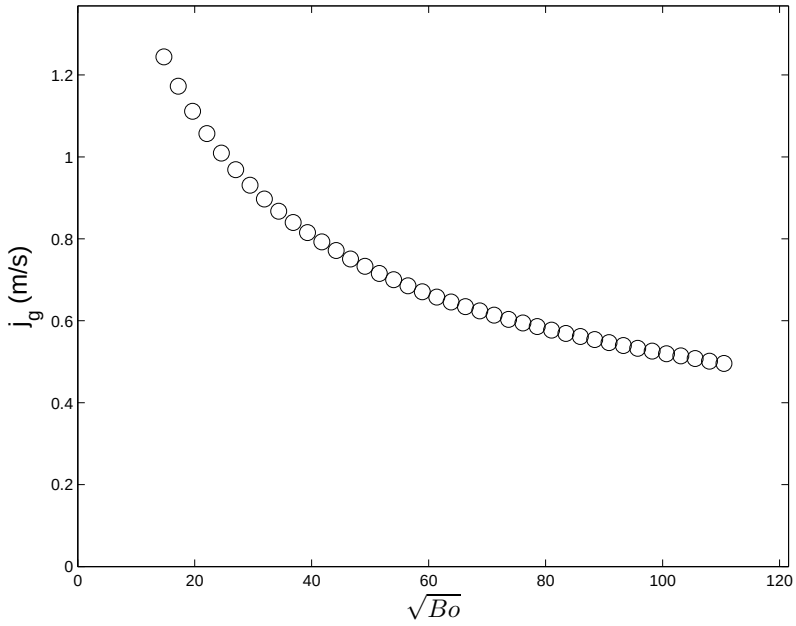

Fig. 6.2. Gas superficial velocity as a function of the square root of the Bond number for diameter dependence demonstration case.

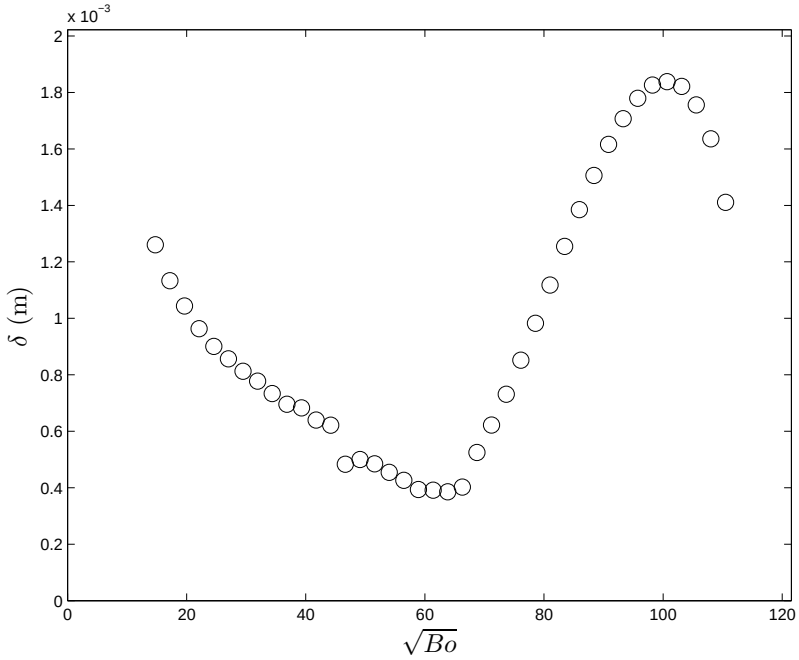

Fig. 6.3. Film thickness as a function of the square root of the Bond number for diameter dependence demonstration case.

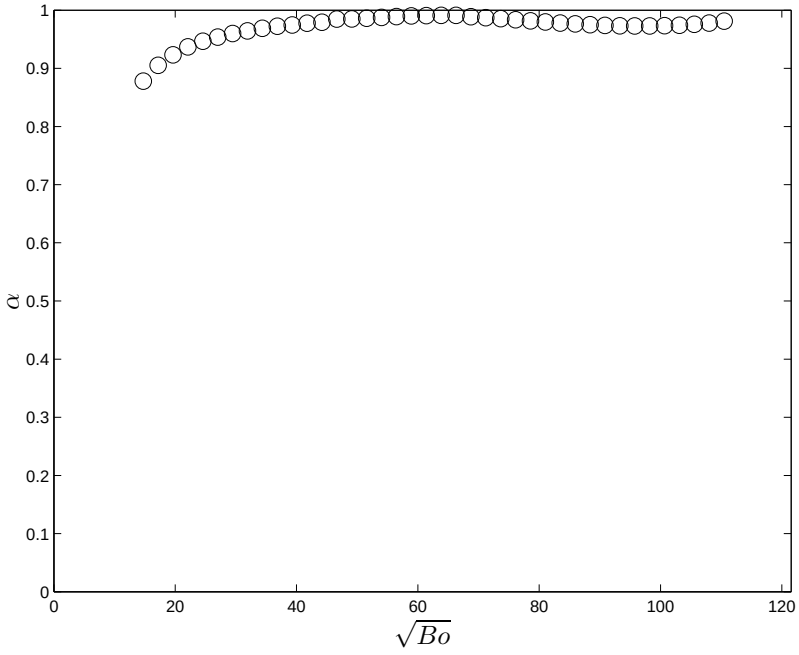

Fig. 6.4. Void fraction as a function of the square root of the Bond number for diameter dependence demonstration case.

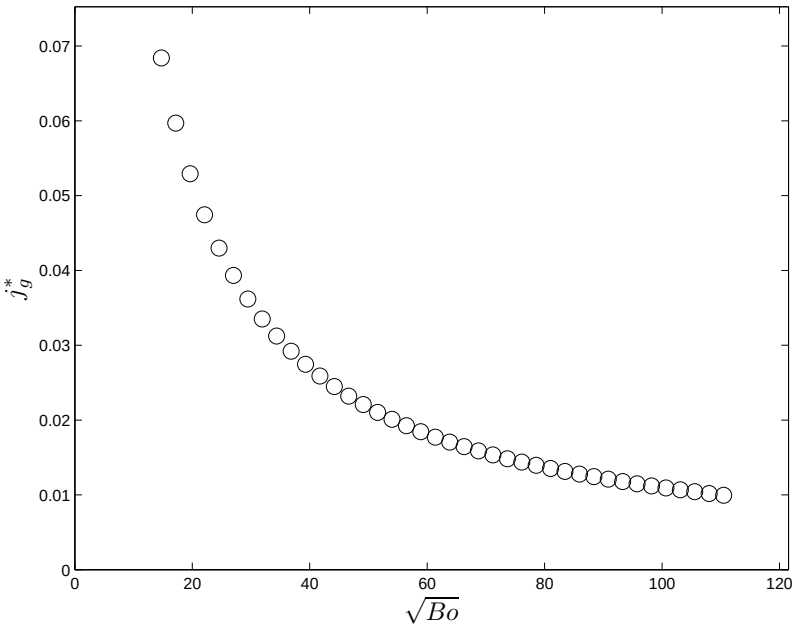

Fig. 6.5. Gas Wallis parameter as a function of the square root of the Bond number for diameter dependence demonstration case.

terize systems where flooding occurs. Specifically, the functional dependence of these three dimensionless numbers on gravity implies that gravity affects the stability of vertical, counter-current annular flow despite the fact that the gravitational field is normal to the forces that would be affecting flow stability. The effect of gravity on film thickness is established by the model developed in Section 3, but this should have significantly less of an effect than is implied by the Bond number. Although flooding data is known to be characterized in the Wallis and Kutateladze correlations using the aforementioned parameters, it can be inferred that the nature of the curve generated by the correlations contributes more to this success than the description of the physics of flooding. Therefore, the suggestion of a new set of dimensionless numbers based on the new model for flooding is proposed as being a more phenomenologically sound method of describing flooding conditions.

Film Thickness Analysis

The model for average annular film thickness in co- and counter-current flow described in Section 3 is characterized by common dimensionless parameters. The wall shear is governed by the Reynolds number, defined by Equation 3.6. The Reynolds number is, in turn, used to calculate a dimensionless friction factor.

The interfacial shear must be characterized by a term developed from the field equation being used, Equation 3.9. Dividing Equation 3.9 by $g_z\left(\rho_g-\rho_f\right)$ yields

$$1=\frac{\tau_{wf}P_{wf}}{g_zA\left(\rho_g-\rho_f\right)\left(1-\langle\alpha_g\rangle\right)}-\frac{\tau_iP_i}{g_zA\left(\rho_g-\rho_f\right)\left(1-\langle\alpha_g\rangle\right)}-\frac{\tau_iP_i}{Ag_z\left(\rho_g-\rho_f\right)\langle\alpha_g\rangle}. \quad (6.31)$$

From this equation, it can be seen that the term

$$T_\tau=\frac{\tau_iP_i}{g_zA\left(\rho_g-\rho_f\right)\langle\alpha_g\rangle} \quad (6.32)$$

represents the momentum loss of the fluid due to interfacial shear stress on the gas flow. Substituting the definition of τ_i, Equation 3.13, into Equation 6.32 results in

$$T_\tau = \frac{\left(\frac{f_i \rho_g \left|\overline{v_r}\right| \overline{v_r}}{2}\right) P_i}{g_z A \left(\rho_g - \rho_f\right) \langle \alpha_g \rangle} \tag{6.33}$$

with $(j_f - j_g)$ used as the definition of relative velocity, v_r. The interfacial friction factor, f_i, is found using a semi-empirical correlation that is dependent on the void fraction and can be neglected in the development of this dimensionless number. Therefore, neglecting f_i and replacing the relative velocity with this quantity, the term can be rewritten

$$T_\tau = \frac{\left(\frac{\rho_g \left(\langle j_f \rangle - \langle j_g \rangle\right)^2}{2}\right) P_i}{g_z A \left(\rho_f - \rho_g\right) \langle \alpha_g \rangle}. \tag{6.34}$$

The interfacial wetted perimeter, P_i, can be calculated as

$$P_i = 2\pi \bar{a}, \tag{6.35}$$

with $\bar{a}$ being the average circumferential radius between the tube centerline and the gas-liquid interface. As the cross-sectional area of the tube, A is

$$A = \pi R^2. \tag{6.36}$$

the presence of the void fraction in Equation 6.34 relates the cross-sectional area of the gas to the tube cross sectional area as

$$\langle \alpha_g \rangle = \frac{\bar{a}^2}{R^2}. \tag{6.37}$$

Therefore,

$$\frac{P_i}{A \langle \alpha_g \rangle} = \frac{2\pi \bar{a}}{\pi R^2 \frac{\bar{a}^2}{R^2}} = \frac{2}{\bar{a}}. \tag{6.38}$$

Using this information, Equation 6.34 reduces to

$$T_\tau = \frac{\rho_g \left(\langle j_f \rangle - \langle j_g \rangle\right)^2}{\bar{a} g_z \left(\rho_f - \rho_g\right)}. \tag{6.39}$$

If the density ratio is then neglected (as it will be considered in the "Stability Analysis"), this equation simplifies to

$$T_\tau = \frac{\left(\langle j_f \rangle - \langle j_g \rangle\right)^2}{\bar{a} g_z}. \tag{6.40}$$

As the average distance from the tube centerline to the gas-liquid interface is the term that is being calculated using Equation 3.9, the term $\bar{a}$ should be replaced by a parameter of the dimension of distance that has a strong relation to the term $\bar{a}$. One such parameter would be the tube diameter, D. This allows T_τ to be written

$$T_\tau = \frac{\left(\langle j_f \rangle - \langle j_g \rangle\right)^2}{g_z D}. \tag{6.41}$$

The term is now cast in terms of the Froude number [71], as

$$\mathrm{Fr}^2 = \frac{\left(\langle j_f \rangle - \langle j_g \rangle\right)^2}{g_z D}. \tag{6.42}$$

The Froude number is a ratio of the inertia force to the gravitational force, and, like the Reynolds number, has a weak effect on the stability of annular counter-current flows via the film thickness closure relation.

Stability Analysis

Though the calculation of the average annular film thickness is clearly defined by several dimensionless numbers, the dependence of flooding on these parameters should be weaker than its dependence on the parameters that can be derived from Equation 6.30. These dimensionless parameters can be determined by non-dimensionalizing Equation 5.40 as

$$0 < -\frac{\gamma\left(k^2a^2-1\right) I_1\left(ka\right)}{ka} + \frac{a\rho_f\rho_g\xi\gamma\left(\langle j_f \rangle - \langle j_g \rangle\right)^2 I_1\left(ka\right) I_0\left(ka\right)\left(\rho_f\xi I_1\left(ka\right) - \rho_g\gamma I_0\left(ka\right)\right)}{\sigma\left(\rho_f\xi I_1\left(ka\right) - \rho_g\gamma I_0\left(ka\right)\right)^2}. \tag{6.43}$$

The first dimensionless parameter considered is ka, a dimensionless wave number, which represents the maximum product of the wave number and distance from the

tube centerline to the gas-liquid interface. This quantity was previously calculated in Section 5.2.8. Using this parameter, dimensionless densities for the liquid and the gas phase can be constructed as

$$\rho_f^* = \frac{\rho_f}{\rho_f \xi I_1(ka) - \rho_g \gamma I_0(ka)} \tag{6.44}$$

and

$$\rho_g^* = \frac{\rho_g}{\rho_f \xi I_1(ka) - \rho_g \gamma I_0(ka)}. \tag{6.45}$$

The unfortunate dependence of the dimensionless liquid and gas densities on the dimensionless wave number can lead to approximations of ρ_f^* and ρ_g^* as

$$\rho_f^* \approx \frac{\rho_f}{\rho_f - \rho_g} \tag{6.46}$$

and

$$\rho_g^* \approx \frac{\rho_g}{\rho_f - \rho_g}. \tag{6.47}$$

Finally, the remaining parameters can be grouped to form a term that resembles a modified Weber number,

$$\widetilde{\mathrm{We}} = \frac{\left(\rho_f \xi I_1(ka) - \rho_g \gamma I_0(ka)\right)\left(\langle j_f \rangle - \langle j_g \rangle\right)^2 a}{\sigma}, \tag{6.48}$$

where the Weber number is a ratio of the inertia force to the surface tension force. Employing the assumptions previously used to describe the density difference and the parameter a, a more practical Weber number can be constructed and written as

$$\mathrm{We} = \frac{\left(\rho_f - \rho_g\right)\left(\langle j_f \rangle - \langle j_g \rangle\right)^2 D}{\sigma}. \tag{6.49}$$

Summary

A summary of the dimensionless parameters that have been determined to characterize the stability-based model of flooding developed in Section 5 is given by Table 6.2. While the inertia force appears in several parameters, these dimensionless terms are derived from two separate but coupled field equations and are therefore the

most appropriate parameters that can be used to model flooding based on the models that have been developed in this dissertation. The derivation of an empirical correlation for flooding based on these parameters could be developed, but this method of correlation would require a plethora of adiabatic flooding data points from numerous experimental facilities. It is important to note the expected relative influence of

Table 6.2
Dimensionless numbers found to characterize flooding.

Number	Definition	Meaning	Model of Origin
Re	$\frac{\rho_f \left\|\langle j_f \rangle\right\| D}{\mu_f}$	$\frac{\text{inertia force}}{\text{viscous force}}$	film thickness
Fr	$\sqrt{\frac{\left(\langle j_f \rangle - \langle j_g \rangle\right)^2}{g_z D}}$	$\frac{\text{inertia force}}{\text{gravitational force}}$	film thickness
k^*	ka	relationship between wave number and gas core radius	stability
We	$\frac{\left(\rho_f - \rho_g\right)\left(\langle j_f \rangle - \langle j_g \rangle\right)^2 D}{\sigma}$	$\frac{\text{inertia force}}{\text{surface tension force}}$	stability
ρ_f^*	$\frac{\rho_f}{\rho_f - \rho_g}$	impact of liquid density	stability
ρ_g^*	$\frac{\rho_g}{\rho_f - \rho_g}$	impact of gas density	stability

each dimensionless number on determining the pairs of data that describe flooding. The dependence of the stability model on the Reynolds and Froude numbers should be less significant than that of the remaining terms due to the limited roll of the film thickness model in the stability model. Overall, the Weber number and the dimensionless wave number should have the most profound effect on the prediction of flooding. Particularly, the method of determining the value of ka used in Section 5 has a controlling effect on the stabilizing term of the flooding model. Previous work

by Zapke and Kroger [72, 73] has identified that flooding can be correlated to the Froude number, defined above, and the Ohnesorge number, which is defined as

$$\mathrm{Oh} = \frac{\sqrt{\mathrm{We}}}{\mathrm{Re}}. \tag{6.50}$$

Using these parameters to correlate flooding data via experimental observation implies possible success in using the newly developed stability model of flooding, though the use of the Ohnesorge number may incorrectly represent the relative importance of the Weber and Reynolds numbers by fixing the relative magnitude of the terms.

6.2 Validation

Quantitative assessment of the stability-based model of flooding is accomplished by validating the model with experimental data. The available literature on flooding in vertical adiabatic tubes that contain annular counter-current flows was surveyed, and two sets of experimental data are used to perform a numerical analysis of the stability-based model for flooding.

6.2.1 Description of Validation Data

Although there has been extensive research on flooding in vertical adiabatic tubes, two major issues preclude the use of this data for validating the stability-based model of flooding that has been developed: unavailability of a majority of data and the low fidelity of a significant set of the data that is attainable. A significant quantity of experimental data issued at Atomic Energy Research Establishment (AERE, see Bankoff and Lee [2] for examples) has been used in work from previous decades, but efforts to find many of these reports either yielded no results or provided documents that did not include experimental data. While numerous sources cite and use experimental data from the work of Bharathan and Wallis [47], including Bankoff and Lee [2] and McQuillan and Whalley [7], it was found that the liquid flow rate into

the test section of their experiment was not measured with appropriate electronic instrumentation, but rather by analyzing the length of time it took the water exiting the test section to fill a vessel of known volume. This method is not only inaccurate but results in experimental data that does not reflect the flow rate actually entering the test section via liquid injection method. Following extensive research, it was concluded that two experimental data sets could best be used to validate the stability-based model of flooding developed in Section 5: the data of Williams [55] and Tien, Chung, and Liu [56].

Data of Williams

The test section for the facility of Williams [55] consists of an approximately 1.8 m long tube that is 76.2 mm in diameter. The working fluids in this experiment are air and water. Water enters the tube via an upper plenum that fills and releases water via twelve equally spaced holes around the periphery of the top of the test section. This water flows down the walls of the tube, forming a liquid annulus. Air is injected into the test section directly by using a nozzle that is placed in the bottom of the test section.

In order to conduct each experiment, the liquid flow rate is fixed before entering the test section and the gas flow rate is increased incrementally until flooding occurs. This flow reverse was noted by detecting a sudden change in the pressure drop over the length of the test section by using a differential pressure transducer.

While the experimental data of Williams [55] does not cover a wide range of operating conditions, the data appears to be of high quality in that none of the reported values appear to be counterintuitive and unphysical. The experimental measurements provided are a good set of validation data, albeit over a limited range of parameters.

Data of Tien, Chung, and Liu

In the experiments of Tien, Chung, and Liu [56], tubes of 15.9 mm, 31.8 mm, 46.0 mm, and 69.9 mm in diameter and 0.914 m in length are used in the battery of experimental tests. Liquid is introduced into the tube by using the "top flood" method, where the liquid is introduced into an upper plenum, accumulates in that plenum, and then overflows down the inside of the tube wall, forming an annulus. The liquid inlet or outlet can be sharp edged or tapered. Gas is introduced into the tube either by directly entering the nozzle in the test section or by indirectly entering from a lower plenum. Air is the only gas used in these experiments, and the liquids used include water, water with Surfynol (a surfactant), silicon oil, and Chevron white oil.

The experimental facility is operated similarly to that of Williams [55] in terms of setting and changing fluid flow rates. Flooding is identified by Tien, Chung, and Lieu as having occured by monitoring the test section pressure for a sudden change, as well as by observing the "chaotic flow pattern" that formed following flooding via the transparent test section. More information regarding the experimental facility or test procedures can be found in reference [56].

Following an initial analysis of the data reported by Tien, Chung, and Liu [56], it was concluded that the overall quality of the reported values was not exceptional in all cases and was unusable in a subset of cases. Several combinations of tube diameters, inlet and outlet conditions, fluids and injection methods provided results that appeared inconsisttnt, and all of the sets of flooding data for white oil appear to display no discernable trend. Additionally, it can be seen in the results shown in Section 6.2.2 that the gas flow rates needed to cause flooding appear to have been "overshot," meaning that care was not taken to identify exactly the conditions causing flooding while the gas flow rate was being increased. The data reported by Tien, Chung, and Lieu that are used as validation data are those sets which include decreasing gas superficial velocities for increasing liquid delivery rates and do not

appear to include flooding conditions that would not allow for momentum to be conserved in the unperturbed system. These data sets are identified in Appendix F.

6.2.2 Model Performance and Results

The stability-based model for the prediction of flooding developed in Section 5 has been used to analyze the experimental data of Williams [55] and Tien, Chung, and Liu [56]. A plot of the results for Williams' data [55] in terms of superficial velocity is shown in Figure 6.6 and a plot of the Wallis parameter is shown in Figure 6.7. It can clearly be seen that there are three distinct sets of data in these figures (from top to bottom): a set of flow reversal values determined by considering a momentum balance between the fluids, experimental data, and a set of values determined by using the new stability theory of flooding. A similar trend can be seen in the calculation of the experimental results of Tien, Chung, and Liu [56], shown in Figure 6.8 and Figure 6.9. The three groups of results are more pronounced due to the increased number of points analyzed, particularly in regards to the plot of Wallis parameters shown in Figure 6.9. It should be noted that Figure 6.8 and Figure 6.9 show all experimental points analyzed without distinction of experimental test sets. Results for each experimental set are provided in Appendix F.

To quantify the assessment of both the momentum balance and stability-based models of flooding, the standard deviation of the relative error is used as the figure of merit. As the standard deviation of the relative error is the same between the superficial velocity comparison and the comparison of Wallis parameters, the error for the momentum balance and stability analysis are defined in terms of the superficial velocity as

$$\sigma_{\text{model}} = \sqrt{\frac{\sum_{i=1}^{N} \left(\frac{\left\langle j_g^* \right\rangle_{\text{model}}}{\left\langle j_g^* \right\rangle_{\text{exp}}} - 1 \right)_i^2}{N-1}}. \tag{6.51}$$

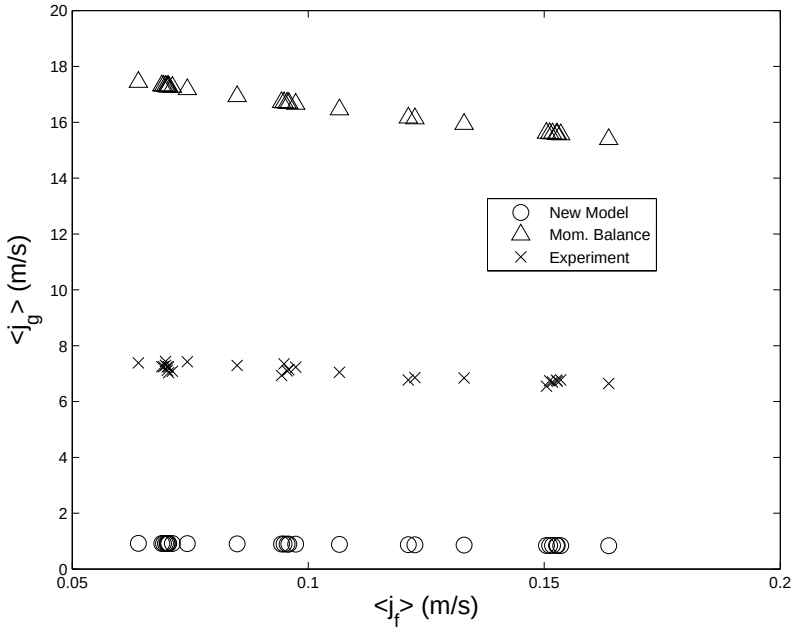

Fig. 6.6. Comparison between Williams' air-water data [55], new stability model, and momentum-based model of superficial velocities for flooding.

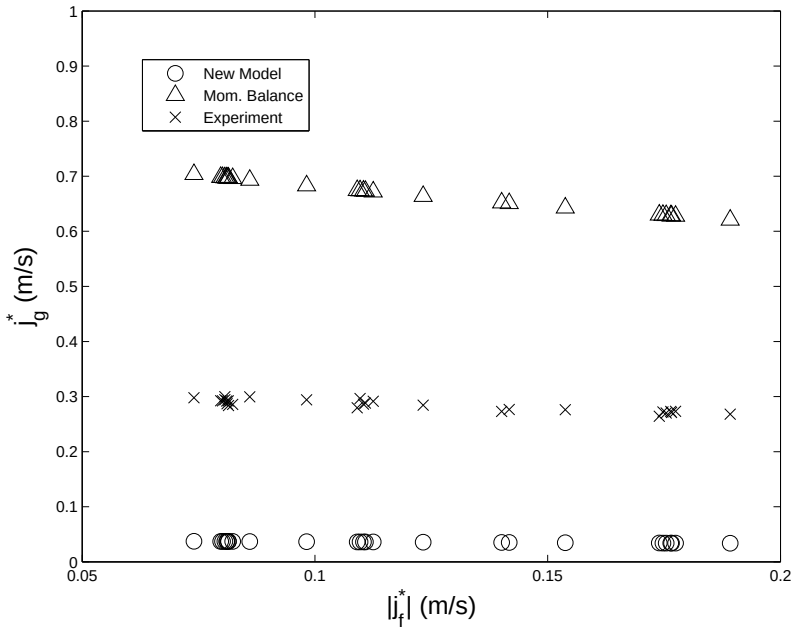

Fig. 6.7. Comparison between Williams' air-water data [55], new stability model, and momentum-based model of Wallis parameters for flooding.

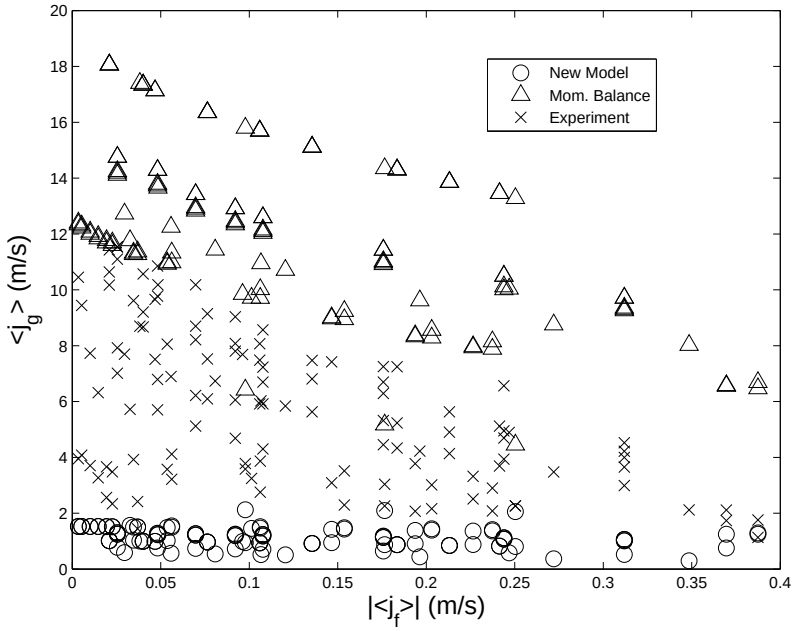

Fig. 6.8. Comparison between Tien, Chung, and Liu's data [56], new stability model, and momentum-based model of superficial velocities for flooding.

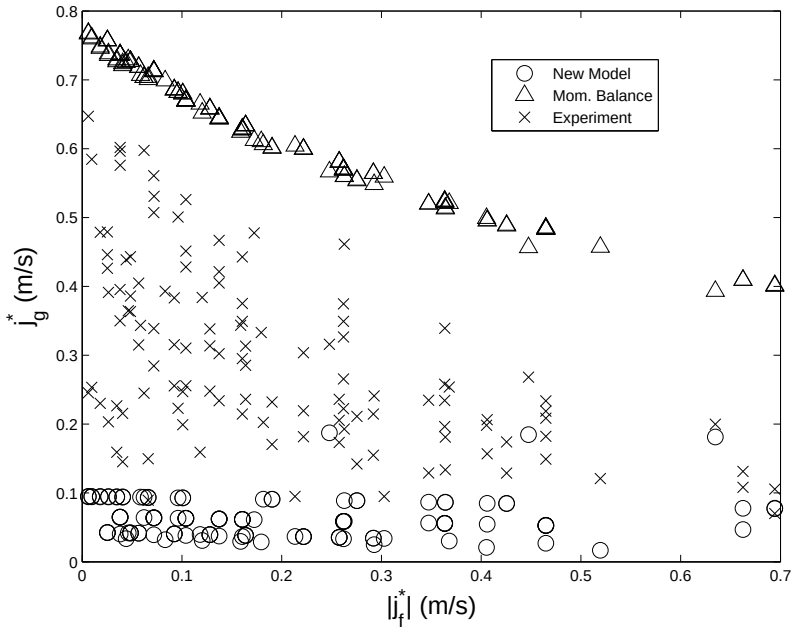

Fig. 6.9. Comparison between Tien, Chung, and Liu's data [56], new stability model, and momentum-based model of Wallis parameters for flooding.

The experimental error reported by Williams [55] is approximately 10%, and that of Tien, Chung, and Liu [56] is not reported. Table 6.3 shows the standard deviation of the relative error for both sets of analyzed data. By comparing Figures 6.6, 6.7, 6.8, and 6.9 and Table 6.3, it can be seen that while, quantitatively, the standard deviation of the relative error of the stability-based model is better than that of the momentum-based model, the graphical representation of the standard deviations show that both sets of predictions are inaccurate. The analysis with the momentum-based model is consistently overpredicting the gas flow rate needed to cause flooding, while the computational results of the stability-based model are consistently conservative.

The underprediction of the gas flow rates when using the stability-based model may be attributable to the use of the finite amplitude wave assumption employeed in Section 5.2.8. The work of Kordyban and Ranov [69] and Mishima and Ishii [61] both demonstrate the underprediction of experimental stability data for two-phase co-current flows in rectangular ducts. It is hypothesized that the cylindrical geometry coupled with the annular flow pattern in this analysis increases the conservatism inherent in applying this method to vertical counter-current annular flows. As the mathematical analysis of the stability-based model in Section 6.1 indicated that the model should be able to predict stability criteria for flooding in principle, further research is suggested in the determination of the closure relations to the model. Using the result of the finite amplitude analysis, the wave number can be found by considering the relation

$$ka = 1.6 \tag{6.52}$$

with $k = 2\pi/\lambda$. Estimating the value of a as the tube radius, 38.1 mm, the wavelength used in determining the stability of the flow is found to be about 30 mm. A continuous wave of this wavelength may not be reasonable to observe in the rough film that has been noted immediately before flooding. An improved estimate of

the dimensionless wave number, $k^* = ka$, should provide a better estimate as to appropriate prediction of the conditions that will cause flooding to occur.

Table 6.3
Standard deviation of the relative error for validation data.

Experiment	Model	σ (%)
Williams [55]	momentum-based	138
	stability-based	89
Tien, Chung, and Liu [56]	momentum-based	188
	stability-based	76

7. CONCLUSIONS

Counter-current flow and flooding in vertical adiabatic tubes have been analytically studied. A literature survey of previous methods of predicting flooding in many systems by using empirical, semi-empirical, and "theoretical" models of flooding was conducted, leading to the conclusions that:

- even as research is conducted on complex phenomena and their relation to flooding, there is no major consensus on what the mechanistic cause of flooding is
- the method of predicting the film thickness in co- and counter-current annular flows did not rigorously model the physics of annular flow systems and did not produce very accurate quantitative results
- most theoretical models of flooding are actually semi-empirical and rely on parameters correlating to experimental data
- models classified as "semi-empirical models" are the primary method of calculating flooding conditions
- the two primary models used to predict flooding, the Wallis and Kutateladze correlations, are essentially methods to curve-fit data using empirical coefficients

These assessments led to the following objectives of this dissertation:

1. the development of a model for average annular film thickness for co- and counter-current flow that produces better quantitative results and provides a better physics-based methodology of calculation
2. the identification of the mechanism of flooding in the simplest configuration, that of counter-current flow in a vertical adiabatic tube, to allow for the devel-

opment of more appropriate models of flooding in more complex systems for future work

3. the derivation of a theoretical model for flooding based on the mechanism identified, an imbalance of momentum of the flow, that can serve as a basis for work in systems such as flooding in the presence of heat transfer and condensation, as well as inclined tubes

A model for average annular film thickness for co- and counter-current flow in vertical adiabatic tubes has been developed that outperforms the commonly used model that was posed by Wallis [11] and based on the models of Nusselt [42] and Belkin, Macleod, Monrad, and Rothfus [43]. Based on a momentum equation previously used for the successful prediction of drift velocity, the field equation for the new film thickness model accurately captures the phenomena necessary to model a flow that is known to be vertical and annular. The new model better considers the effects of interfacial shear and tube curvature by using closure relations known to appropriately represent forces in co- and counter-current flow. Supplementing this model with improved closure relations for annular flow can augment its predictive capabilities. The new model shows significant quantitative improvement when compared to experimental data and is recommended for future film thickness calculations. Future work to improve the new film thickness model should include validation with additional experimental data sets, including microgravity systems and additional counter-current film thickness data.

The equation posed as a new model for annular film thickness was used to investigate semi-empirical models of flooding using work by Ohkawa and Lahey [40]. The result of this analysis is the theory that flooding is the result of the need for momentum to be conserved in a counter-current flow following a decrease in void fraction due to interfacial wave growth. Therefore, the calculation of the conditions that cause this interfacial wave growth is requisite to predict flooding.

A model was derived to represent wave growth due to interfacial instability in a two-phase counter-current vertical adiabatic tube. Using the assumption that the liquid and gas flows can be modeled using potential flow, a condition for instability was derived by considering exponential wave amplitude growth when the wave speed was found to have an imaginary component. This stability model appropriately represents the boundary conditions of a solid wall at the tube periphery, a wave evolving in time and space at the gas-liquid interface, and the need for the fluid properties to be finite at the tube center. Following the formulation of this stability criteria, closure relations for the unknown wave numbers in the flow were developed by using the assumption of waves of finite amplitude.

An analytical assessment of the stability-based model of flooding was conducted to verify the physical basis of the model. It was shown that this model can be simplified to represent Rayleigh's model of the stability of a vibrating jet in an infinitely large fluid with neither fluid moving in the axial direction. The dependence of the stability model on the tube diameter and system Bond number was investigated and was found to be similar to the dependence that is experimentally observed. By analyzing the flooding stability equation and film thickness model, dimensionless numbers, including the Reynolds number, Froude number, Weber number, and dimensionless densities and wave number were found to characterize the flow. Finally, a quantitative validation of the new stability model was conducted against two experimental data sets. The new model for flooding underestimated the gas superficial velocity needed to cause flooding for a specific liquid superficial velocity, most likely due to the fact that the finite wave amplitude assumption is known to underpredict the stability condition of one flow rate in a system when the other fluid flow rate is fixed. When applied to the analysis of nuclear reactors, specifically pressurized water reactors, the new stability is conservative in that the gas flow rate predicted to cause flooding for a fixed liquid flow rate will be less than the flow rate found experimentally. Therefore, the liquid delivery to the reactor core during an accident would be

safely underestimated. Future work will include procuring of, and validation with, more sets of experimental data and improved theoretical closure relations for the wave number. Following this, this model can be extended to analyze flooding in the presence of heat transfer, condensation, and additional system geometries, as well as serve as a theoretical basis for the prediction of flooding in complex flow geometries.

REFERENCES

[1] K. Takeuchi, M.Y. Young, A.F. Gagnon, Flooding in the pressurizer surge line of AP600 plant and analyses of APEX data, Nucl. Eng. Des. 192 (1) (1999) 45–58.

[2] S.G. Bankoff, S.C. Lee, A critical review of the flooding literature, NUREG/CR-3060, Northwestern University, Evanston, IL, July 1983.

[3] M.A. Navarro, Study of countercurrent flow limitation in a horizontal pipe connected to an inclined one, Nucl. Eng. Des. 235 (10–12) (2005) 1139–1148.

[4] Y. Liao, K. Vierow, MELCOR analysis of steam generator tube creep rupture in station blackout severe accident, Nucl. Eng. Des. 152 (3) (2005) 302–313.

[5] A.H. Govan, G.F. Hewitt, H.J. Richter, A. Scott, Flooding and churn flow in vertical pipes, International J. Multiphase Flow 17 (1) (1991) 27–44.

[6] Deendarlianto, A. Ousaka, A. Kariyasaki, T. Fukano, Investigation of liquid film behavior at the onset of flooding during adiabatic counter-current air–water two-phase flow in an inclined pipe, Nucl. Eng. Des. 235 (21) (2005) 2281–2294.

[7] K.W. McQuillan, P.B. Whalley, Comparison between flooding correlations and experimental flooding data for gas-liquid flow in vertical circular tubes, Chem. Eng. Sci. 40 (8) (1985) 1425–40.

[8] D. Bessette, M. Di Marzo, Transition from depressurization to long term cooling in AP600 scaled integral test facilities, Nucl. Eng. Des. 188 (3) (1999) 331–344.

[9] G.B. Wallis, Flooding velocities for air and water in vertical tubes, AEEW-R-123, United Kingdom Atomic Energy Authority. Reactor Group. Atomic Energy Establishment, Winfrith, Dorset, UK, December 1961.

[10] A. Zapke, D.G. Kroger, The influence of fluid properties and inlet geometry on flooding in vertical and inclined tubes, Int. J. Multiphase Flow 22 (3) (1996) 461–472.

[11] G.B. Wallis, One-Dimensional Two-Phase Flow, first ed., McGraw-Hill Book Company, New York, 1969, pp. 315–344.

[12] N.E. Todreas, M.S. Kazimi, Nuclear Systems I: Thermal Hydraulic Fundamentals, first ed., Taylor & Francis, New York, 1993, pp. 463–467.

[13] M. Solmos, An experimental investigation of the countercurrent flow limitation, MS thesis, Texas A&M University, College Station, TX, 2008.

[14] H. Richter, Flooding in tubes and annuli, Int J. Multiphase Flow 7 (6) (1981) 647–658.

[15] S. Levy, Two-Phase Flow in Complex Systems, first ed., Wiley, New York, 1999, pp. 264–299.

[16] Y. Taitel, D. Barnea, A.E. Dukler, Modelling flow pattern transitions for steady upward gas-liquid flow in vertical tubes, AIChE Journal 26 (3) (1980) 345–354.

[17] S.M. Ghiaasiaan, X. Wu, D.L. Sadowski, S.I. Abdel-Khalik, Hydrodynamic characteristics of counter-current two-phase flow in vertical and inclined channels: effects of liquid properties, Int. J. Multiphase Flow 23 (6) (1997) 1063–1083.

[18] D. Barnea, A unified model for predicting flow-pattern transitions for the whole range of pipe inclinations, Int. J. Multiphase Flow 13 (1) (1987) 1–12.

[19] G.B. Wallis, J.T. Kuo, The behavior of gas-liquid interfaces in vertical tubes, Int. J. Multiphase Flow 2 (5-6) (1976) 521–536.

[20] G.B. Wallis, S. Makkenchery, The hanging film phenomenon in vertical annular two-phase flow, J. Fluids Eng 3 (1) (1974) 297–298.

[21] C.J. Shearer, J.F. Davidson, The investigation of a standing wave due to gas blowing upwards over a liquid film; its relation to flooding in wetted-wall columns, J. Fluid Mech. 22 (02) (1965) 321–335.

[22] D. Nicklin, J. Davidson, The onset of instability in two-phase slug flow, in: Proceedings of the Symposium on Two-Phase Fluid Flow, 1962.

[23] A.A. Mouza, S.V. Paras, A.J. Karabelas, Incipient flooding in inclined tubes of small diameter, Int. J. Multiphase Flow 29 (9) (2003) 1395–1412.

[24] D. Moalem Maron, A.E. Dukler, Flooding and upward film flow in vertical tubes II: Speculations on film flow mechanisms, Int. J. Multiphase Flow 10 (5) (1984) 599–621.

[25] R. Clift, C.L. Pritchard, R.M. Nedderman, The effect of viscosity on the flooding conditions in wetted wall columns, Chem. Eng. Sci. 21 (1) (1966) 87–95.

[26] Deendarlianto, C. Vallee, D. Lucas, M. Beyer, H. Pietruske, H. Carl, Experimental study on the air/water counter-current flow limitation in a model of the hot leg of a pressurized water reactor, Nucl. Eng. Des. 238 (12) (2008) 3389–3402.

[27] S. Wongwises, Flooding in a horizontal pipe with bend, Int. J. Multiphase Flow 22 (1) (1996) 195 – 201.

[28] S. Wongwises, Effect of inclination angles and upper end conditions on the countercurrent flow limitation in straight circular pipes, International Communications in Heat and Mass Transfer 25 (1) (1998) 117–125.

[29] S. Fiedler, H. Auracher, D. Winkelmann, Effect of inclination on flooding and heat tranfer during reflux condensation in a small diameter tube, International Communications in Heat and Mass Transfer 29 (3) (2002) 289–302.

[30] K.Y. Choi, H.C. No, Experimental studies of flooding in nearly horizontal pipes, Int. J. Multiphase Flow 21 (3) (1995) 419–436.

[31] J.I.H. Jeong, H.C. No, Classification of flooding data according to type of tube-end geometry, Nucl. Eng. Des. 148 (1) (1994) 109–117.

[32] K.H. Ardron, S. Banerjee, Flooding in an elbow between a vertical and a horizontal or near-horizontal pipe II: Theory, Int. J. Multiphase Flow 12 (4) (1986) 543–558.

[33] H. Siddiqui, S. Banerjee, K.H. Ardron, Flooding in an elbow between a vertical and a horizontal or near-horizontal pipe I: Experiments, Int. J. Multiphase Flow 12 (4) (1986) 531–541.

[34] G.P. Celata, M. Cumo, T. Setaro, Flooding in inclined pipes with obstructions, Exp. Therm. Fluid Sci. 5 (1) (1992) 18–25.

[35] M. Ishii, T. Hibiki, Thermo-Fluid Dynamics of Two-Phase Flow, first ed., Springer Verlag, New York, 2006, pp. 48–54,387-405.

[36] S.S. Kutateladze, Elements of the hydrodynamics of gas-liquid systems, Fluid Mechanics-Soviet Research 1 (4) (1972) 29-50.

[37] O.L. Pushkina, Y.L. Sorokin, Breakdown of liquid film motion in vertical tubes, Heat Transfer Sov. Res 1 (5) (1969) 56–64.

[38] C.L. Tien, A simple analytical model for counter-current flow limiting phenomena with vapor condensation, Lett. Heat Mass Transfer 4 (3) (1977) 231–238.

[39] S.K. Chung, L.P. Liu, C.L. Tien, Flooding in two-phase counter current flows–I analytical modeling, Physicochem. Hydrodyn. 1 (2-3) (1980) 195–207.

[40] K. Ohkawa, R.T. Lahey, The analysis of CCFL using drift-flux models, Nucl. Eng. Des. 61 (2) (1980) 245–255.

[41] N. Zuber, J.A. Findlay, Average volumetric concentration in two-phase flow systems, J. Heat Transfer 87 (3) (1965) 453–468.

[42] W. Nusselt, Die oberflachen-kondensation des wasserdampfes, Z. Ver. Deutch. Ing 60 (27) (1916) 541–546.

[43] H. Belkin, A. Macleod, C. Monrad, R. Rothfus, Turbulent liquid flow down vertical walls, AIChE Journal 5 (2) (1959) 245–248.

[44] R.W. Fox, P.J. Pritchard, A.T. McDonald, Introduction to Fluid Mechanics, seventh ed., Wiley, New York, 2006, pp. 19–44,215–255.

[45] M. Ishii, T.C. Chawla, N. Zuber, Constitutive equation for vapor drift velocity in two-phase annular flow, AIChE Journal 22 (2) (1976) 283–289.

[46] S.G. Bankoff, S. Lee, A critical review of the flooding literature, Multiphase Science and Technology 2 (1-4) (1984) 95–180.

[47] D. Bharathan, G.B. Wallis, H.J. Richter, Air-water countercurrent annular flow, EPRI Report No. NP-786, Dartmouth College, Hanover, NH, interim report 1978.

[48] C.E. Lacy, Flooding and wavy films in vertical annular gas-liquid flows, PhD thesis, University of Houston, Houston, TX, 1992.

[49] J.C. Asali, Entrainment in vertical gas-liquid annular flows, PhD thesis, University of Illinois, Urbana, 1983.

[50] L.B. Fore, A.E. Dukler, Droplet deposition and momentum transfer in annular flow, AIChE Journal 41 (9) (1995) 2040–2046.

[51] R.M. MacGillivray, Gravity and gas density effects on annular flow average film thickness and frictional pressure drop, PhD thesis, University of Saskatchewan, Saskatoon, Saskatchewan, Canada, 2004.

[52] A. Wolf, S. Jayanti, G.F. Hewitt, Flow development in vertical annular flow, Chemical Engineering Science 56 (10) (2001) 3221–3235.

[53] S.A. Klein, EES–Engineering Equation Solver, Academic Commercial, V8.181-3D, F-Chart Software 2008.

[54] M. Abramowitz, I.A. Stegun, Handbook of Mathematical Functions with Formulas, Graphs, and Mathematical Tables, ninth ed., Dover Publications, New York, 1972, pp. 374–378.

[55] S.N. Williams, Flooding experiments with steam and water in a large diameter vertical tube, MS thesis, Texas A&M University, College Station, TX, 2009.

[56] C.L. Tien, K.S. Chung, C.P. Liu, Flooding in two-phase countercurrent flows, EPRI Report No. NP-1283, University of California, Berkeley, CA, December 1979.

[57] H. Lamb, Hydrodynamics, sixth ed., Dover Publications, New York, 1945, pp. 471–473.

[58] P.G. Drazin, W.H. Reid, Hydrodynamic Stability, second ed., Cambridge University Press, New York, 2004, pp. 14–26.

[59] L. Rayleigh, On the instability of jets, Proceedings of the London Mathematical Society 1 (1) (1878) 4.

[60] N. Zuber, Hydrodynamic aspects of boiling heat transfer, PhD thesis, University of California, Los Angeles, CA, 1959.

[61] K. Mishima, M. Ishii, Theoretical prediction of onset of horizontal slug flow, J. Fluids Eng. 102 (1) (1980) 441–445.

[62] V. Georgevich, Analytical modeling and experimental investigation of interfacial waves in annular microgravity two phase flow, PhD thesis, Texas A&M University, College Station, TX, 1991.

[63] H. Imura, H. Kusuda, S. Funatsu, Flooding velocity in a countercurrent annular two-phase flow, Chem. Eng. Sci. 32 (1) (1977) 79–87.

[64] L.S. Yao, K.H. Sun, On the prediction of the hydrodynamic flooding criterion, in: ASME Symposium on Fluid Flow and Heat Transfer over Rod or Tube Bundles, 1979.

[65] Y. Shibata, F. Kaminaga, Instability of interfacial waves on countercurrent two-phase flow in a vertical tube, JSME International Journal Series B 44 (3) (2001) 352–360.

[66] V.P. Carey, Liquid-Vapor Phase-Change Phenomena, first ed., Hemisphere, Lillington, NC, 1992, pp. 98–105.

[67] G.E. Fischer, I.J. Schwatt, Higher Algebra, first ed., Norwood Press, Norwood, MA, 1901, pp. 491.

[68] G.K. Batchelor, An Introduction to Fluid Dynamics, first ed., Cambridge University Press, New York, 2000, pp. 77-78.

[69] E.S. Kordyban, T. Ranov, Mechanism of slug formation in horizontal two-phase flow, Journal of Basic Engineering 92 (1) (1970) 857–864.

[70] I.G. Currie, Fundamental Mechanics of Fluids, second ed., McGraw-Hill, New York, 2003, pp. 59–61.

[71] B.R. Munson, D.F. Young, T.H. Okiishi, Fundamentals of Fluid Mechanics, fifth ed., Wiley, New York, 2002, pp. 3-1–3-6.

[72] A. Zapke, D.G. Kroger, Countercurrent gas-liquid flow in inclined and vertical ducts II: The validity of the Froude-Ohnesorge number correlation for flooding, Int. J. Multiphase Flow 26 (9) (2000) 1457–1468.

[73] A. Zapke, D.G. Kroger, Countercurrent gas-liquid flow in inclined and vertical ducts II: Flow patterns, pressure drop characteristics and flooding, Int. J. Multiphase Flow 26 (9) (2000) 1439–1455.

[74] L.C. Andrews, Special Functions of Mathematics for Engineers, second ed., McGraw-Hill, New York, 1992, pp. 287–292.

APPENDIX A
MODIFIED BESSEL FUNCTIONS

The following equation is referred to as the modified Bessel equation in rectangular coordinates [54, 74]:

$$x^2\frac{d^2y}{dx^2} + x\frac{dy}{dx} - (x^2 + s^2)y = 0 \tag{A.1}$$

If $s \geq 0$, the solution to Equation A.1 is

$$y = C_1 I_s(x) + C_2 K_s(x). \tag{A.2}$$

where I_s and K_s are the modified Bessel functions of the first and second kind, respectively, of order s. The modified Bessel function of the first kind, I_s, can be defined in terms of a Bessel function of the first kind as

$$I_s(x) = i^{-s} J_s(ix) \tag{A.3}$$

and the modified Bessel function of the second kind, K_s, can be defined as

$$K_s(x) = \frac{\pi}{2}\frac{I_{-s}(x) - I_s(x)}{\sin(s\pi)}. \tag{A.4}$$

Plots of each modified Bessel function for $s = 0, 1, 2, 3$ are shown in Figures A.1 and A.2 and limits of each function are given in Table A.1.

The derivatives with respect to an argument x of the modified Bessel function of the first and second kind are

$$\frac{dI_s(x)}{dx} = I_{s+1}(x) + \frac{sI_s(x)}{x} \tag{A.5}$$

$$\frac{dK_s(x)}{dx} = -K_{s+1}(x) + \frac{sK_s(x)}{x}. \tag{A.6}$$

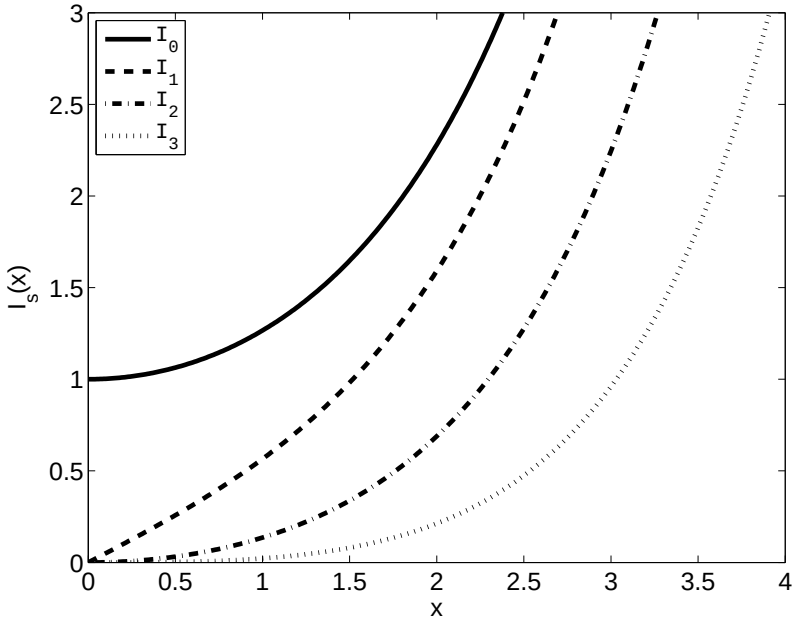

Fig. A.1. Plot of modified Bessel functions of the first kind.

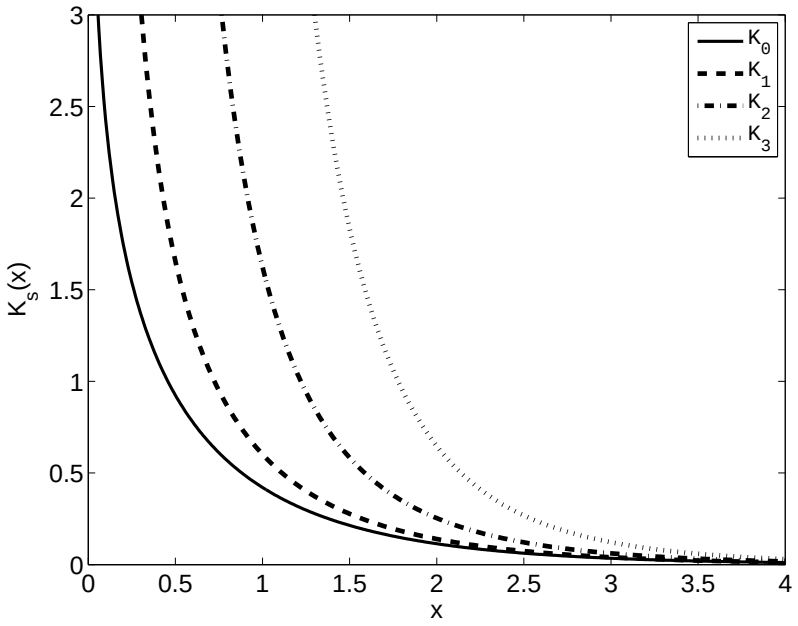

Fig. A.2. Plot of modified Bessel functions of the second kind.

Table A.1
Limits of modified Bessel functions.

Function	$\lim_{x\to 0}$	$\lim_{x\to\infty}$
$I_s(x)$	finite value	∞
$K_s(x)$	∞	0

APPENDIX B
A SOLUTION TO THE REDUCED FORM OF THE LIQUID FILM POTENTIAL FLOW EQUATION

The potential flow of the liquid film is given by Equation 5.7 as

$$\frac{\partial^2 \Phi_{1,f}}{\partial r^2} + \frac{1}{r}\frac{\partial \Phi_{1,f}}{\partial r} + \frac{1}{r^2}\frac{\partial^2 \Phi_{1,f}}{\partial \theta^2} - \Phi_{1,f}k^2 = 0. \tag{5.7}$$

The general solution of this equation has been posed as

$$\Phi_{1,k} = C_1 I_s(kr)\cos(s\theta) + C_2 K_s(kr)\cos(s\theta). \tag{5.8}$$

A unique solution is to be found that satisfies the boundary condition

$$-\frac{\partial \Phi_{1,f}(R)}{\partial r} = 0. \tag{5.10}$$

To determine this solution, the derivative of Equation 5.8 can be calculated to be

$$\frac{\partial \Phi_{1,k}}{\partial r} = C_1\left(I_{s+1}(kr) + \frac{sI_s(kr)}{kr}\right) + C_2\left(-K_{s+1}(kr) + \frac{sK_s(kr)}{kr}\right). \tag{B.1}$$

Substituting Equation B.1 into Equation 5.10 yields

$$0 = C_1\left(I_{s+1}(kR) + \frac{sI_s(kR)}{kR}\right) + C_2\left(-K_{s+1}(kR) + \frac{sK_s(kR)}{kR}\right). \tag{B.2}$$

Equation B.2 can be satisfied for all values of R by choosing values of C_1 and C_2 that cause the first term to always be equivalent to the negative of the second term. This can be accomplished by choosing C_1 and C_2 such that

$$C_1 = \frac{1}{\left(I_{s+1}(kR) + \frac{sI_s(kR)}{kR}\right)} \tag{B.3a}$$

$$C_2 = \frac{-1}{\left(-K_{s+1}(kR) + \frac{sK_s(kR)}{kR}\right)}. \tag{B.3b}$$

When Equation 5.12 is substituted into Equation 5.8, which is then substituted into Equation 5.10, the result can be reduced to

$$0 = 1 - 1 \tag{B.4}$$

which is true for any given value of R.

APPENDIX C
GENERAL WAVE STABILITY CRITERIA FOR ANNULAR COUNTER-CURRENT FLOW

Using Equation 5.32, stability criteria for an annular counter-current flow can be developed for all values of s. In order to develop this criteria, Equation 5.32 must be solved for the wave speed, c. The values which make c imaginary cause the flow to become unstable. This leads to the general stability criterion for counter-current annular flow for all orders, s, of the modified Bessel functions of the first and second kind as

$$0 \leq \Psi_1 + \Psi_2 \tag{C.1}$$

where

$$\Psi_1 = -\frac{\sigma\left[\left(k^2a^2+s^2-1\right)A_1\left(A_2s^2+A_3s+A_4\right)\right]}{k^2a^3\left[\left(A_5\rho_g+A_6\rho_f\right)s^2+\left(A_7\rho_g+A_8\rho_f\right)s+A_9\rho_g+A_{10}\rho_f\right]} \tag{C.2}$$

and

$$\Psi_2 = \frac{\rho_f\left(B_1s+B_2\right)B_3\left(\left(B_4\rho_g+B_5\rho_f\right)s^2+\left(B_6\rho_g+B_7\rho_f\right)s+B_8\rho_g+B_9\rho_f\right)}{4\left[\left(B_{10}\rho_g+B_{11}\rho_f\right)s^2+\left(B_{12}\rho_g+B_{13}\rho_f\right)s+B_{14}\rho_g+B_{15}\rho_f\right]^2}. \tag{C.3}$$

Each variable A_i and B_i were defined to allow for the concise expression of Equation C.2 and Equation C.3 and are defined by the following equations.

$$
\begin{aligned}
A_1 =& kaI_{s+1}(ka) + sI_s(ka) \\
A_2 =& I_s(ka)\,K_s(kR) - I_s(kR)\,K_s(ka) \\
A_3 =& -kRI_{s+1}(kR)\,K_s(ka) + kRI_s(ka)\,K_{s+1}(kR) \\
&+ kaI_{s+1}(ka)\,K_s(kR) + kaK_{s+1}(ka)\,I_s(kR) \\
A_4 =& k^2aRI_{s+1}(ka)\,K_{s+1}(kR) + k^2aRI_{s+1}(kR)\,K_{s+1}(ka) \\
A_5 =& I_s(kR)\,K_s(ka)\,I_s(ka) - (I_s(ka))^2\,K_s(kR) \\
A_6 =& (I_s(ka))^2\,K_s(kR) - I_s(kR)\,K_s(ka)\,I_s(ka) \\
A_7 =& -kaI_s(ka)\,K_s(kR)\,I_{s+1}(ka) - kaI_s(ka)\,K_{s+1}(ka)\,I_s(kR) \\
&- kR(I_s(ka))^2\,K_{s+1}(kR) + kRI_{s+1}(kR)\,K_s(ka)\,I_s(ka) \\
A_8 =& kaI_s(ka)\,K_s(kR)\,I_{s+1}(ka) - kRI_{s+1}(kR)\,K_s(ka)\,I_s(ka) \\
&- kaI_s(kR)\,K_s(ka)\,I_{s+1}(ka) + kR(I_s(ka))^2\,K_{s+1}(kR) \\
A_9 =& -k^2aRI_s(ka)\,K_{s+1}(kR)\,I_{s+1}(ka) - k^2aRI_s(ka)\,I_{s+1}(kR)\,K_{s+1}(ka) \\
A_{10} =& k^2aRI_s(ka)\,K_{s+1}(kR)\,I_{s+1}(ka) - k^2aRI_{s+1}(kR)\,K_s(ka)\,I_{s+1}(ka)
\end{aligned}
$$

$$
\begin{aligned}
B_1 =& I_s(ka)\,K_s(kR) - I_s(kR)\,K_s(ka) \\
B_2 =& kRI_s(ka)\,K_{s+1}(kR) - kRI_{s+1}(kR)\,K_s(ka) \\
B_3 =& kaI_{s+1}(ka) + sI_s(ka) \\
B_4 =& -4U_g^2 I_s(ka)\,I_s(kR)\,K_s(ka) + 4U_g^2\left(I_s(ka)\right)^2 K_s(kR) \\
& - 4U_fU_g\left(I_s(ka)\right)^2 K_s(kR) + 4U_fU_g I_s(ka)\,I_s(kR)\,K_s(ka) \\
B_5 =& -U_f^2 I_s(ka)\,I_s(kR)\,K_s(ka) + U_f^2\left(I_s(ka)\right)^2 K_s(kR) \\
B_6 =& -4kaU_fU_g I_s(ka)\,K_{s+1}(ka)\,I_s(kR) + 4kaU_g^2 I_{s+1}(ka)\,I_s(ka)\,K_s(kR) \\
& - 4kaU_fU_g I_{s+1}(ka)\,I_s(ka)\,K_s(kR) + 4kRU_fU_g I_s(ka)\,I_{s+1}(kR)\,K_s(ka) \\
& - 4kRU_fU_g K_{s+1}(kR)\left(I_s(ka)\right)^2 + 4kaU_g^2 I_s(ka)\,K_{s+1}(ka)\,I_s(kR) \\
& + 4kRU_g^2\left(I_s(ka)\right)^2 K_{s+1}(kR) - 4kRU_g^2 I_s(ka)\,I_{s+1}(kR)\,K_s(ka) \\
B_7 =& -kaU_f^2 I_{s+1}(ka)\,I_s(kR)\,K_s(ka) + akU_f^2 I_{s+1}(ka)\,I_s(ka)\,K_s(kR) \\
& - kRU_f^2 I_s(ka)\,I_{s+1}(kR)\,K_s(ka) + kRU_f^2 K_{s+1}(kR)\left(I_s(ka)\right)^2
\end{aligned}
$$

$$
\begin{aligned}
B_8 =& 4k^2aRU_g^2 I_s(ka)\, I_{s+1}(kR)\, K_{s+1}(ka) \\
&+ 4k^2aRU_g^2 I_{s+1}(ka)\, K_{s+1}(kR)\, I_s(ka) \\
&- 4k^2aRU_fU_g I_s(ka)\, I_{s+1}(kR)\, K_{s+1}(ka) \\
&- 4k^2aRU_fU_g I_{s+1}(ka)\, K_{s+1}(kR)\, I_s(ka) \\
B_9 =& -k^2aRU_f^2 I_{s+1}(ka)\, I_{s+1}(kR)\, K_s(ka) \\
&+ k^2aRU_f^2 I_{s+1}(ka)\, K_{s+1}(kR)\, I_s(ka) \\
B_{10} =& I_s(kR)\, K_s(ka)\, I_s(ka) - (I_s(ka))^2 K_s(kR) \\
B_{11} =& (I_s(ka))^2 K_s(kR) - I_s(kR)\, K_s(ka)\, I_s(ka) \\
B_{12} =& -kaI_s(ka)\, K_s(kR)\, I_{s+1}(ka) - kaI_s(ka)\, K_{s+1}(ka)\, I_s(kR) \\
&- kR(I_s(ka))^2 K_{s+1}(kR) + kRI_{s+1}(kR)\, K_s(ka)\, I_s(ka) \\
B_{13} =& kaI_s(ka)\, K_s(kR)\, I_{s+1}(ka) - kRI_{s+1}(kR)\, K_s(ka)\, I_s(ka) \\
&- kaI_s(kR)\, K_s(ka)\, I_{s+1}(ka) + kR(I_s(ka))^2 K_{s+1}(kR) \\
B_{14} =& -k^2aRI_s(ka)\, K_{s+1}(kR)\, I_{s+1}(ka) - k^2aRI_s(ka)\, I_{s+1}(kR)\, K_{s+1}(ka) \\
B_{15} =& k^2aRI_s(ka)\, K_{s+1}(kR)\, I_{s+1}(ka) - k^2aRI_{s+1}(kR)\, K_s(ka)\, I_{s+1}(ka)
\end{aligned}
$$

APPENDIX D
DERIVATION OF UNIQUE FLUID PRESSURES FOR ANNULAR COUNTER-CURRENT FLOW

As described in Section 5.2.5, the value of the parameter s can be determined to be zero for the case of annular counter-current flow stability. With this information, the relationship between the gas and liquid pressures can be developed in a mathematically succinct manner.

By assuming $s = 0$, the general solution to the differential equation posed by Equation 5.7 can be rewritten

$$\Phi_{1,k} = B_k \left(C_1 I_0 \left(kr \right) + C_2 K_s \left(kr \right) \right). \tag{D.1}$$

Using methods described in Section 5.2, Equation D.1 can be written as

$$\Phi_{1,g} = B_g \left(I_0 \left(kr \right) + K_s \left(kr \right) \right) \tag{D.2}$$

for the gas flow and

$$\Phi_{1,f} = B_f \left(C_1 I_0 \left(kr \right) + C_2 K_s \left(kr \right) \right) \tag{D.3}$$

for the liquid flow. The wall boundary condition of the liquid, fulfilled by the parameters C_1 and C_2, are found to be

$$C_1 = \frac{1}{I_1 \left(kR \right)} \tag{D.4a}$$

$$C_2 = \frac{1}{K_1 \left(kR \right)}. \tag{D.4b}$$

The wave at the gas-liquid interface, defined by

$$\eta = \eta_0 e^{ik(z-ct)} + \bar{a}, \tag{D.5}$$

can then be used to determine B_f and B_g. Using Equations 5.13 and 5.21, these coefficients can be found to be

$$B_g = \frac{i\eta_0 \left(c - U_g \right)}{I_1 \left(ka \right)} \tag{D.6}$$

and

$$B_f = \frac{i\eta_0 I_1(kR) K_1(kR)(c - U_f)}{I_1(ka) K_1(kR) - K_1(ka) I_1(kR)}. \tag{D.7}$$

Finally, using the Bernoulli equation, the pressure of the gas and liquid can be calculated to be

$$P_g = \frac{\rho_g k \eta I_0(ka)(c - U_g)^2}{I_1(ka)} \tag{D.8}$$

and

$$P_f = \frac{\rho_f k \eta (c - U_f)^2 (I_0(ka) K_1(kR) + K_0(ka) I_1(kR))}{I_1(ka) K_1(kR) - K_1(ka) I_1(kR)}. \tag{D.9}$$

APPENDIX E

ALTERNATIVE PRESENTATION OF RESULTS OF TUBE DIAMETER STUDY

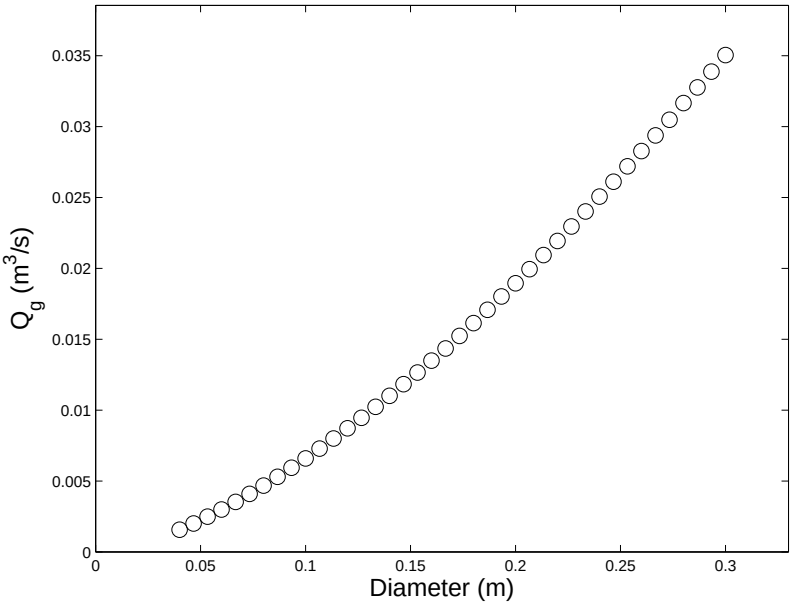

Fig. E.1. Gas volumetric flow rate as a function of the tube diameter for diameter dependence demonstration case.

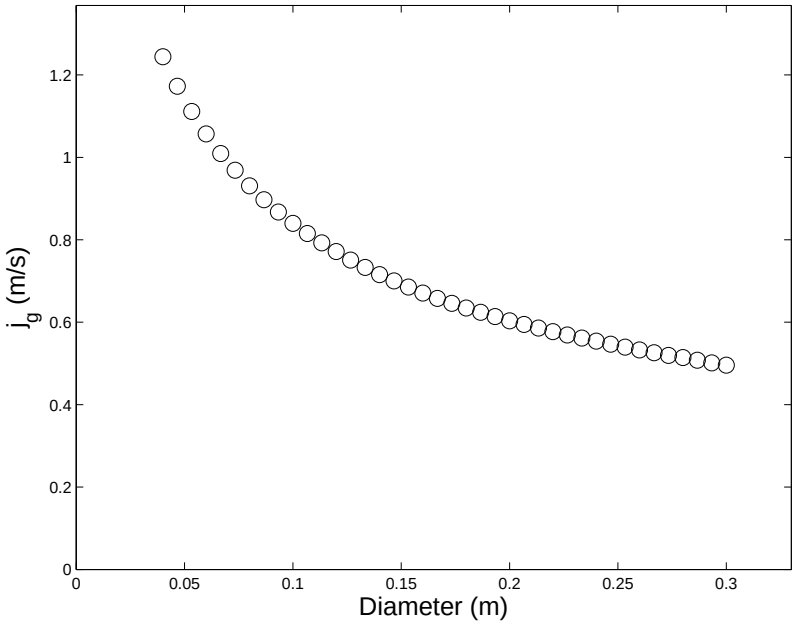

Fig. E.2. Gas superficial velocity as a function of the tube diameter for diameter dependence demonstration case.

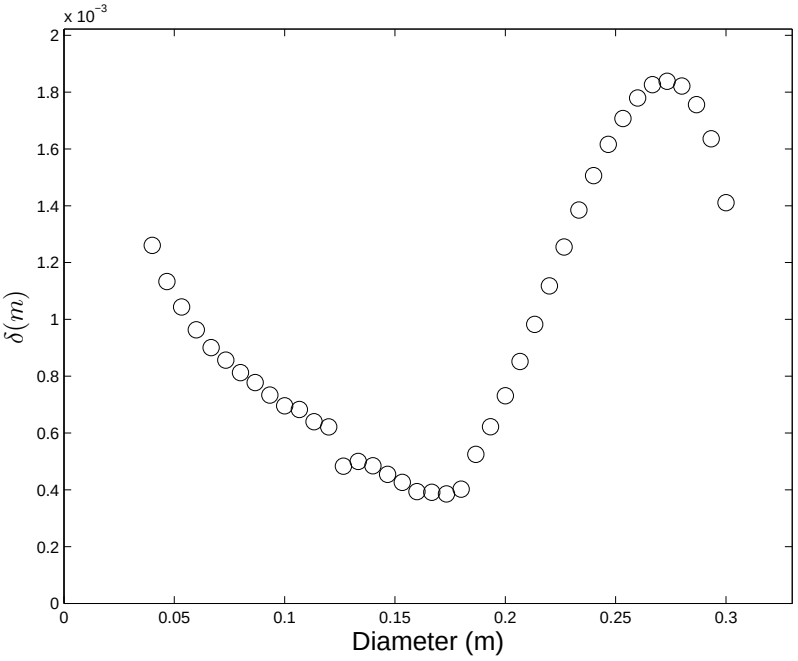

Fig. E.3. Film thickness as a function of the tube diameter for diameter dependence demonstration case.

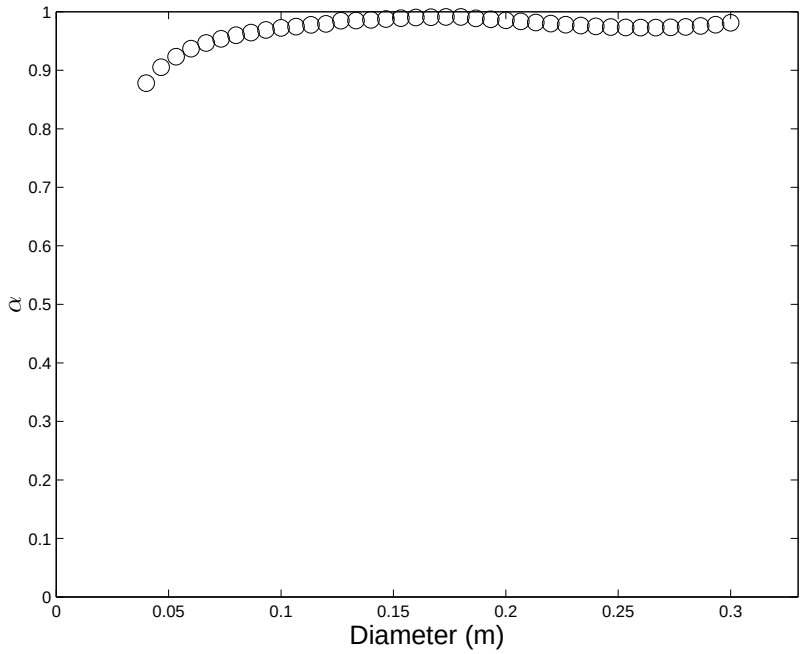

Fig. E.4. Void fraction as a function of the tube diameter for diameter dependence demonstration case.

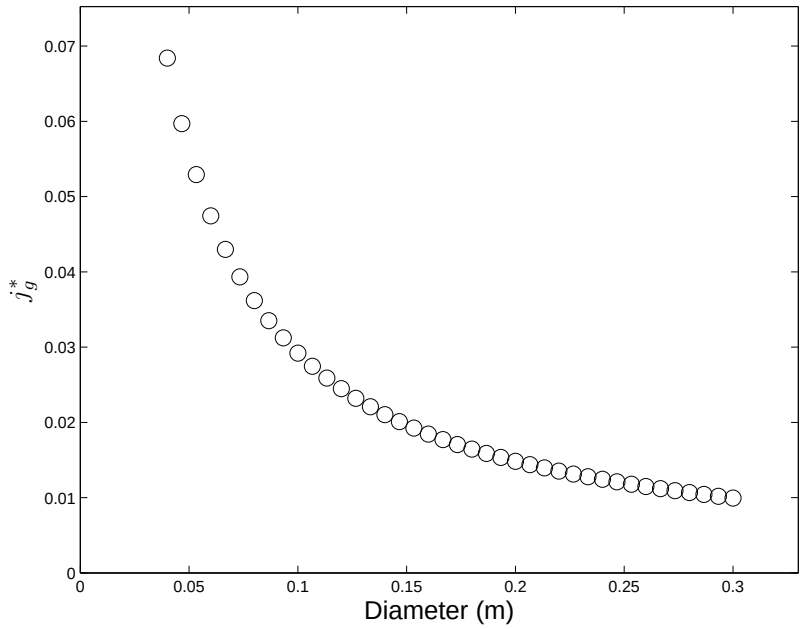

Fig. E.5. Gas Wallis parameter as a function of the tube diameter for diameter dependence demonstration case.

APPENDIX F

ANALYSIS OF THE DATA OF TIEN, CHUNG, AND LIU

The experimental flooding data presented by Tien, Chung, and Liu [56] represent several sets of experimental conditions. As mentioned in Section 6.2, all the data that was given was assessed, and a group of experimental sets were dismissed. The data sets presented in this validation of the stability-based and momentum-based models of flooding are given in Table F.1. The corresponding table for the data to be found in the original reference is given by the page number followed by a letter which indicates the first or second table on that page (e.g. 7-7A, 7-7B). The set of data is then given a corresponding case number for this assessment in order to match data sets to the graphical and quantitative results. The gas in each experiment presented is air, with a density of $\rho = 1.2\ \mathrm{kg/m^3}$, and the viscosity of all liquids used in these experiments is $0.001\ \mathrm{Pa \cdot s}$. The liquid inlet and outlet were either straight-edged (s) or tapered (t), and the air could be delivered via a nozzle into the test section (n) or indirectly (i), by way of a lower plenum on the test section.

The results of the validation of the stability-based and momentum-based model, as well as corresponding figures comparing dimensionless velocities and Wallis parameters, are tabulated in Table F.2.

Table F.1
Experimental conditions for the data of Tien, Chung, and Liu [56].

Original Table	Case	Liquid	D (mm)	ρ_f (kg/m^3)	σ (N/m)	Inlet	Exit	Air Supply
7-2B	1	water	31.8	997	0.072	t	s	n
7-3A	2	water	46.0	998	0.073	t	s	n
7-5B	7	water	69.9	998	0.073	t	s	n
7-5A	8	water	46.0	988	0.073	s	t	n
7-6A	9	water	15.9	998	0.073	s	t	i
7-6B	10	water	31.8	998	0.073	t	s	i
7-7A	11	water	46.0	998	0.073	t	s	i
7-7B	12	water	69.9	998	0.073	t	s	i
7-8A	13	water	69.9	998	0.073	t	s	i
7-8B	14	water	31.8	998	0.073	s	t	i
7-9A	15	water	46.0	998	0.073	s	t	i
7-9B	16	water	69.9	998	0.072	s	t	i
7-10A	17	water	31.8	998	0.073	t	t	i
7-10B	18	water	31.8	998	0.073	s	s	i
7-12A	21	water with Surfynol	31.8	998	0.029	t	s	n
7-12B	22	silicon oil	46.0	820	0.017	t	s	n
7-13A	23	water with Surfynol	46.0	998	0.029	t	s	n

Table F.2

Standard deviation of the relative error for validation data sets of Tien, Chung, and Liu [56].

Original Table	Case	σ_{momentum}	$\sigma_{\text{stability}}$	Figure of $\langle j_g \rangle$	Figure of j_g^*
7-2B	1	205.76%	75.939%	F.1	F.18
7-3A	2	56.387%	91.506%	F.2	F.19
7-5B	7	109.82%	93.584%	F.3	F.20
7-5A	8	80.814%	89.149%	F.4	F.21
7-6A	9	101.42%	36.826%	F.5	F.22
7-6B	10	247.98%	53.433%	F.6	F.23
7-7A	11	182.17%	78.8%	F.7	F.24
7-7B	12	174.21%	90.4%	F.8	F.25
7-8A	13	559.63%	82.184%	F.9	F.26
7-8B	14	398.83%	53.012%	F.10	F.27
7-9A	15	128.02%	83.989%	F.11	F.28
7-9B	16	159.81%	91.418%	F.12	F.29
7-10A	17	199.6%	60.91%	F.13	F.30
7-10B	18	342.33%	42.418%	F.14	F.31
7-12A	21	116.93%	87.69%	F.15	F.32
7-12B	22	144.19%	96.773%	F.16	F.33
7-13A	23	79.266%	96.67%	F.17	F.34

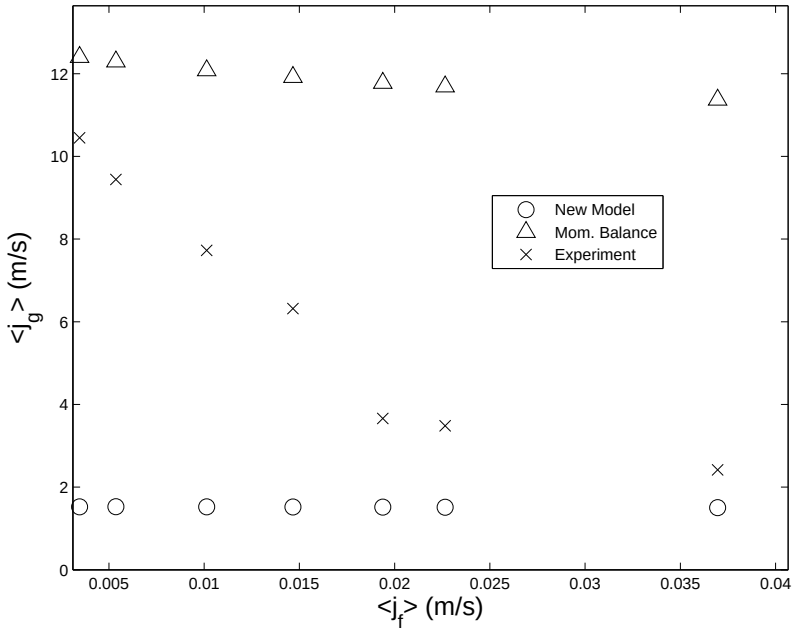

Fig. F.1. Comparison between Case 1, new stability model, and momentum-based model of superficial velocities for flooding.

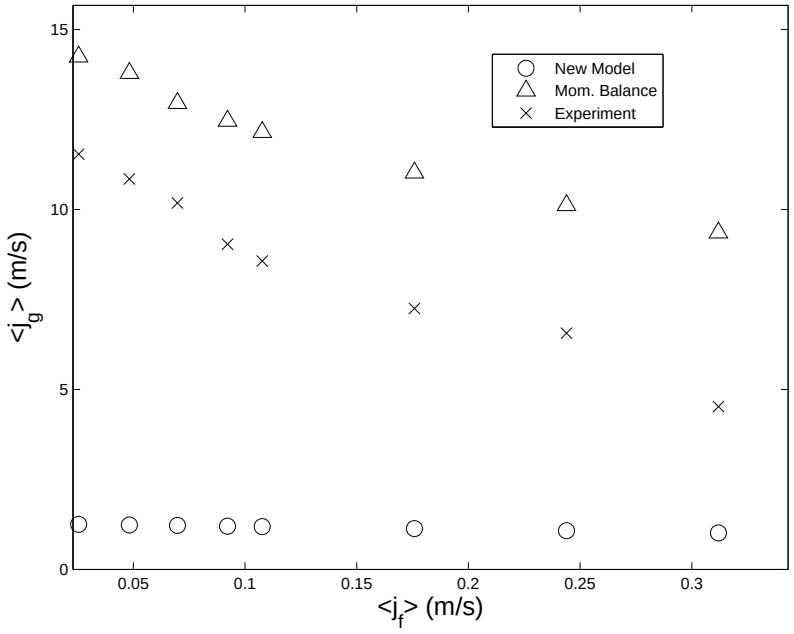

Fig. F.2. Comparison between Case 2, new stability model, and momentum-based model of superficial velocities for flooding.

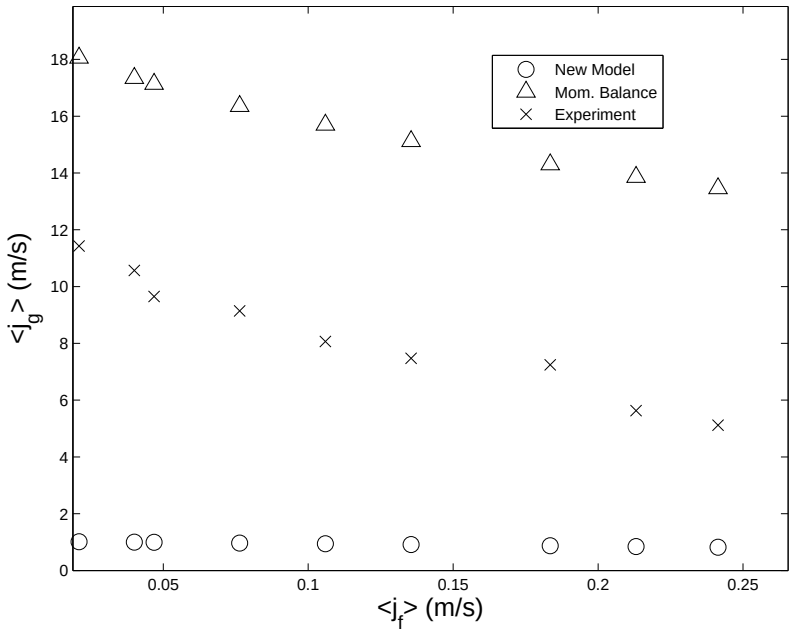

Fig. F.3. Comparison between Case 3, new stability model, and momentum-based model of superficial velocities for flooding.

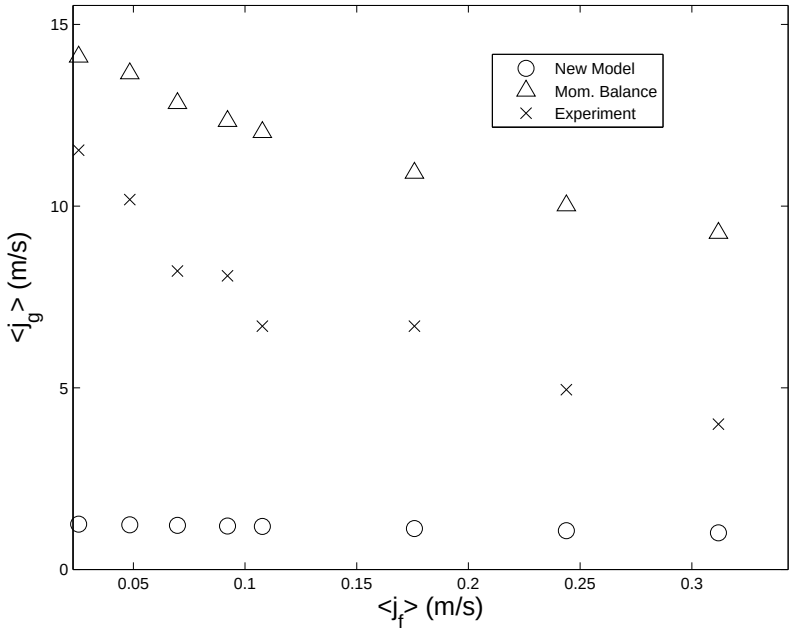

Fig. F.4. Comparison between Case 4, new stability model, and momentum-based model of superficial velocities for flooding.

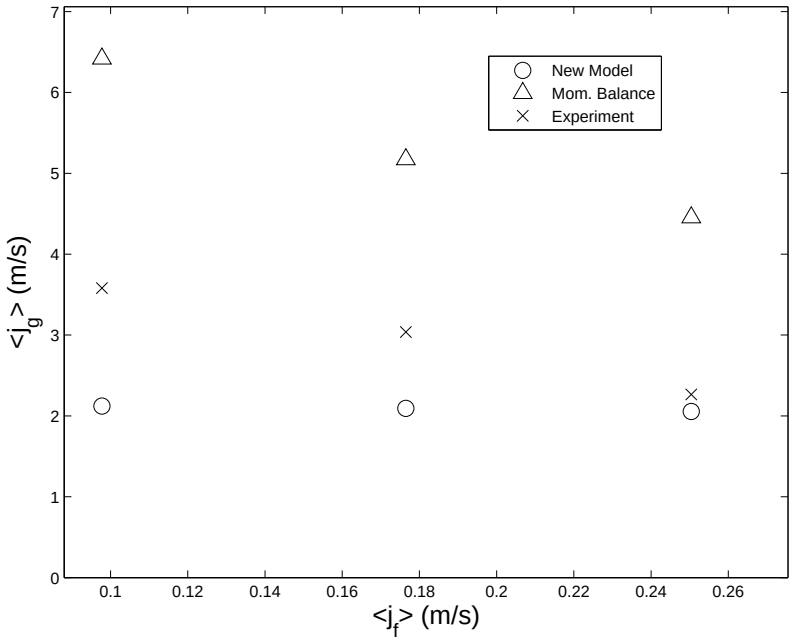

Fig. F.5. Comparison between Case 5, new stability model, and momentum-based model of superficial velocities for flooding.

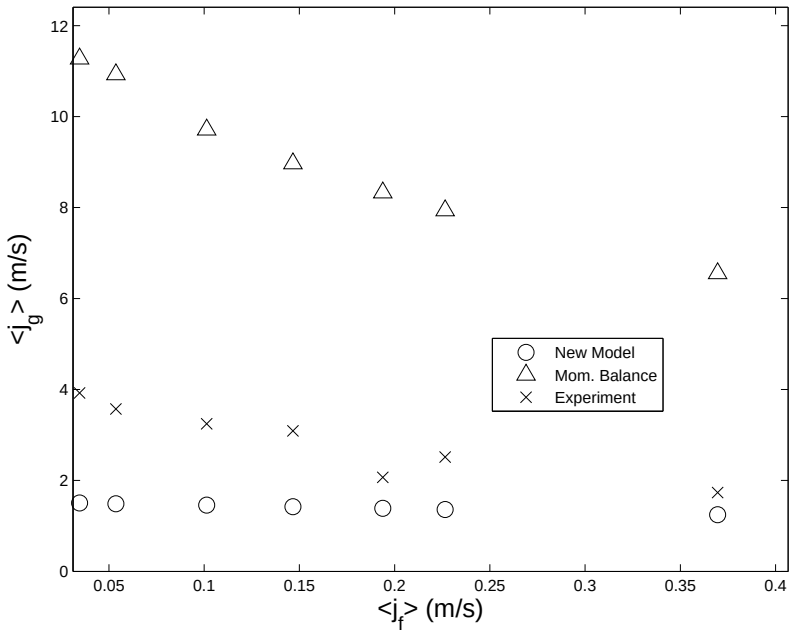

Fig. F.6. Comparison between Case 6, new stability model, and momentum-based model of superficial velocities for flooding.

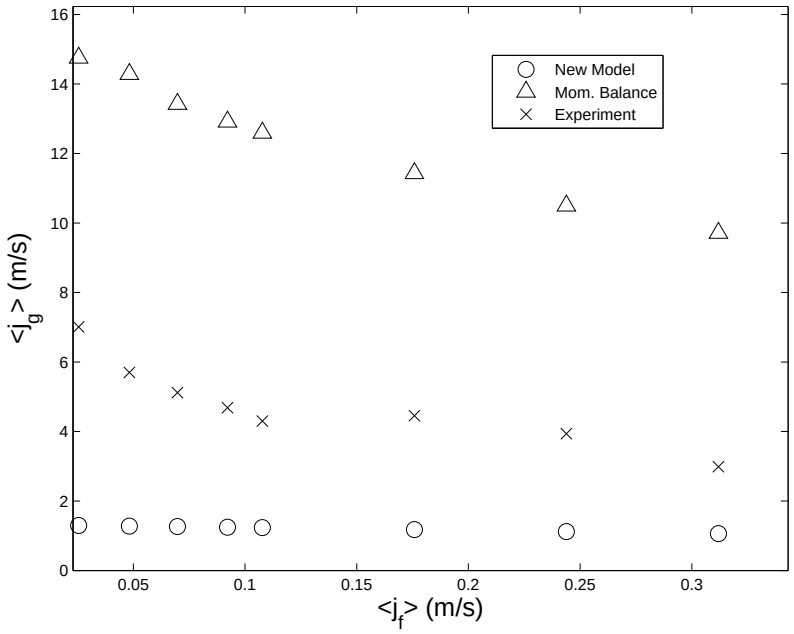

Fig. F.7. Comparison between Case 7, new stability model, and momentum-based model of superficial velocities for flooding.

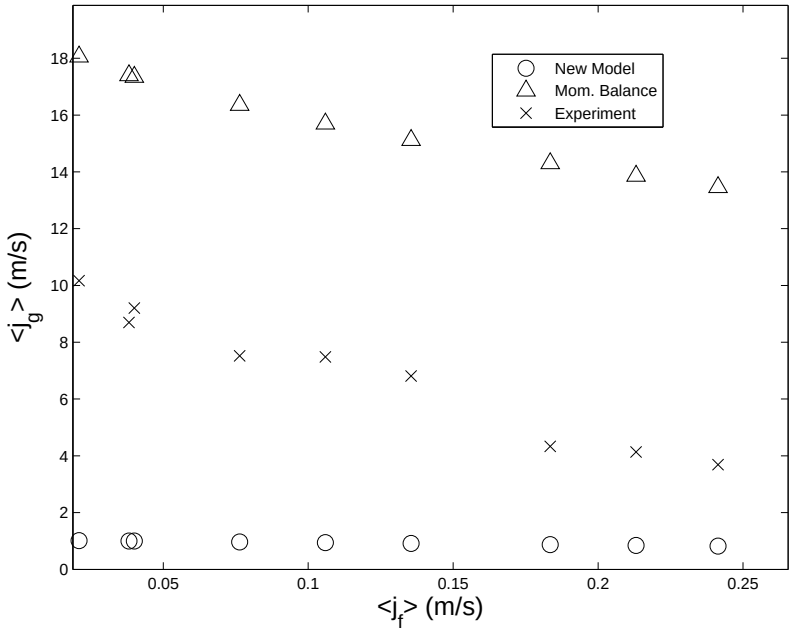

Fig. F.8. Comparison between Case 8, new stability model, and momentum-based model of superficial velocities for flooding.

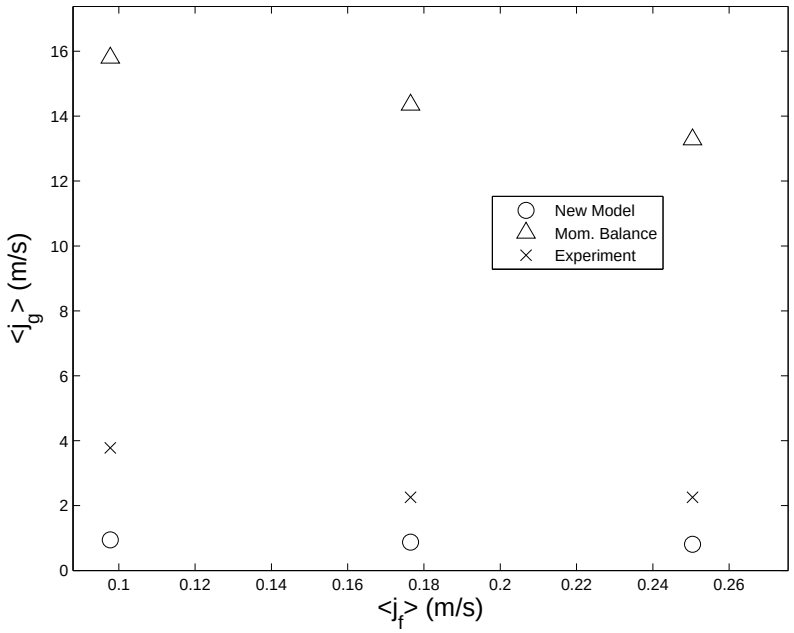

Fig. F.9. Comparison between Case 9, new stability model, and momentum-based model of superficial velocities for flooding.

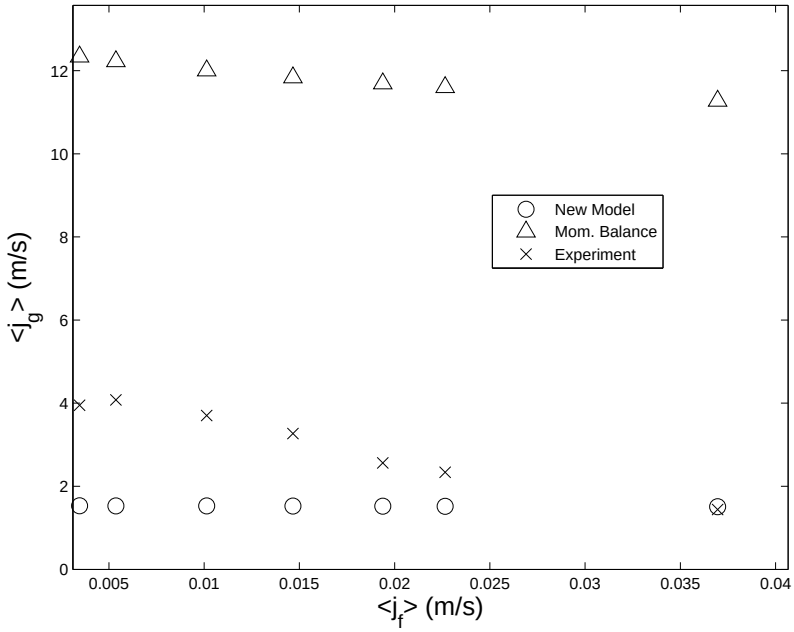

Fig. F.10. Comparison between Case 10, new stability model, and momentum-based model of superficial velocities for flooding.

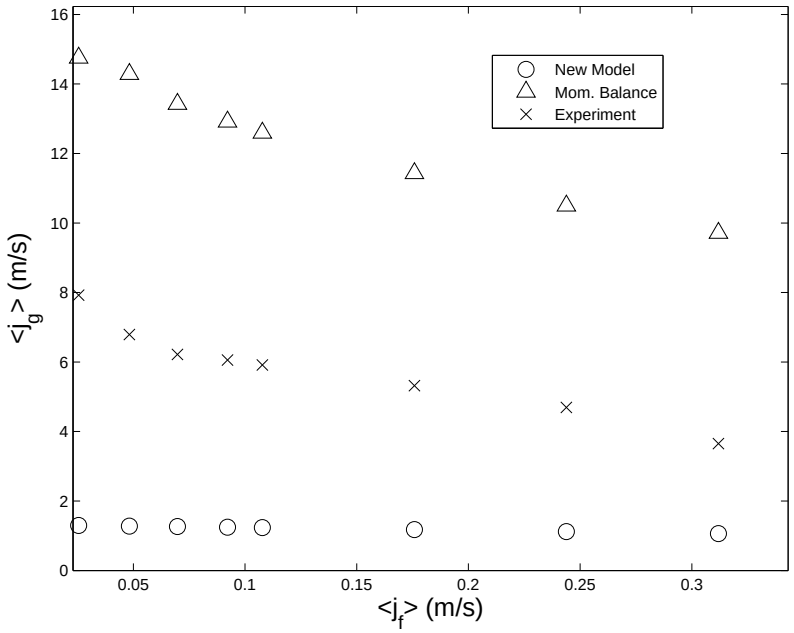

Fig. F.11. Comparison between Case 11, new stability model, and momentum-based model of superficial velocities for flooding.

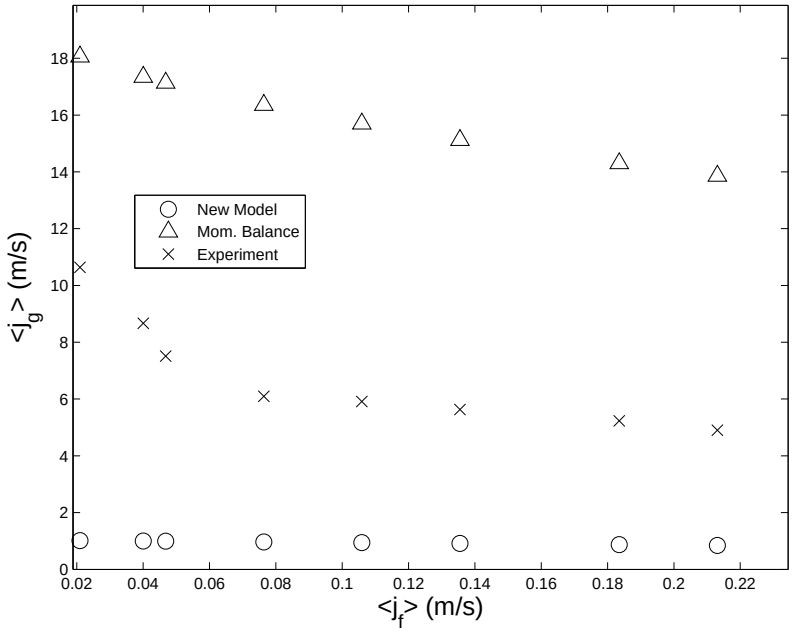

Fig. F.12. Comparison between Case 12, new stability model, and momentum-based model of superficial velocities for flooding.

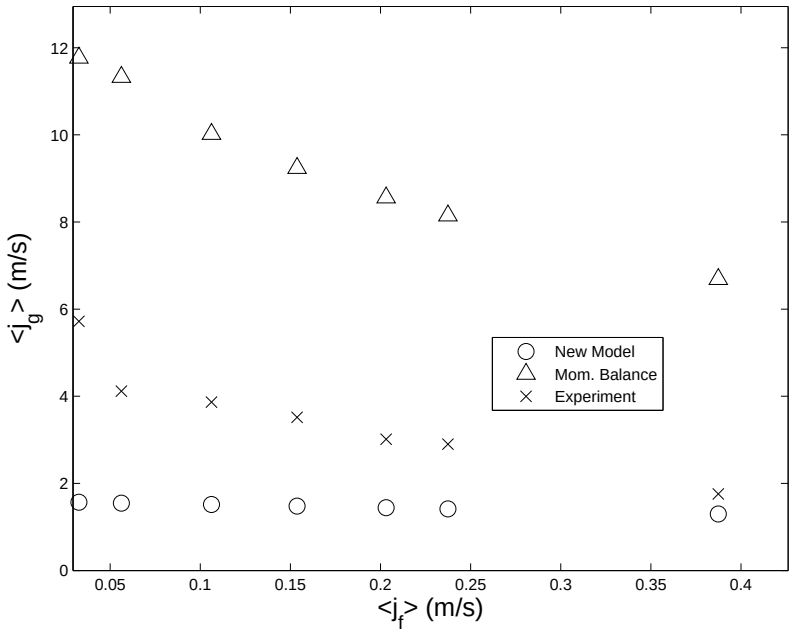

Fig. F.13. Comparison between Case 13, new stability model, and momentum-based model of superficial velocities for flooding.

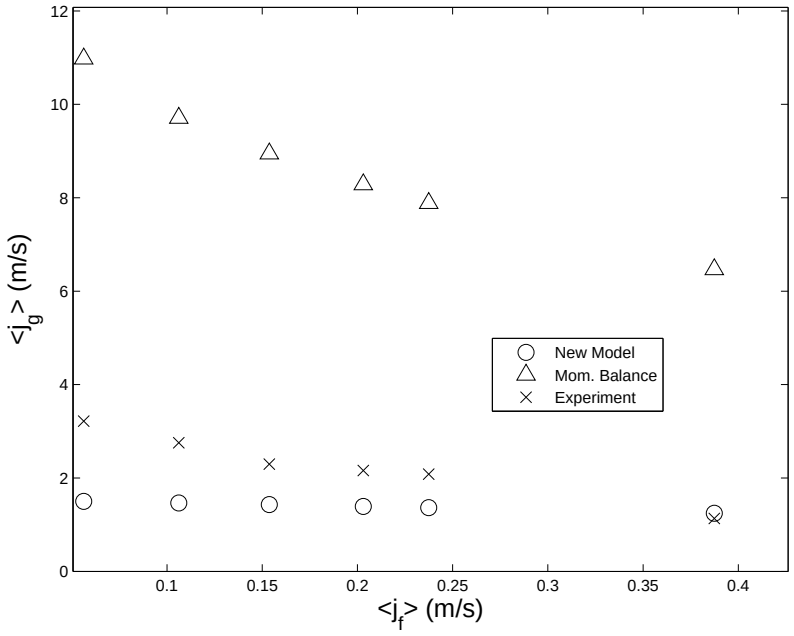

Fig. F.14. Comparison between Case 14, new stability model, and momentum-based model of superficial velocities for flooding.

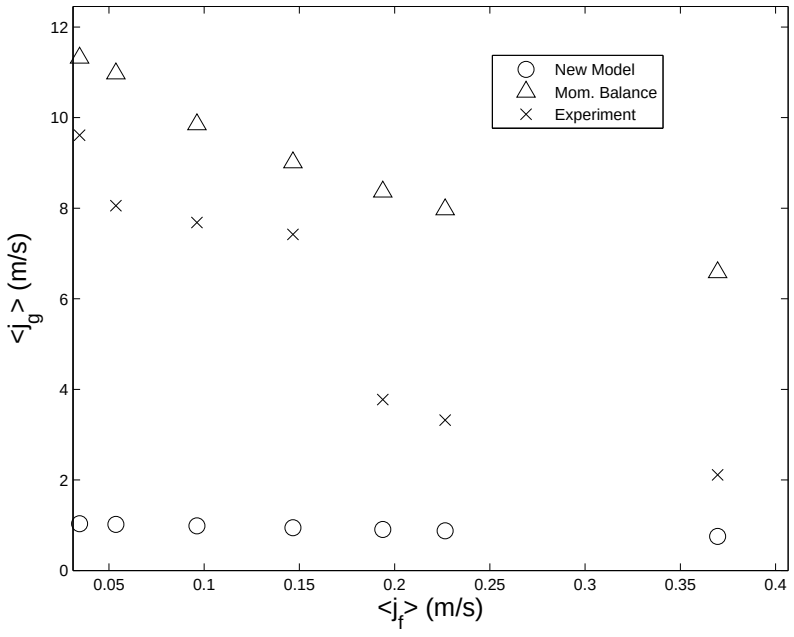

Fig. F.15. Comparison between Case 15, new stability model, and momentum-based model of superficial velocities for flooding.

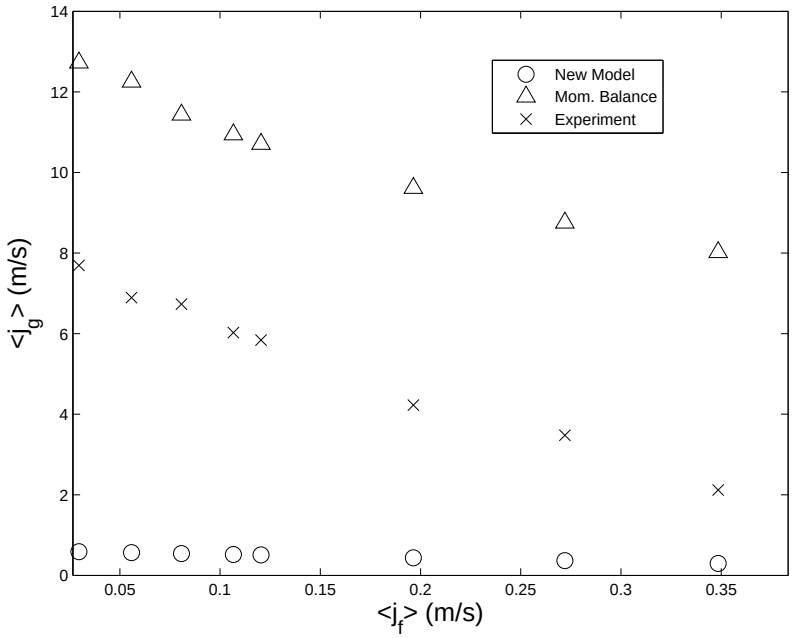

Fig. F.16. Comparison between Case 16, new stability model, and momentum-based model of superficial velocities for flooding.

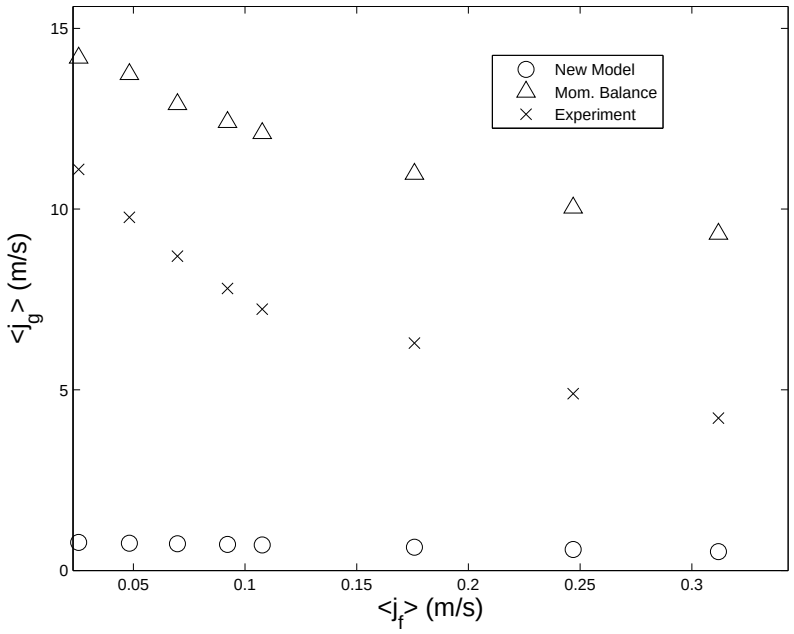

Fig. F.17. Comparison between Case 17, new stability model, and momentum-based model of superficial velocities for flooding.

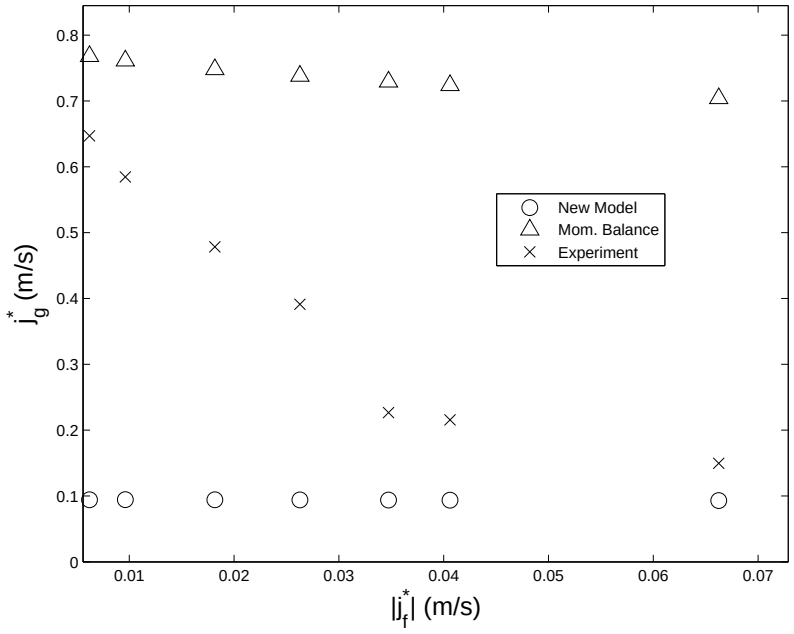

Fig. F.18. Comparison between Case 1, new stability model, and momentum-based model of Wallis parameters for flooding.

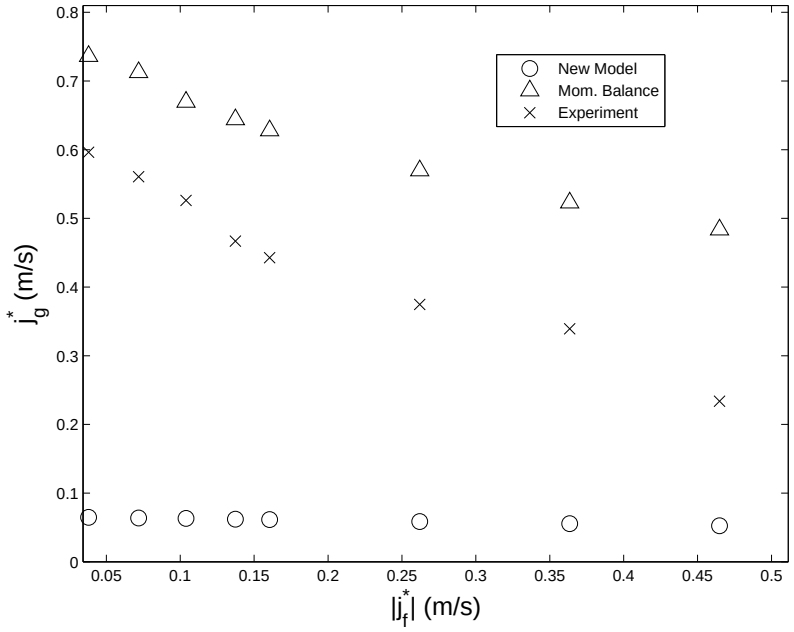

Fig. F.19. Comparison between Case 2, new stability model, and momentum-based model of Wallis parameters for flooding.

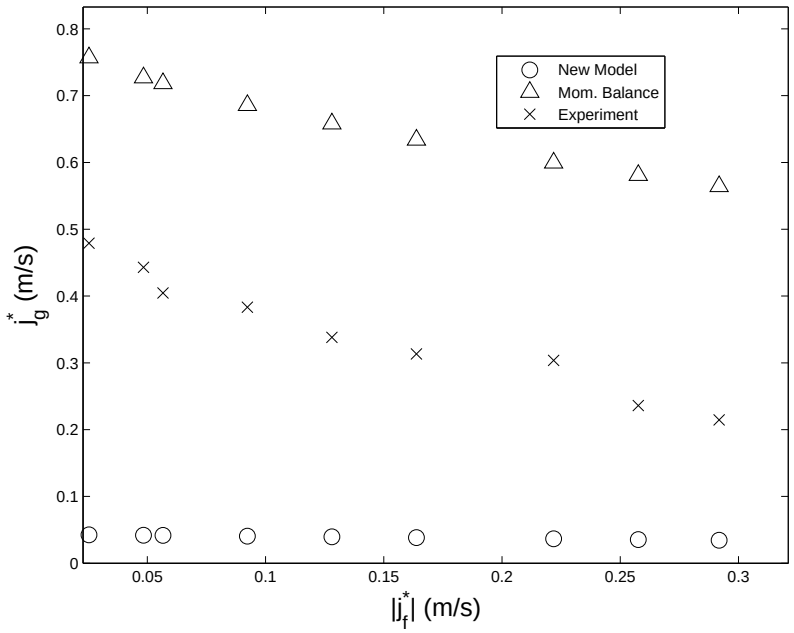

Fig. F.20. Comparison between Case 3, new stability model, and momentum-based model of Wallis parameters for flooding.

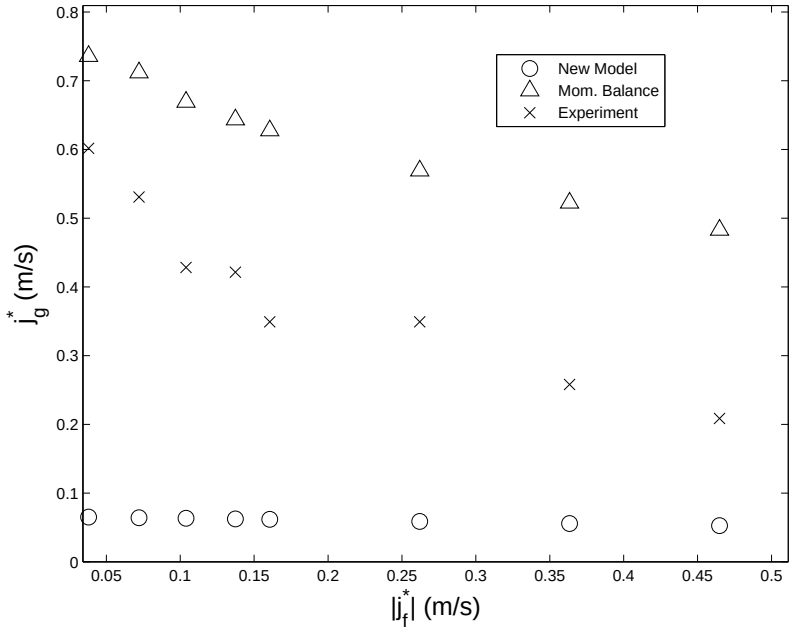

Fig. F.21. Comparison between Case 4, new stability model, and momentum-based model of Wallis parameters for flooding.

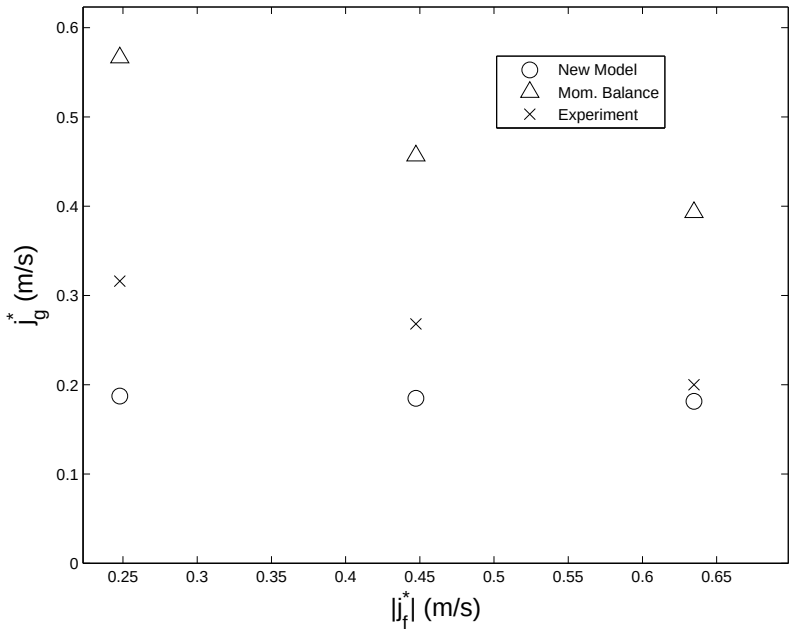

Fig. F.22. Comparison between Case 5, new stability model, and momentum-based model of Wallis parameters for flooding.

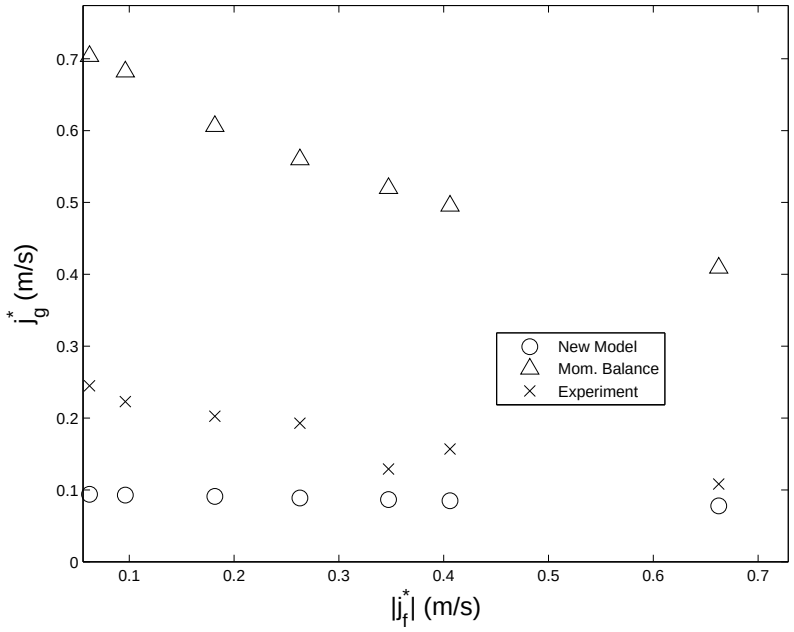

Fig. F.23. Comparison between Case 6, new stability model, and momentum-based model of Wallis parameters for flooding.

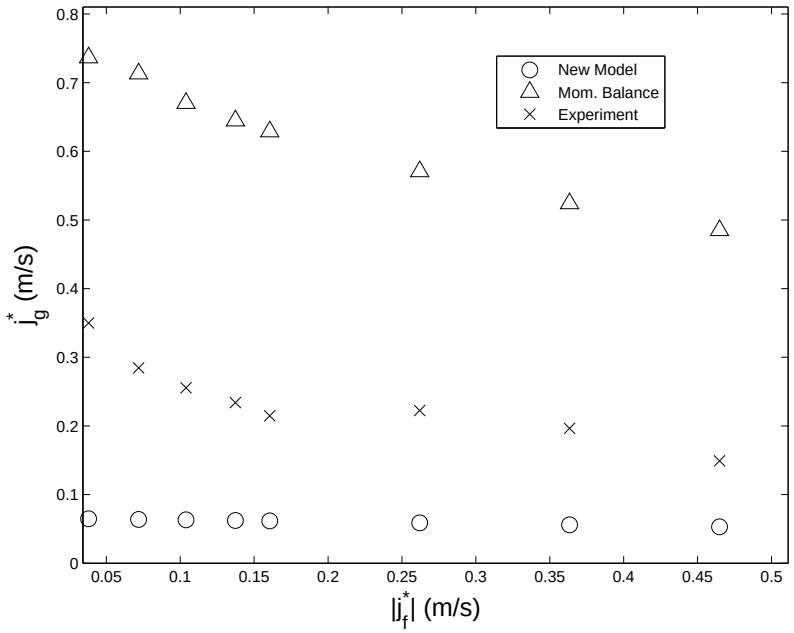

Fig. F.24. Comparison between Case 7, new stability model, and momentum-based model of Wallis parameters for flooding.

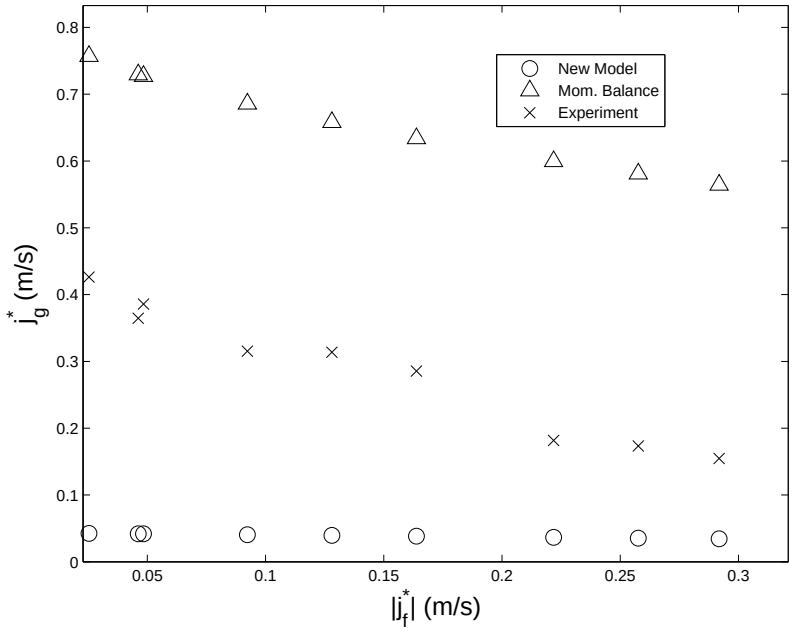

Fig. F.25. Comparison between Case 8, new stability model, and momentum-based model of Wallis parameters for flooding.

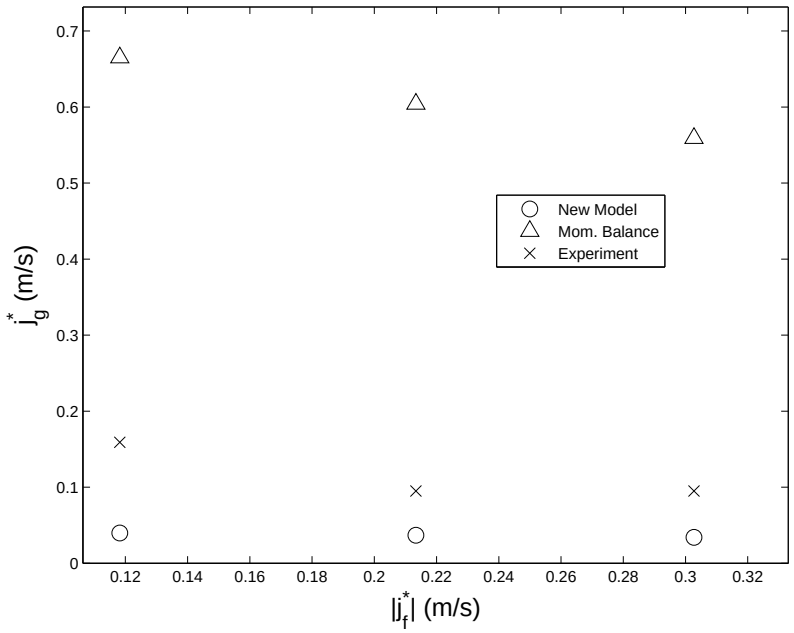

Fig. F.26. Comparison between Case 9, new stability model, and momentum-based model of Wallis parameters for flooding.

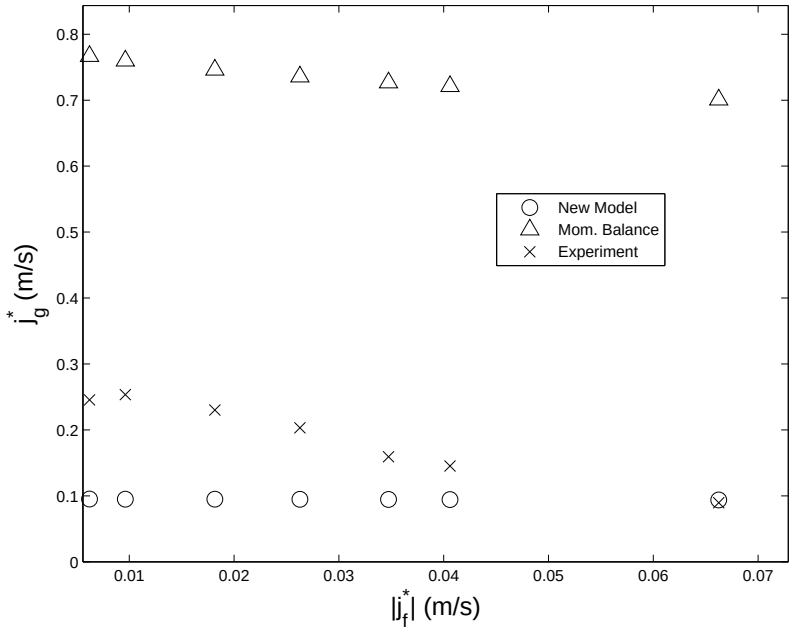

Fig. F.27. Comparison between Case 10, new stability model, and momentum-based model of Wallis parameters for flooding.

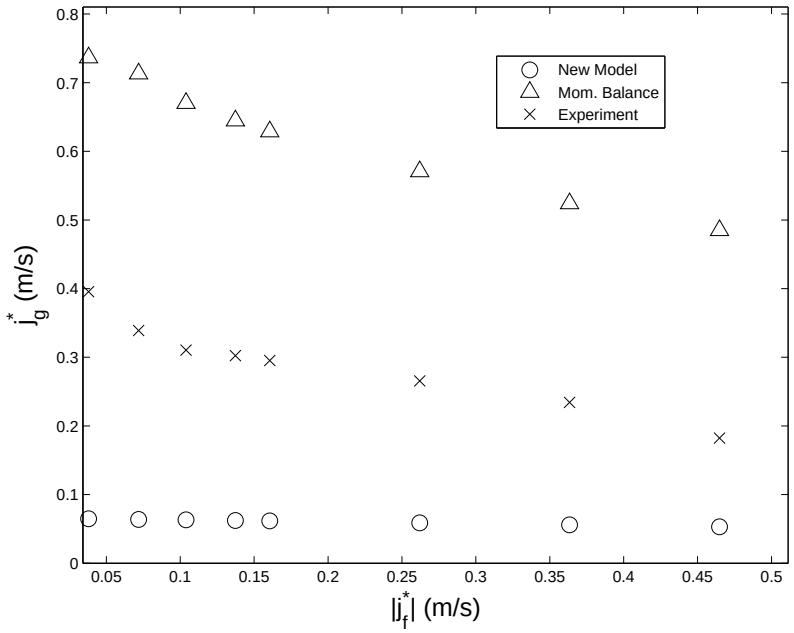

Fig. F.28. Comparison between Case 11, new stability model, and momentum-based model of Wallis parameters for flooding.

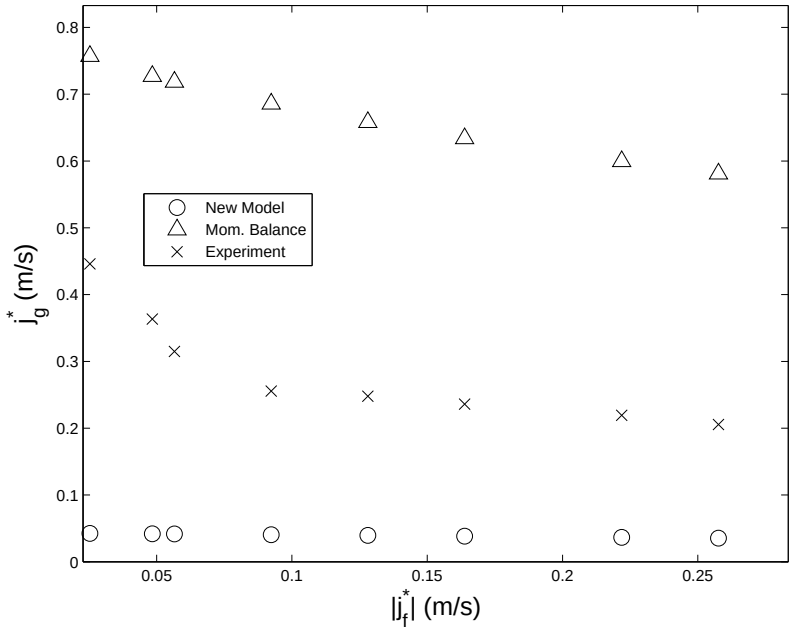

Fig. F.29. Comparison between Case 12, new stability model, and momentum-based model of Wallis parameters for flooding.

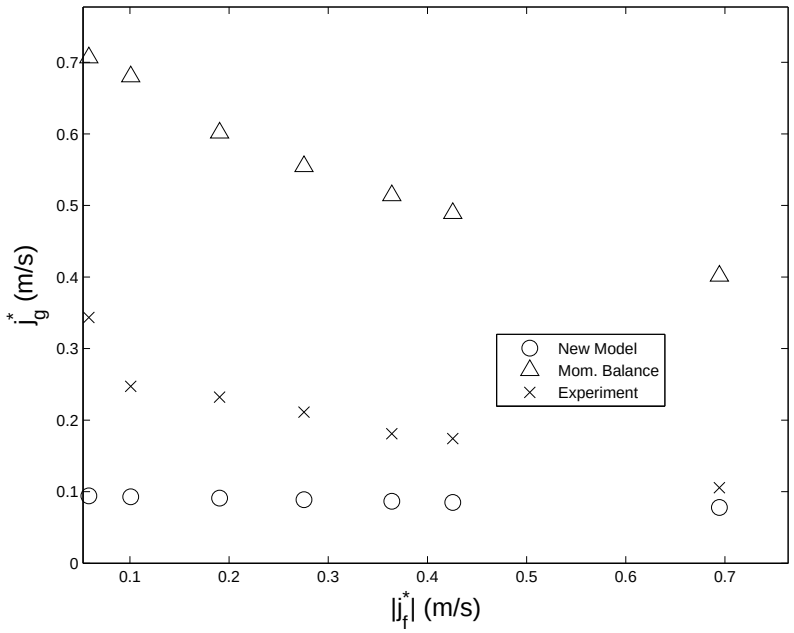

Fig. F.30. Comparison between Case 13, new stability model, and momentum-based model of Wallis parameters for flooding.

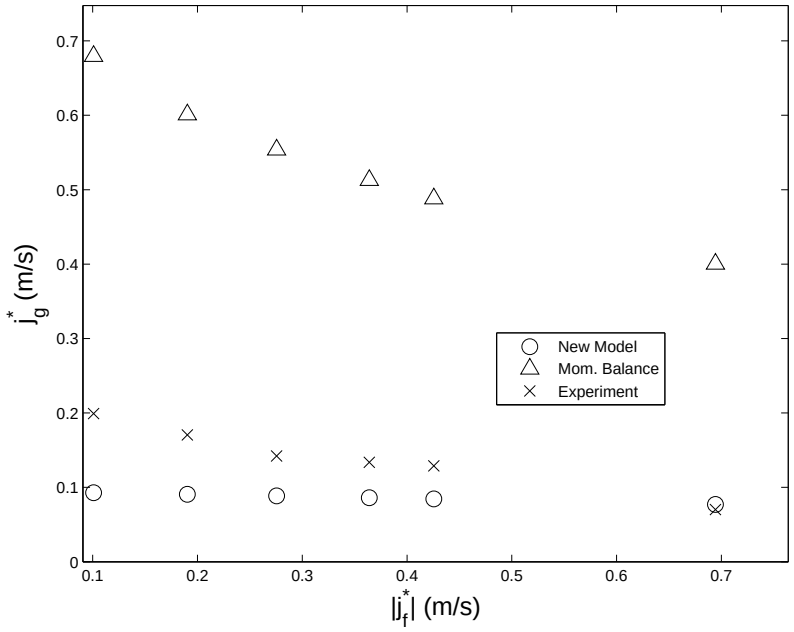

Fig. F.31. Comparison between Case 14, new stability model, and momentum-based model of Wallis parameters for flooding.

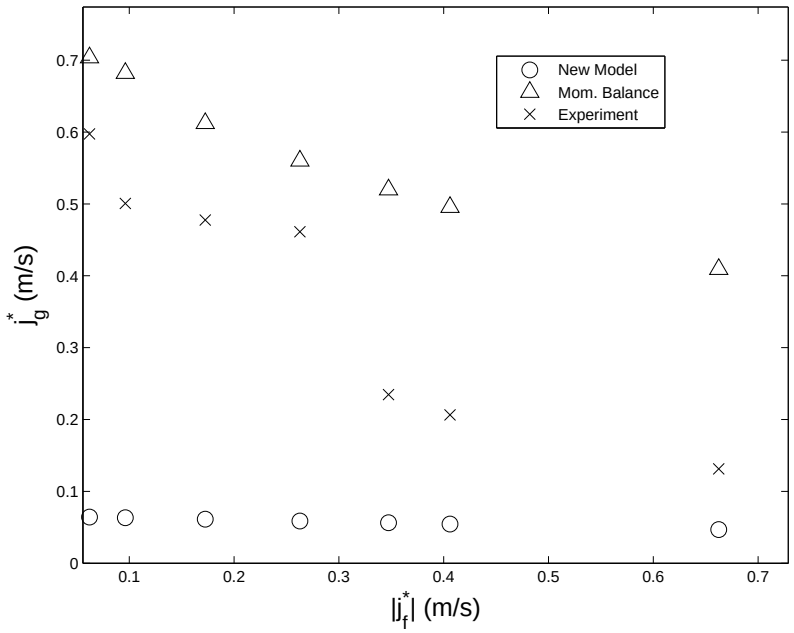

Fig. F.32. Comparison between Case 15, new stability model, and momentum-based model of Wallis parameters for flooding.

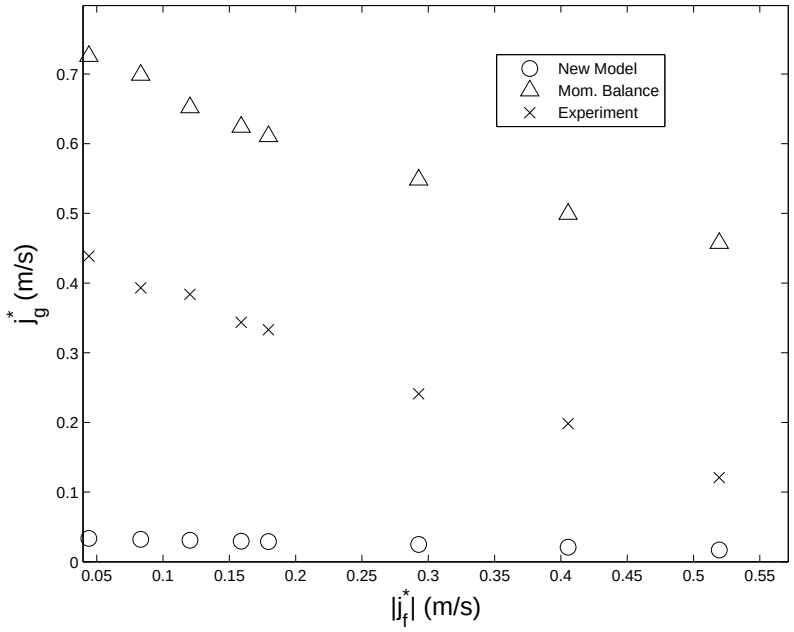

Fig. F.33. Comparison between Case 16, new stability model, and momentum-based model of Wallis parameters for flooding.

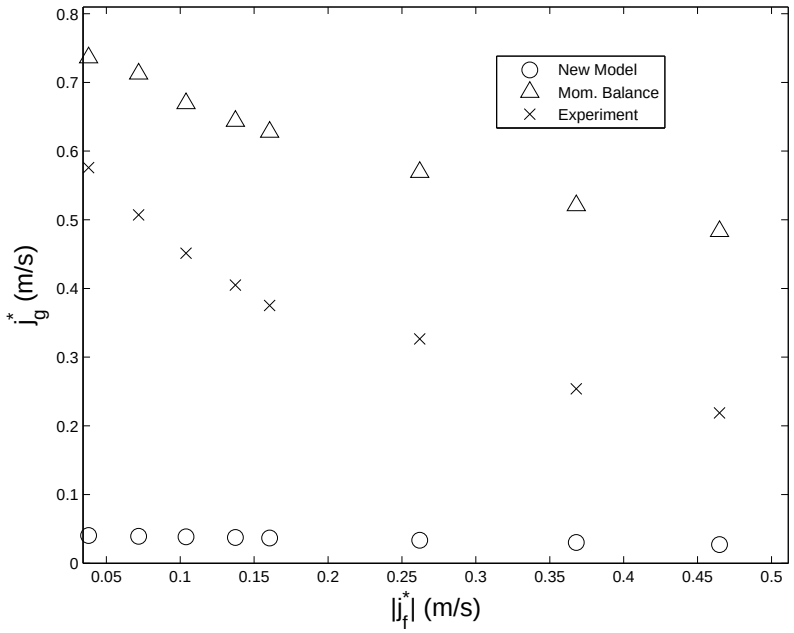

Fig. F.34. Comparison between Case 17, new stability model, and momentum-based model of Wallis parameters for flooding.

VITA

Name: Kevin J. Hogan

Email: kjhogan@tamu.edu

Address: Kevin Hogan
c/o Karen Vierow
Texas A&M University
3133 TAMU
129 Zachry Engineering Center
College Station, TX 77843-3133

Education:

· Ph.D.		Texas A&M University
Nuclear Engineering		August 2009
· M.S.N.E.		Purdue University
Nuclear Engineering		August 2006
· B.S.		University of Maryland
Nuclear Engineering		May 2004